Pulsed Laser Deposition (PLD) of Magnetic Multilayer and Granular Thin Films

by

Li Ming Fai

A Thesis Submitted in Partial Fulfilment
of the Requirements for the Degree of
Master of Philosophy

The Hong Kong Polytechnic University

1999

This thesis is dedicated to my dear shepherd,

Jesus Christ,

and my lovely family.

Abstract

CoAg granular and multilayer films as well as the Ti/Si based films have been fabricated by pulsed laser deposition (PLD) method. A special split target and a rotating multi-target holder have been developed to facilitate the PLD process. X-ray diffraction and Atomic Force Microscopy (AFM) were used to examine the structure and topography of the films respectively. The electrical properties and the magnetoresistance (MR) of these films were measured by a standard four-probe method. The effects of film thickness, substrate temperature and post-annealing on Ti/Si based films were investigated. In the CoAg granular films a MR ratio of 9% at 77 K and 5.5% at room temperature were obtained under the influence of a magnetic field of 1 Tesla. The PLD CoAg multilayer films in this work however showed a relatively poor MR. Some possible explanations for this result are suggested. Anomalous electrical properties were obtained in the Ti/Si based films. In addition, an unusual and rather large positive magnetoresistance (PMR) was also observed in these samples. Maximum PMR of +37% at about 170 K and +10% at room temperature were recorded. Thin films based on the Ti/Si and other related materials systems can have very good potentials for integrated sensor applications. It is one of the purpose of the present work to explore this material system and to report some of the interesting findings.

Acknowledgments

I would like to acknowledge my supervisor, Dr. K. H. Wong, for his close supervision, valuable advice and fruitful discussion through thses two years. Special thanks to Dr. W. B. Wu who gave me enlightening suggestions and discussion. I would like also to thank my research companion, Mr. Y. S. Leung, for his useful suggestions and lending help in some experiments.

I wish to thank Dr. K .H. Pang for his assistance in AFM charaterization. I would also like to thank Dr. Alec Pakhomov (The Hong Kong University of Science and Technology) for helping some of the assistance in magnetic measurement. Extended thanks should go to my companions Mr. Albert Luk, W. L. and Miss Melanie Ho, M. T. for their support in this research period. Finally, I would thank my brothers and sisters in my church for their encouragement.

This work is supported by a Research Grant of the Hong Kong Polytechnic University under the Code No.350.695.A3.110. I am grateful for the award of a research studentship from the Hong Kong Polytechnic University.

Table of Contents

Chapter 4 Experiments and Set-up

Chapter 5 Split Target

Chapter 1

Introduction

Due to the small volume involved, highly integratable and excellent performance quality, thin films of various functional materials systems and structural configurations have been the interests of many researches. They have been fabricated for numerous microelectronics device applications. There are many thin film fabrication methods. In recent years, however, the Pulsed Laser Deposition (PLD) method has been shown to a be very successful technique in producing high quality thin films. This is largely due to the fact that the PLD method is relatively simple and it is virtually applicable to any kinds of target materials. Besides, the PLD process can atomize the target associated with very high quenching and deposition rates [Zhang et al, 1997]. Other distinct advantage of PLD is the "congruent" evaporation of materials from target. The stoichiometry of multi-component materials can be preserved in the deposited films. This is especially suitable and useful for fabrication of multi-element ceramic films. Nevertheless, by some clever arrangement in the target holders, the PLD technique is expected to be equally useful in preparing metallic multilayer and granular films.

The Giant Magnetoresistance (GMR) effect, that is the change of resistivity of the sample by an external magnetic field, was discovered to occur in metallic multilayer and granular thin films. These metallic thin films are composed of

ferromagnetic and nonferromagnetic material system such as FeCr, CoCu and CoAg. The phenomenon of GMR in these materials systems can be attributed to the change of the magnetic moment of the ferromagnetic material from an antiparallel alignment in multilayer and from a randomly alignment in granular films to parallel and ordered arrangement. These new class of materials has provided promising application potentials in magnetic recording and magnetic sensor [White, R. L.,1992]. The studies of GMR effect in different material systems have been the themes of many research groups.

In this study, a conventional PLD technique with a "split target" arrangement was used to fabricate CoAg multilayer and granular thin films with different layer thickness and varied composition respectively on Si(100) substrates. The GMR effect in the CoAg thin films has also been characterized and examined.

Apart from the CoAg multilayer and granular films, a new material system, Ti/Si thin film, also has been investigated. It shows an anomalous resistance-temperature profile and exhibited an exceptionally large positive magnetoresistance effect even at room temperature. This new material system is expected to be valuable in device applications because the Ti is directly grown on silicon wafer at low temperature, which is well compatible in microelectronics processing technology.

In Chapter 2 the background and the possible origin of GMR effect in multilayer and granular thin films will be discussed. The magnetoresistance ratio of both the negative and positive magnetoresistance effects will also be defined.

In Chapter 3 a brief history and the mechanism of pulsed laser deposition will be presented. We will discuss the advantages and the limitations of PLD for fabrication of thin films. A review on PLD of GMR granular and multilayer films will also be given.

Our experimental set-up and instrumentation for PLD will be presented in Chapter 4. The working principles of some major measuring and characterization equipment such as the Atomic Force Microscope (AFM), X-Ray Diffraction (XRD), four-terminal probe and the electromagnet will be briefly introduced. Procedures for fabrication of CoAg multilayer and granular films as well as the Ti/Si thin films will be described.

In Chapter 5 the detailed working principle of split target will be shown and explained. Fabrication of multilayer and granular thin films by the split target arrangement will be discussed. Studies of the relationship between the laser track length ratio and atomic percentage of Co in CoAg films will be presented.

The results of CoAg multilayer and granular films on silicon(100) will be shown in Chapter 6. The magnetoresistance ratio dependence on the atomic percentage of Co, processing parameters such as substrate temperature and post-annealing will be discussed.

Fabrication and characterization of PLD of Ti thin film on silicon will be presented in Chapter 7. The effect of the film thickness, substrate and annealing temperatures will be reported. The results of positive magnetoresistance and the anomalous R-T profiles of the Ti/Si system will be discussed.

Conclusion of our present experimental results and suggestions for future investigation and development are given at the end of this report.

Chapter 2

Giant Magnetoresistance (GMR)

2.1 Introduction

There was a sudden surge of interest in research of magnetic multilayers [Baibich, et al, 1988; Binash et al, 1989; Bennett, L. H. and Wastson, R. E.,1994] in the late 80`s when reports on the exceptional properties of these artificially structured materials, such as the perpendicular anisotropy, giant magnetoresistance, and magneto-optical activity emerged. The first application of magnetic mutilayers, however, goes back to the 60`s and it was in the field of neutron physics [Turchin, V. F., 1967]. The supperlattices of magnetic/nonmagnetic thin films are still extensively used in neutron scattering technology, as monochromators [Schoenborn et al, 1974; Saxena et al, 1981; Majkrzak, C. F., 1984], polarizers [Lynn, et al, 1976; Hamelin, B., 1976; Moon et al; 1969; Majkrzak et al, 1982] and reflectors [Mezei, F.,1981]. The present interest are motivated by the prospective use of magnetic mutilayers as magnetic/magnetoptic recording materials and sensors of magnetic fields and the development of new structure such as granular films.

Magnetoresistance is the change in electrical resistance of a material in response to a magnetic field. All metals have an inherent, albeit small, magnetoresistance (MR) owing to the Lorentz force that a magnetic field exerts on moving electrons. However, metallic alloys containing atoms with net magnetic

moment can have an enhanced MR because the scattering that produces the electrical resistance is controlled by a magnetic field [Levry, Peter M., 1994].

Although earlier studies reported unusual magnetoresistive effects in layered structures [Sato et al, 1987; Velu et al, 1988], it was discovered in 1988 that the application of magnetic fields to atomically engineered materials known as magnetic superlattices, which are special form of multilayered structure, greatly reduced their electrical resistance [Baibich et al, 1988]; that is, the superlattices have a Giant Magnetoresistance (GMR) and this effect can revolutionize the recording and magnetic sensor industry.

2.2 Background and Theory

2.2.1 Giant Magnetoresistance in Metal Multilayer

There has been a great deal of interest in recent years in artificially engineered nanostructure materials with novel physical properties. One area of particular interest is that of metal multilayers. These materials have been studied for the past 30 years or more, but it is only relatively recently that detailed expertise has been developed to prepare and characterize the structure of such systems. These metal multilayers have attracted great interest largely because of the possibility of creating artificial materials with potentially new properties or new combinations of properties [Shinjo, T. and Takada, T., 1987; Schuller, I. K., 1988; Falicov et al, 1990a; Falicov et al, 1990b]. Magnetic multilayers are of particular interest because of the

importance of magnetic materials for many technological applications. The simplest form of such multilayer [Parkin, S. S. P., 1994] structure is comprised of alternating thin layers of magnetic and non-magnetic metal as shown in Figure 2.1.

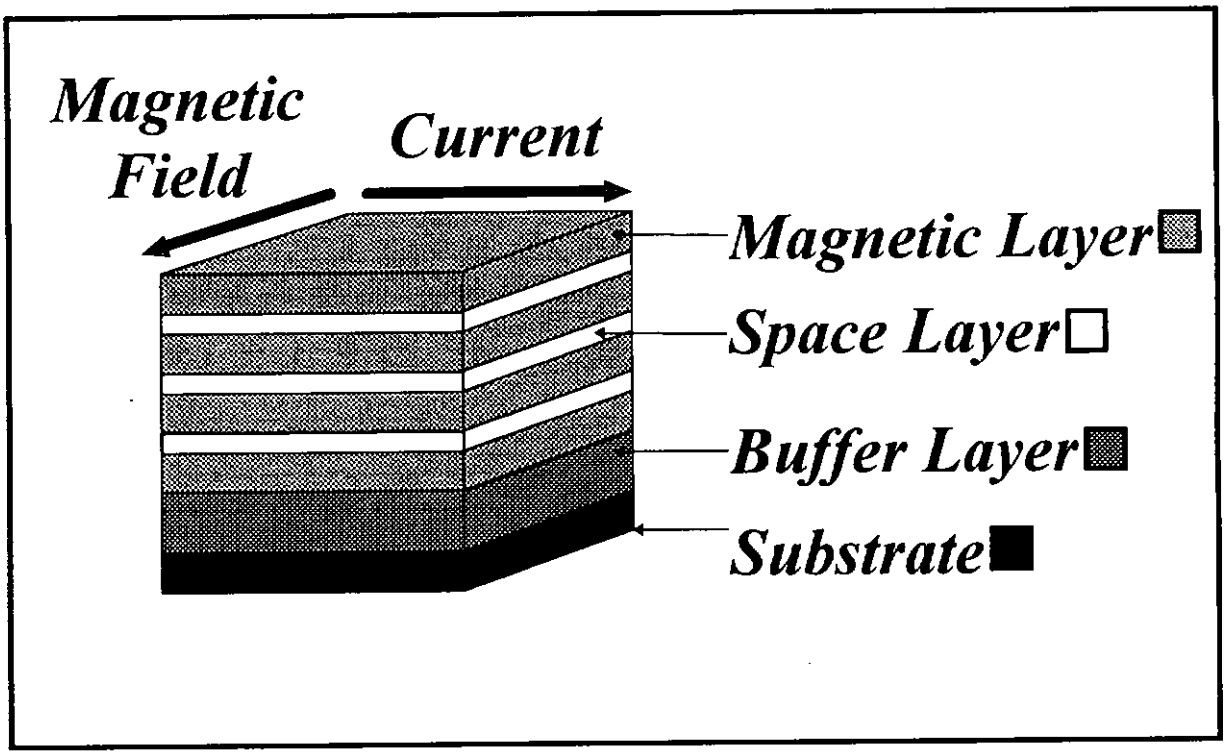

Figure 2.1 The schematic diagram of the multilayer structure.

The magnetic superlattice is formed by alternate layers of ferromagnetic transition metal layers (TM), usually iron and cobalt, and non-magnetic spacer layers, normally a non-magnetic transition metal or noble metals (NM). It would not be surprising, given the delocalized nature of metallic electrons that the magnetic layers would be magnetically coupled via the conduction electrons of the non-magnetic layers.

The magnetic moments of the neighbouring magnetic layers are usually aligned either in a parallel or an antiparallel direction, depending on the thickness of the spacer layer. However other configurations, for example, "90° coupling" with the neighbouring magnetic layers perpendicularly aligned, also occur. The coupling between magnetic layers is usually dominated by exchange coupling mediated by electrons in the spacer although under certain conditions, in particular with rough interfaces between layers, purely magnetic dipole and dipole interactions may play a role [Edwards, D. M., 1996].

It is found that the resistance of the multilayer structure to an electric current flowing parallel and perpendicular to the layer plane depends on the magnetic configuration. Besides, the antiparallel alignment of ferromagnetic layers in the absence of an applied magnetic field has been observed in these mutilayers. It is believed to be caused by an antiferromagnetic interlayer exchange coupling of the magnetic layers. The application of a sufficiently large magnetic field causes the magnetic moment to align parallel to each other. The MR is defined by

$$MR = \frac{\rho_{H=0} - \rho_{H=Hs}}{\rho_{\min}} \qquad (2.1)$$

where $\rho_{H=0}$ and $\rho_{H=Hs}$ are the resistivities in antiferromagnetic (AF) (without magnetic field) and ferromagnetic (FM) (with magnetic field) alignments of the magnetic layers, respectively. ρ_{min} is the minimum resistivity. For negative magnetoresistnace, ρ_{min} is $\rho_{H=0}$ and for positive magnetoresistance, ρ_{min} is $\rho_{H=Hs}$. Resistivity is lower in

the FM configuration, in which all magnetic moments are parallel, than in the AF one, in which the magnetic moment of neighboring layers are antiparallel.

An AF configuration can be changed by an applied magnetic field, attaining a FM configuration in a saturation field H_s, which is a measure of the AF exchange coupling [Zhang et al, 1996]. A schematic drawing is shown in Figure 2.2. The MR ratio can be as high as 220% [Schad, et al, 1994] and this sensitivity to applied field, known as GMR, can be exploited as a magnetic sensor, for example as a read head in magnetic recording.

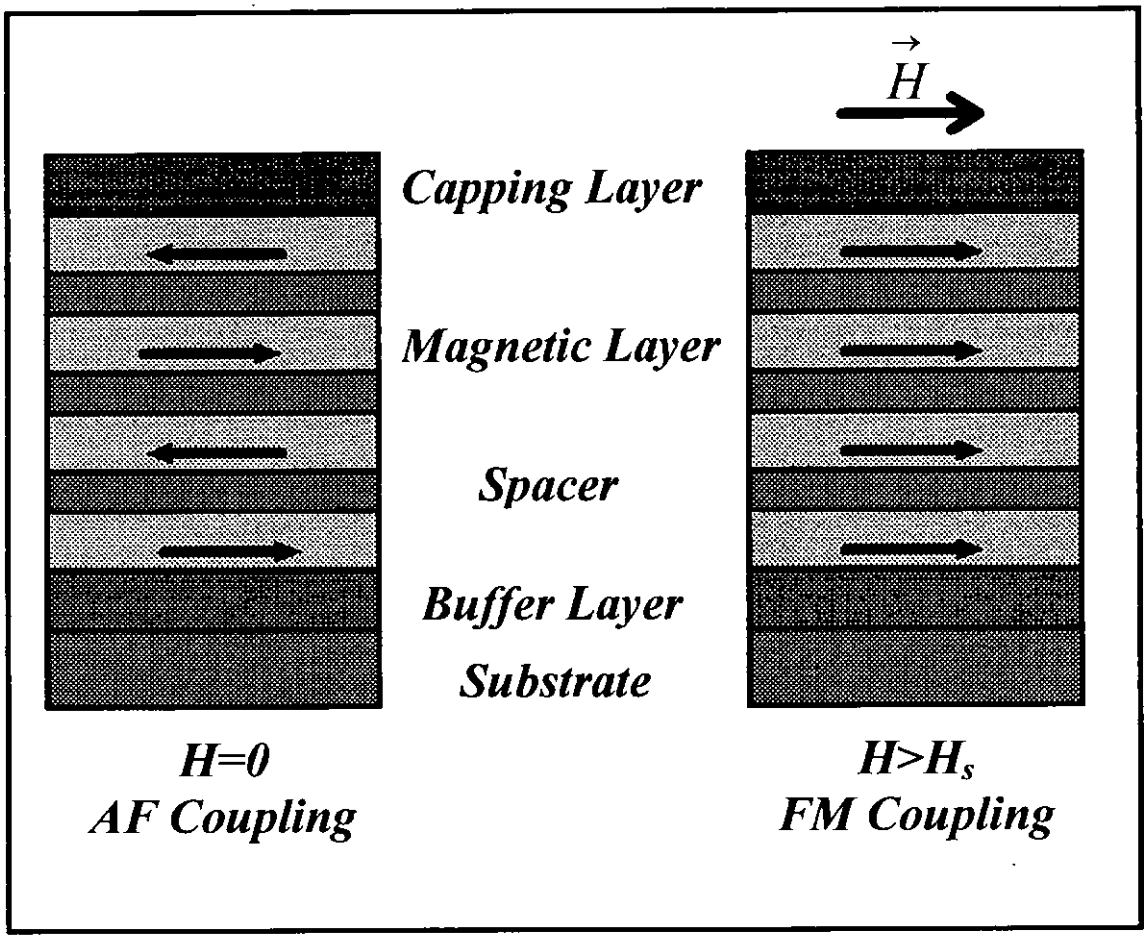

Figure 2.2 Antiferromagnetic coupling multilayer structure in H=0 and H>H_s

2.2.2 Oscillatory Coupling

Oscillation coupling is manifested as an oscillating exchange interaction, alternating between AF and FM coupling depending on the separation of magnetic layers. This coupling can be explained by the Ruderman-Kittel-Kasuya-Yosida (RKKY) interaction [White, R. M., 1983]], first proposed by Ruderman and Kittel [Ruderman, M. A. and Kittel, C.,1954] for the coupling between nuclear spins by the hyperfine contact interaction, and latter extended by Kasuya [Kasuya, T,1956] and Yosida [Yosida, K, 1957] to indirect coupling between electronic localized states through the s-d or s-f exchange interaction in the rare earth metals [Freeman, A. J.,1972; Coqblin, B., 1977].

The discovery of oscillations in the interlayer magnetic exchange coupling in multilayers comprised of thin ferromagnetic layer of Fe, Co, Ni and their various alloys separated by thin layers of virtually all the non-ferromagnetic transition and noble metals was reported by Parkin et al [Parkin et al , 1990; 1991a; 1991b; 1991c]. For example, the magnetic moments of successive magnetic layers in the Co/Cu mutilayer are arranged anti-parallel to one another in small fields. This is a consequence of an antiferromagnetic interlayer exchange coupling propagated through the intervening Cu layers. As the Cu layer thickness is varied the exchange coupling of the magnetic layers is found to vary in sign, oscillating back and forth between AF and FM coupling [Parkin et al , 1990; 1991a]. Since the coupling between magnetic layers changes with the thickness of the spacer layers, it exhibits an oscillation in magnitude of the GMR effect with increasing separation of the magnetic

layers. This was first observed in sputtered Fe/Cr and Co/Ru Multilayers [Parkin et al , 1990], and subsequently in transition metal multilayers grown by conventional sputter deposition techniques and only later in single crystalline multilayers prepared in ultra high vacuum (UHV) deposited systems using electron beam or thermal evaporation cells. Figure 2.3 shows results for a series of Co/Cu multilayers in which the magnitude of the saturation magnetoresistance is found to oscillate with increasing Cu spacer layer thickness with an oscillation period of ~ 0.9 nm. Large GMR values are found for Cu layer thickness for which the Co layers are coupled antiferromagnetic.

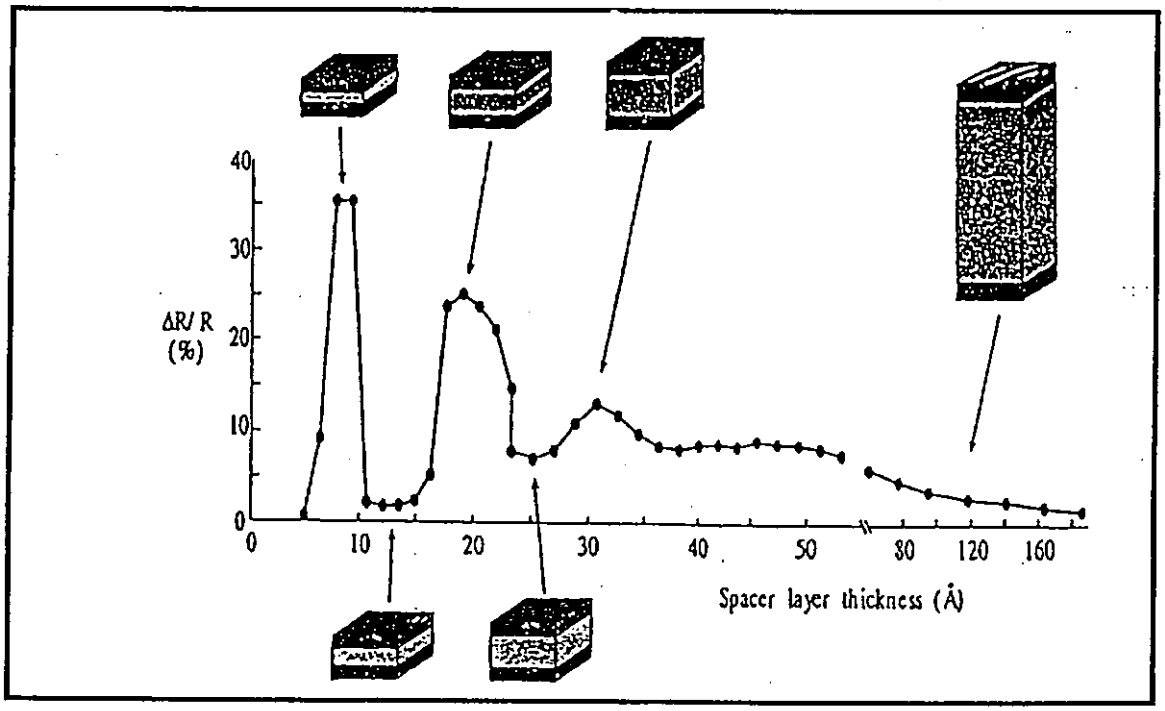

Figure 2.3 Room temperature saturation magnetoresistance vs Cu spacer layer thickness for a series of polycrystalline sputter-deposited Co/Cu multilayers. The magnetic state of the multilayer is shown schematically for various Cu layer thicknesses (only two magnetic layers are shown) [Parkin, et al, 1990].

2.2.3 The Origin of GMR

The theory of electron transport properties of thin metallic films is based on the Boltzman transport equation. The transport in thin film differs from in bulk metals because of the thickness of a thin film is comparable to the mean free path of the electrons. The classical Fuchs-Sondheimer theory described the interplay between film thickness (t) and the mean free path (λ) effects, leading to a relationship between the conductivity of a thin film σ_t and the bulk metal σ_b.

$$\frac{\sigma_t}{\sigma_b} \sim \frac{t}{\lambda(\ln\frac{\lambda}{t})} + const. \qquad for \quad \frac{t}{\lambda} << 1. \tag{2.2}$$

In order to understand the electron transport process in mutilayer thin film, one has to know the electron scattering first. The scattering mechanisms include all of the usual scattering mechanisms in metals, including scattering from impurities, structural defects, phonons and magnons, etc. The density of states at the Fermi level for the up-spin and down-spin d electron bands can be very different , particularly for the strong ferromagnetic metals such as Co and Ni. This means that the scattering rates into these states will be significantly different for the two conduction channels. Consequently this leads to the possibility of substantially different mean free path $\lambda^{\pm}$ and conductivities $\sigma^{\pm}$ in the two conduction channels.

A review of the theory of magnetic and transport properties of mutilayers is given by Fert [Fert, A., 1990]. A simple way to describe the GMR is via spin dependent electron scattering in magnetic layers, i.e. the scattering rates differ for majority (parallel to the field) and minority (antiparallel to the field) electrons [Fert et al, 1976]. In the FM coupled state, when the magnetic moments of all the layers are parallel, the scattering is weak in one spin channel, i.e. for electrons whose spin is parallel to the magnetization direction. A majority spin electron can move through the system without spin flip. However, the scattering of the electrons with spins opposite to the magnetization, is strong. Consequently the mean free path becomes short and the resistivity increases. Shunting by their weak scattering channel results in a small resistivity. In contrast, when the layers are coupled antiferromagnetically, the scattering is alternating between weak and strong for both spin-up and spin-down channels, and the resultant resistivity is higher. If, due to the strong scattering, the mean free path becomes shorter than the thickness of the layer, then the scattering in successive layers is decoupled and the GMR vanishes. In FM coupling the electrons can go through the system without spin flipping but in AF coupling the electrons are hard to go to the next magnetic layer due to the need of spin flipping. This model is illustrated in Figure 2.4, where F1 and F2 are magnetic layers and M is nonmagnetic layer.

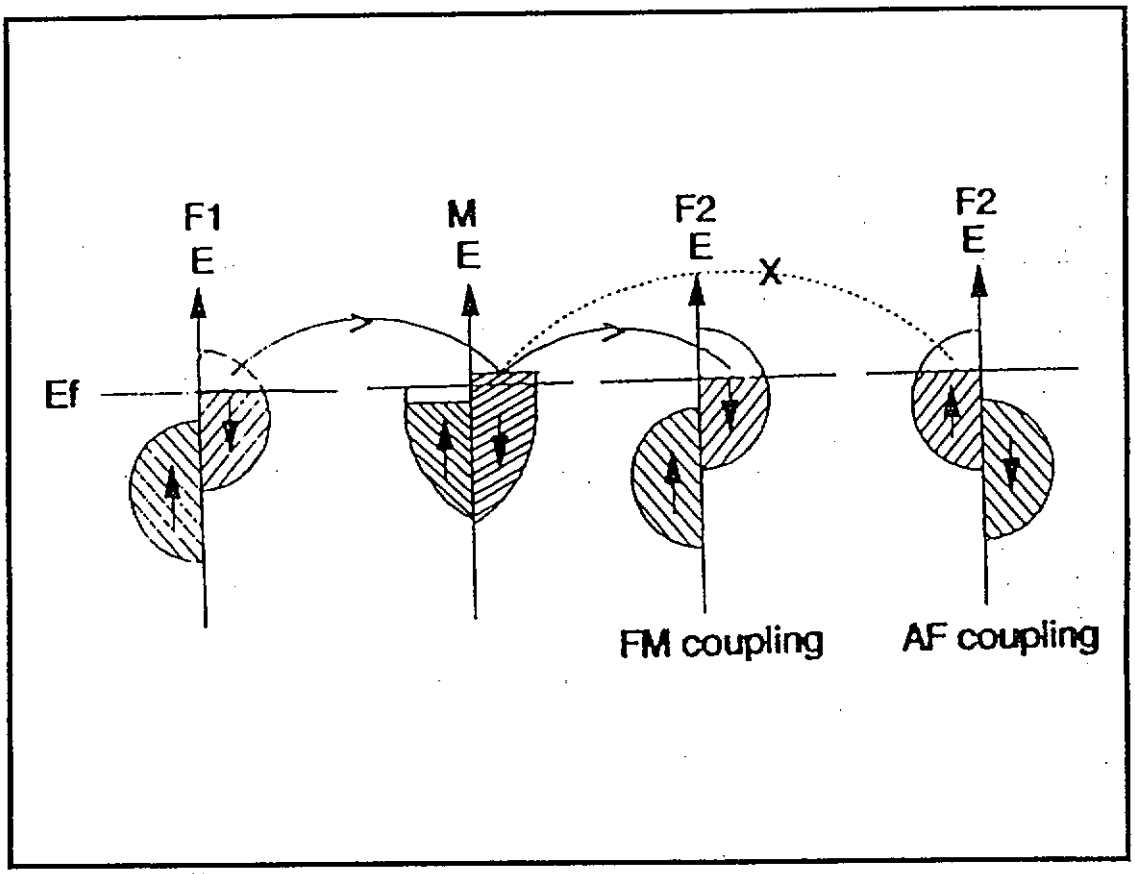

Figure 2.4 Origin of GMR: spin dependent electron scattering in FM coupling and AF coupling in multilayer, F1, F2 -magnetic layer, M - nonmagnetic metallic spacer, E_f -Fermi level.

The origin GMR effect can be explained by a simple resistance diagram shown in Figure 2.5. It has two spin conduction channels of spin up and spin down as mentioned above. Their spin scattering dependent are different in different magnetic moment states. Thus, the resistance of the two conduction channels of the two anti-parallel and parallel magnetic moment states (on the right hand side) can be represented by the resistance box diagrams (on left hand side). For parallel alignment, the scattering probabilities for the two spin channels are different so the

resistivities $\rho_\uparrow$ and $\rho_\downarrow$ are also different. Electron with spin direction as same as the magnetic moment can go through the sample and the current is shunted by this channel so a resistivity channel is formed. Then the total resistivity

$$\rho_{FM} = \frac{\rho_\uparrow \rho_\downarrow}{\rho_\uparrow + \rho_\downarrow} \tag{2.3}$$

is low. For anti-parallel alignment, the low resistivity electron in a layer becomes the high resistivity electron in next layer. Therefore, each channel has an average resistivity $(\rho_\uparrow + \rho_\downarrow)/2$ and the final resistivity

$$\rho_{AF} = \frac{\rho_\uparrow + \rho_\downarrow}{4} \tag{2.4}$$

is high.

By the MR definition (2.1)

$$MR = \frac{\rho_{AF} - \rho_{FM}}{\rho_{FM}}$$

$$= \frac{(\rho_\uparrow - \rho_\downarrow)^2}{4\rho_\uparrow \rho_\downarrow}$$

$$= \frac{(\alpha - 1)^2}{4\alpha} \tag{2.5}$$

with $\alpha = \rho_\uparrow / \rho_\downarrow$

if $|\alpha| >> 1$, MR can be very large.

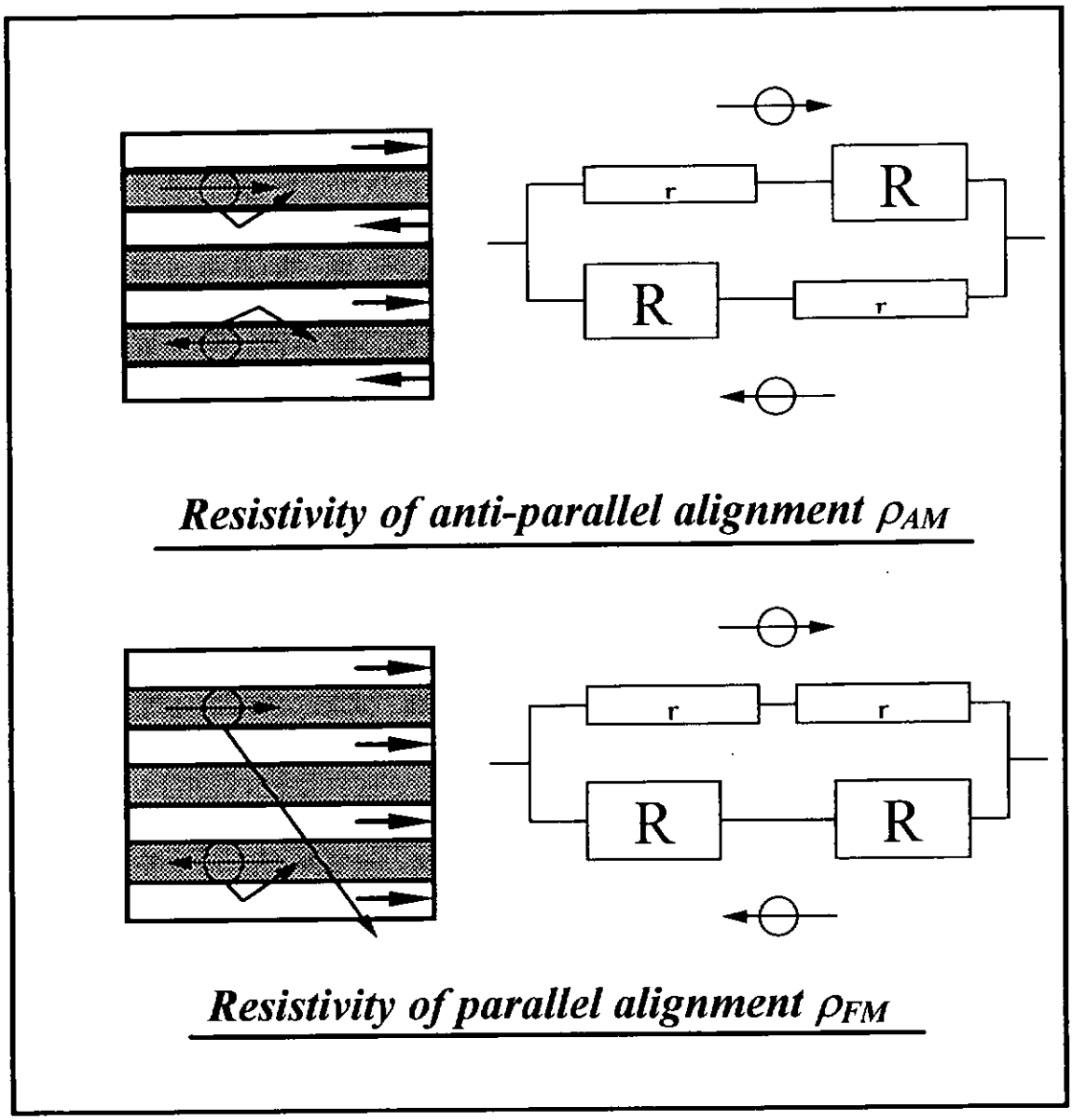

Figure 2.5 The schematic diagram of the resistance of the mutilayer film.

2.2.4 Giant Magnetoresistance in Metal Granular Film

A similar GMR effect to that found in magnetic mutilayers has recently been reported to occur in metal granular films. A schematic diagram of the structure of the class of GMR granular metals films is shown in Figure 2.6. In this case, nanometer size (essentially single domain) magnetic metal particles are embedded in an immiscible nonmagnetic metal matrix. At present, for these granular metals, there are two main categories, namely the silver system such as CoAg, FeAg, FeNiAg and FeCoAg, and the copper system such as CoCu, FeCu and FeCoCu.

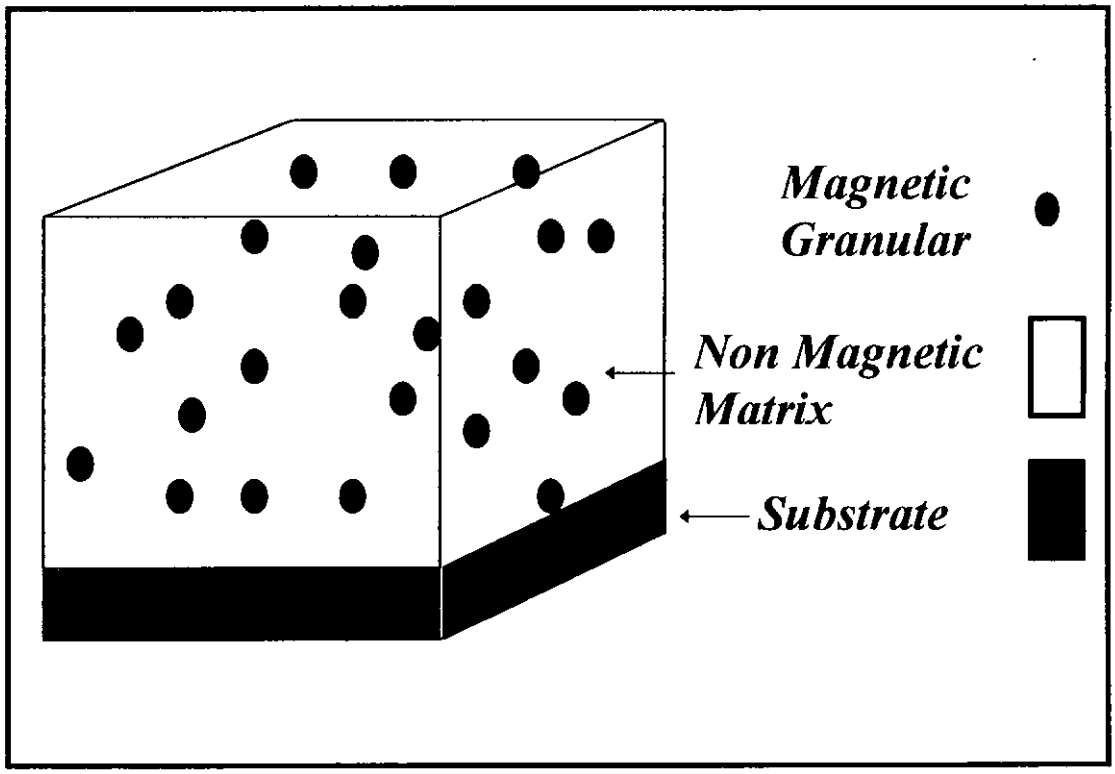

Figure 2.6 The schematic diagram of granular structure.

Figure 2.7 shows the granular structure with and without an external magnetic field. The essentially superparamagnetic, single domain magnetic entities, if their magnetization vectors are completely disordered in zero external magnetic field, have a zero magnetization - like the multilayers with AF coupling. Upon application of a magnetic field, the magnetization of the system increases toward a saturated paramagnetic state, analogous to the FM coupling in multilayers. The resistivity of the system is maximum at H=0. It decreases as the square of the magnetization in the external field, as described by the classical theories of the galvanomagnetic effects [Paradavi-Horvath, Martha, 1994a]. The saturation field for a superparamagnetic system at room temperature is quite high, on the order of tens of kG, and the GMR cannot be obtained easily. In reality, however, a quite substantial GMR effect is observed . As a consequence , GMR is expected to occur in magnetically inhomogeneous systems containing non-aligned, isolated ferromagnetic or superparamagnetic particles on a length scale of the mean free path, which is in the order of a 10 nanometer [Hathaway, K. B., 1994] . The larger the original misalignment of the particles, the larger is the GMR effect.

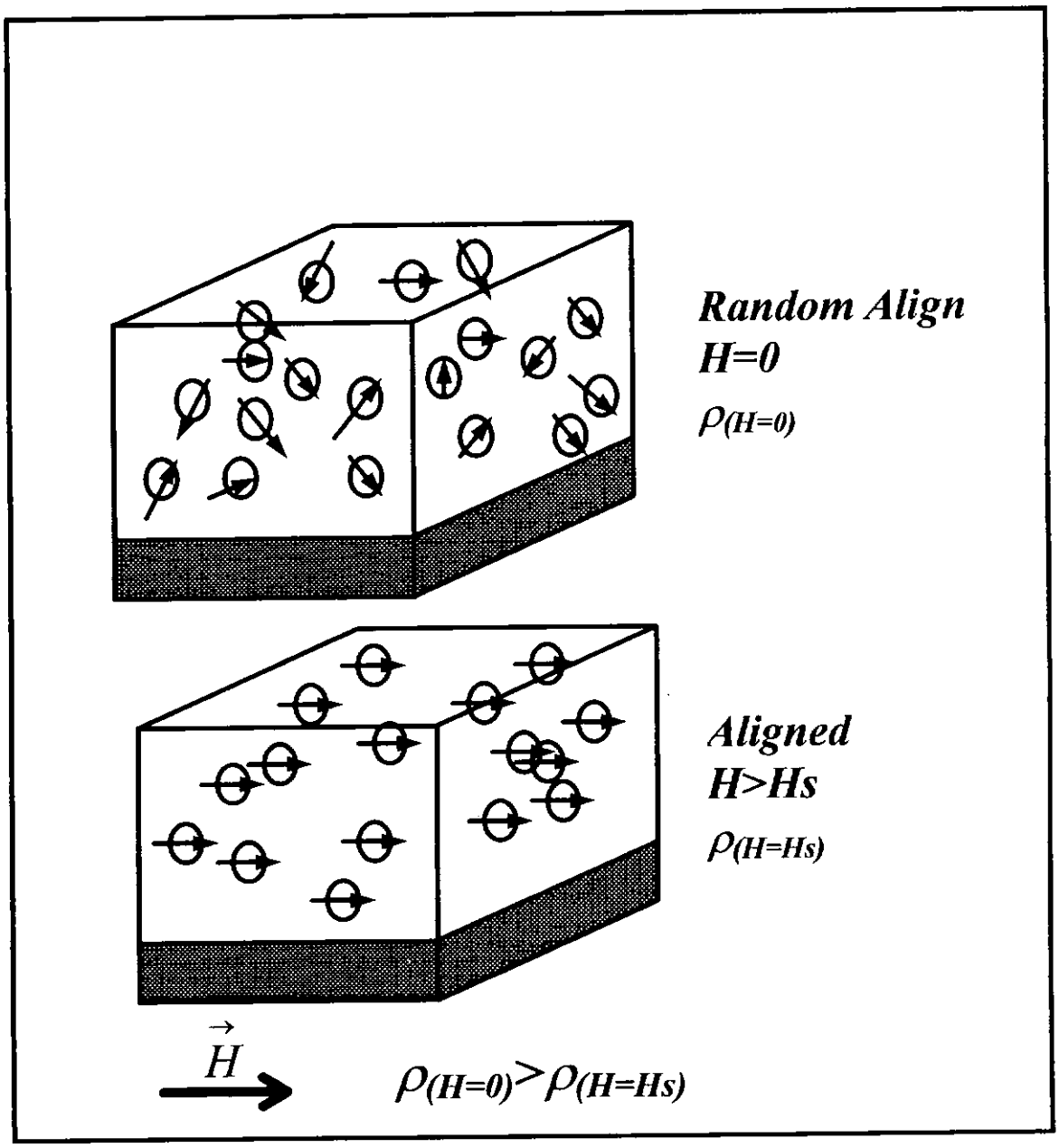

Figure 2.7 Magnetic alignment of granular film with and without a magnetic field.

2.2.5 Obtain GMR Mechanism

In order to observe the GMR effect, there has to be mechanism to induce the AF coupling between alternate layers in the multilayer structure . This can be achieved by several ways [Daughton, J. M., 1992] :

1) in AF coupled mutilayers, where the AF coupling can be overcome by an external field;
2) by making alternating layers with high and low coercivities, so that one of the magnetic moment can be reversed without reversing the other one [Chaiken et al, 1991];
3) by exchange coupling one of the two kinds of soft magnetic layers to a magnetically hard layer , thus allowing the direction of the magnetization of the other soft layer to be controlled relatively easily by the external magnetic field [Dieny et al, 1992];
4) by etching a magnetic sandwich in a way that when demagnetizing effects and currents through a bilayer strip orient the magnetization in an antiparallel direction, the external fields can orient it in parallel [Daughton, J. M., 1991]

Systems based on method 2) and 3) are called Spin Valves (SV) [Pardavi-Horvath, Martha, 1994b].

In our studies only 1) is used. However, there should be no particular difficulties in using the rest mechanisms if other appropriate material system are selected.

2.2.6 Positive Magnetoresistance

The giant magnetoresistance of multilayer and granular structures are always negative and this negative magnetoresistance NMR effect can be attributed to the change of spin configuration from anti-ferromagnetic to ferromagnetic coupling. The positive magnetoresistance PMR, on the other hand, has been scarcely reported. Small positive magnetoresistance, of about 0.03% under 1 Tesla magnetic field at 1.55K, in binary and ternary metallic glasses [Lindqvist et al, 1989] such as CaAl(Au) [Howson, M. A.,1985], YAl [Olivier, M.,1986], CuTi [Fritsch et al, 1987], VSi [Ousset et al, 1987] and LuPd [Poon et al, 1985] have been demonstrated. The effect can be explained within the theories of weak localization and electron-electron interaction effect [Al'tshuler et al, 1984; Lee et al, 1985]. Dy/Sc superlattices [Tsui et al, 1994] have also been observed to show a small PMR effect due to the interfacial reflectivity and this effect are also small. More recently, a PMR of +30% under a magnetic field of 5 T and at 10 K has been obtained in Co/Cr supperlattices with Mo buffer layers [Huang et al, 1996]. In our study, we found that Ti films grown on Si substrate by PLD produce large PMR effect even at room temperature. A detailed of this work will be presented in Chapter 7.

Chapter 3

Pulsed Laser Deposition (PLD)

3.1 History of Pulsed Laser Deposition

The first high power ruby laser was demonstrated in 1960 by T. H. Maiman at the Hughes Research Laboratories [Maiman, 1960]. Immediately afterwards, a lot of theoretical and experimental studies on the intense laser beam interaction with solid surfaces [Ready, 1963; White, 1963], liquids [Askar'yan et al., 1963], and gaseous materials [Meyerand, and Haughty, 1963] have been reported. The ease with material being vaporized suggested that the intense laser radiation could be used to deposit thin films. This idea was quickly picked up and demonstrated a few years later [Smith and Turner, 1965]. However, the development and investigations of pulsed laser deposition did not gather the expected momentum. At that time the laser technology was immature. The types of laser were limited and the laser repetition rate was too low for any realistic film grow processes. Thus PLD was inferior in comparison with other methods technologies, such as sputtering to produce high quality films.

The rapid progress of the laser technology, such as the CO_2 lasers [Hass and Ramsey, 1969; Bykovskii et al., 1978; Cali et al., 1976] and the Nd: Glass lasers [Schwarz and Tourtellotte, 1968], however, enhanced the competitiveness of PLD. These lasers have a higher repetition rate than the early ruby lasers, making the thin

film growth possible. In 1970s, there were two major improving elements for PLD. Firstly, reliable electronic Q-switches became available for generation of very shot optical pulses to attain peak powers exceeding 10^8 W/cm^2. Thus material that absorbs laser radiation of this power level, will be transformed to form a plasma. In other words, PLD can be used to vaporize and to deposit thin films of any material if the absorbed laser power density is high enough. Besides, the use of short laser pulses for ablation is more likely to achieve congruent ablation that allows PLD to preserve stoichiometry during mass transfer from the target to the thin film. The second significant technical advance was the development of a high-efficiency second harmonic generator to deliver shorter wavelength radiation. Therefore, the absorption depth is shallower and the splashing is reduced. In addition, a smaller heated volume also favors congruent evaporation. Together, these two developments allow a wide selection of ablation target materials and an improved film quality.

The other major breakthrough, which was triggered by the successful growth of high-temperature *Tc* superconducting films in 1987, that literally lifted PLD off the ground. The success of in situ growth of these oxide films by PLD brought an overwhelming interest to this field [Dijkkamp et al., 1987]. Although the first PLD growth of perovskite-type oxides was demonstrated in 1983 [Zeitsev-Zotov et al., 1983], the process was perfected by the Bellcore group, which provided the catalyst that initiated an explosive growth in PLD. This deposition technique allows the fabrication of many different thin films such as superconductor, ferroelectric, metallic

oxide, metal, metallic multilayers, and various supperlattices. Accordingly, the total number of publications in PLD has rocketed since 1987.

The latest trends in PLD development include the heteroepitaxy of ceramic on semiconductors such as YSZ/Si [Fork et al., 1990], MgO/GaAs [Change et al., 1992; Fork et al., 1992; Prusseit et al., 1992] and STO/TiN/Si [Leung, Y. S., 1998]. This area has found successes in research unmatched by any other techniques. It opens up a new frontier of material research by providing the possibility of new devices based on the integration of semiconductors and oxides. The growth of ferroelectric perovskite oxide films is another area showing potential promise [Ramesh et al., 1990; Horwitz et al., 1991]. The growth of perovskite ferroelectric films is a natural extension of the work on high *Tc* oxide superconductors because of the structural similarity between these two materials. These layers can be grown by PLD in situ without high-temperature post annealing. Therefore, epitaxial multilayer structures can be grown by incorporating matching electrodes to improve the performance endurance of the devices subjected to repetitive cycling. Nitrides are another material system that researchers have attempted to grow by PLD. Epitaxial layers of TiN have been grown by PLD on (100) Si substrate [Narayan et al., 1992; Leung, Y. S., 1998]. Some other nitrides, AlN [Norton et al., 1991] and BN [Doll et al., 1991] are still difficult to grow especially due to the inactivity of nitrogen. This problem can be solved by a hybrid approach using a plasma-excited nitrogen source combined with PLD. PLD can also be applied to deposit diamond-like-carbon using a graphite target [Rengan and Narayan, 1992]. Some new ideas of using PLD are applied to the synthesis of buckminster fullerenes (i.e., C60) [Curl and Smalley, 1991] and

nanopowders and they are gaining recognition. Production-related issues concerning reproducibility [Cheung et al., 1992], large-area scale-up [Greer and Van Hook, 1990], and multiple-level devices have also begun to be addressed. It is the dawn of a new age of PLD.

3.2 Advantages and Disadvantages of PLD

There are numerous physical deposition methods to produce thin films such as dc. and r.f. magnetron sputtering [Lee et al., 1988 and Humphreys et al., 1989], thermal evaporation, electron-beam or ion-beam sputtering [R. F. Bunshsh., 1982], molecular beam epitaxy (MBE) [E. H. C. Parker., 1986]. However, PLD have many advantages over another techniques. For example, in using PLD method one can easily change the targets in situ during the deposition of films. This is enormously useful in fabrication of multilayers such as metallic multilayered thin films having giant magnetoresistance (GMR) properties. In addition, film thickness control down to atomic level is simple in PLD. Essentially the minimum deposition is governed by a single shot of laser ablation, which quite often yields a less than an atomic layer film. By increasing the laser repetition rate one can achieve very high deposition rate so that the film growth time can be shorten. Other advantageous features of PLD include with the use of small targets, in contrast to the large size targets required for sputtering. In addition, the highly energetic ablated species can have beneficial effects for certain film properties. For example, epitaxial films can be deposited at a relatively lower substrate temperatures.

Conceptually and experimentally, PLD is extremely simple, probably the simplest among all thin film growth techniques. A schematic diagram of PLD is shown in Figure 3.1. The decoupling of the evaporation power source makes this technique so flexible that it is easily adaptable to different operational modes without the constraints imposed by the use of internally powered evaporation source. Film growth can be carried out in a reactive environment containing different kind of gas. In a hybrid approach, PLD can be also operated simultaneously with other types of evaporation sources.

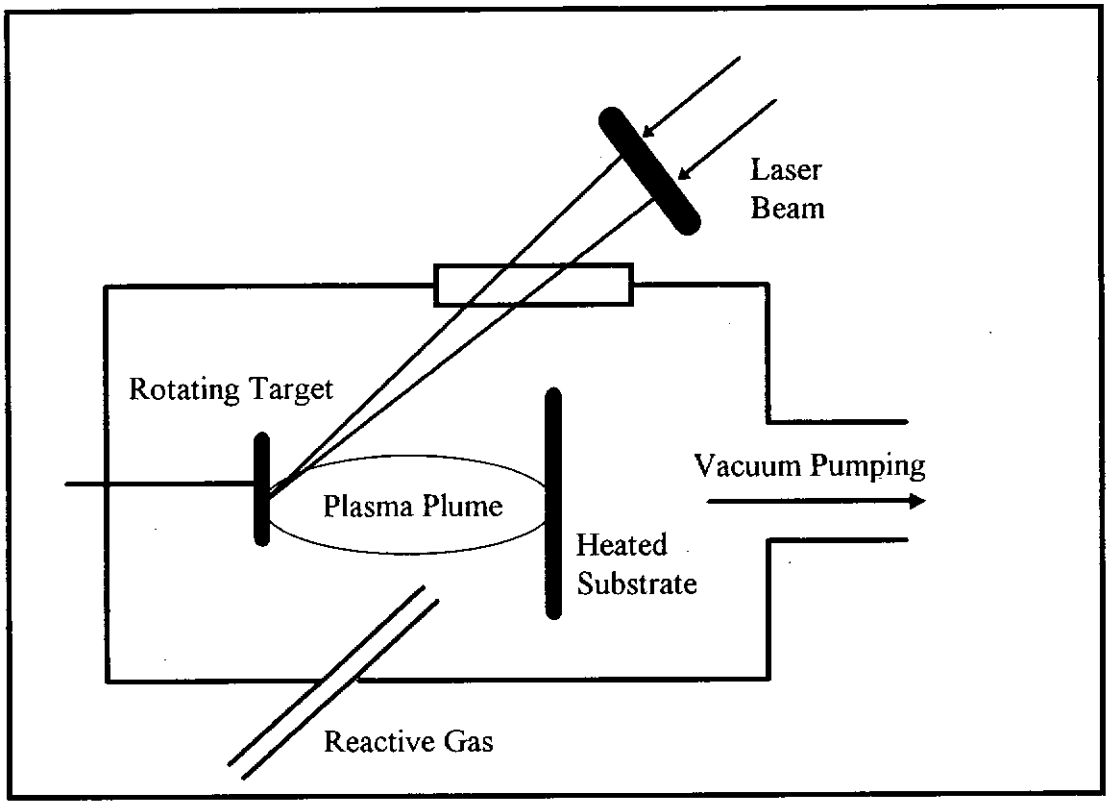

Figure 3.1 Schematic diagram of a pulsed laser deposition apparatus.

In contrast to the simplicity of the hardware, the laser-target interaction is a very complex physical phenomenon. The mechanism that leads to materials ablation depends on the laser characteristics, as well as the optical, topological, and thermodynamical properties of the target. When the laser is absorbed by a solid surface, electromagnetic energy is converted first into electronic excitation and then into thermal, chemical, and even mechanical energy to cause evaporation, ablation, excitation, plasma formation, and exfoliation. Evaporants form a "plume" consisting of a mixture of energetic species including atoms, molecules, electrons, ions, cluster, micro-sized solid particulates, and molten globules. The collision dominated mean free path inside the dense plume rapidly expands into the vacuum from the target surface to form a nozzle jet with hydrodynamic flow characteristics. This process attributes to many advantages as well as disadvantages. The advantages are flexibility, fast response, energetic evaporants and congruent evaporation.

On the other hand, there are disadvantages in using PLD method to deposit thin films. PLD films often carry large particulates and globules formed from the ablation process. The size of particulates can be as large as a few microns. For the multilayer films, these large particulates adhered on the surface of every layer and it will greatly affect the growth of the coming layer as well as the electrical and magnetic properties of the films. This intrinsic problem, however, can be eliminated by shadow mask deposition [Iwabuchi et al., 1994], in which an opaque mask is inserted between the target and the substrate to block off the large particulates emitted from the target in the forward direction. Particulate free thin films with smooth and clean surface can be obtained [Wu et al, 1997]. The non-uniformity of the film's thickness remains an

acute problem in PLD process. Due to hydrodynamic flow of the plasma plume in vacuum, the film thickness is highest at the center of the plasma plume normally to the target surface. It decreases rapidly with the distance away from this point [Venkatesan, 1998]. This feature will limit the use of PLD in producing a large uniform area thin films. There are, however, techniques to tackle this problem. For example, by tilting and rotating the target, a much larger scanning area of the plasma plume to the substrates so that the uniformity area of the film can be enlarged.

3.3 Review on PLD of GMR Granular and Multilayer Films

Usually the change in resistance of metal films with the application of a magnetic field is very small. However, in 1988, the GMR was first discovered in the magnetic (100) oriented Fe/Cr multilayers. The resistance of the multilayers was found to decrease by almost a factor of two when a field of ~20 KOe was applied at low temperature (4.2 K) [Baibich et al, 1988]. The film was prepared by molecular beam epitaxy (MBE), which is a very sophisticated and expensive ultra high vacuum deposition technique.

To date the largest GMR effects measured at room temperature, is about 70% for a field of 10 KOe applied orthogonal to the current in the plane of the layers, in polycrystalline Co/Cu multilayers system. For polycrystalline Fe/Cr mutilayers it is 25% at 25 KOe. However, higher GMR values have been reported in single crystalline (100) Fe/Cr multilayers. GMR values exceeding 150% at 4.2 K have been found in magnetron sputtered samples [Fullertton et al, 1993] and a value of more

than 220% at 1.5 K have been reported recently in MBE deposited multilayers [Schad et al, 1994].

In fact, there are many potential mutilayer compositions and structures other than those mentioned above that exhibit strong GMR effect. For example granular structures, in which the ferromagnetic particles embedded in nonmagnetic metallic matrix have also shown prominent GMR effect. Typical material systems are CoAg, CoCu and FeAg granular films deposited by magnetron sputtering [Xiao et al, 1992].

Pulsed Laser Deposition (PLD) technique has been , in recent years, extensively and successfully used to fabricate ceramic oxide films. However, PLD of metallic multilayer and granular film has scarcely been reported in open literature. In 1993, Enrech, M et al produced Co/Pd metallic mutilayers thin films by PLD. They have characterized the transport and magnetic properties of the films [Enrech et al, 1993]. Ferromagnetic resonance and GMR studies of CoCu granular materials fabricated by PLD has also been reported in 1994 [Rubinstein et al, 1994]. Only two research groups have studied the CoAg granular thin film by PLD method. Dupuis et al reported a maximum of MR ratio of 12% at 4.2 K for granular films having 25 atomic % of Co-clusters content embedded in the Ag matrix [Dupuis et al, 1996]. Wei Zhang et al studied the phase segregation and giant magnetoresistance behavior in as-deposited Co-Ag film grown on Si by PLD. Their main motivations for applying PLD to produce granular thin films are that PLD usually proceeds congruently, so that the composition of the ablation-induced plasma is very close to that of the target material. It thus provides an easy and convenient path in controlling

the composition of the thin film grown. PLD is also associated with very high quenching and deposition rates. These latter properties in particular introduce the possibility for producing phase segregation in the as-deposited films, unlike in, e.g. sputtering, where a post-annealing step is normally required for the formation of segregation phases. Therefore in order to enhance the phase segregation and to produce larger magnetoresistance characteristics, PLD is the preferred route. The largest magnetoresistance ratio for PLD granular films is 27% measured at 4.2K under a magnetic field of 4.7 T [Zhang et al, 1997].

In this project, we emphasis the use of PLD with a rotating split targets arrangement to prepare metallic multilayers and granular films. The rotating split target arrangement has made the fabrication process easy and quickly. The studies of varying the deposition conditions to grow Co, Ag and CoAg thin films on Si substrate will be described. Structural and surface morphology of the films will be examined by SEM and AFM. MR ratio of different samples will also be presented and discussed.

Chapter 4

Experimental Set-up and Procedures

4.1 Instruments

4.1.1 PLD System

4.1.1.1 Excimer Laser

We have used a Xenon Chloride (XeCl) excimer laser (Lumonic TE-860-4) and a Krypton Fluoride (KrF) excimer laser (Lamda Physik Compex 205) to deposit different thin films. For the XeCl excimer laser, the excimer molecules are formed in a gaseous mixture of their component gases of Xe, HCl and Ne. The total gas pressure of the laser chamber is 60 psi (1 psi = 51.7151 Torr) with of 40 Torr Xe, 60 Torr HCl and the remaining gas pressure balanced by Ne. For the KrF excimer laser, the gases used are F_2, Kr , He and Ne. The total gas pressure of the laser chamber is 3400 mBar (1 Bar = 750.06 Torr) where the partial pressure of F_2 is 4 mBar, Kr is 130 mBar, He is 56 mBar and Ne is 3210 mBar. The ionic and electronically excited species are created by the avalanche electric discharge excitation (about 40 kV). Then the excited species react chemically to produce the excimer molecules, of which the ground state is repulsive and tends to dissociate rapidly. The wavelength of the emitted light is 308 nm for XeCl and 248 nm for KrF. The maximum energy of XeCl laser is about 100 mJ per pulse for a pulse duration of ~12 ns. The KrF laser, on the other hand, can deliver up to 600 mJ in a 25 ns pulse duration.

4.1.1.2 Vacuum System and Deposition Chamber

We have used two experimental vacuum chambers for the deposition of different thin films. One chamber of a volume of ~ 10 litres was evacuated by a system comprised of a rotary roughing pump and a diffusion pump. The base pressure achieved was about 1×10^{-5} Torr. It was measured by an ionization gauge (Type WI-T), which was controlled by an ionization vacuum gauge controller (GI-TL3). The other chamber with a volume of ~ 5 litres was evacuated by a turbo molecular pump (UTM50) and a rotary roughing pump. The ultimate vacuum was about 4×10^{-6} torr in a normal working condition.

Figures 4.1 and 4.2 show the schematic diagrams of the vacuum chambers. Apart from the size, shape and orientation of target, both chambers have similar fixtures and attachments. The axis of the rotating target is along the target-substrate direction in larger chamber and perpendicular to the target-substrate direction in the other chamber. A viewing port at the top of the chamber was for in-situ visual inspection and target alignment. The laser port consisted of a fused silica window. It allowed the laser beam to enter the chamber to ablate the target surface.

At the substrate heater port, there was an electrical feedthrough for the K-type thermocouple connection and a pair of copper conducting wire for supplying the heater power. The heater was made of stainless steel and it was heat-shielded by two thin plates of stainless steel wrapped around the side. The heating filament was a Kanthal wire (25% chromium, 5% aluminium, 3% coblat and 67% iron) curled around the inside of the heating block. The diameter of the Kanthal wire was 0.559 mm and the resistance per unit length was 5.1 Ωm^{-1}. A total resistance of the

Kanthal wire used was 15 Ω. A K-type (Nickel-Chromium, Nickel-Aluminium) thermocouple was inserted into the heating block for measuring the substrate temperature. The temperature was controlled by a temperature controller (PAC25-0321) that can conveniently keep the substrate temperature between room temperature and 750 °C with an accuracy of ± 1.0 °C. Quick drying silver paint (G3691) was used to adhere the substrates onto the top of the heater and to provide a good thermal contact between the heating block and the substrates.

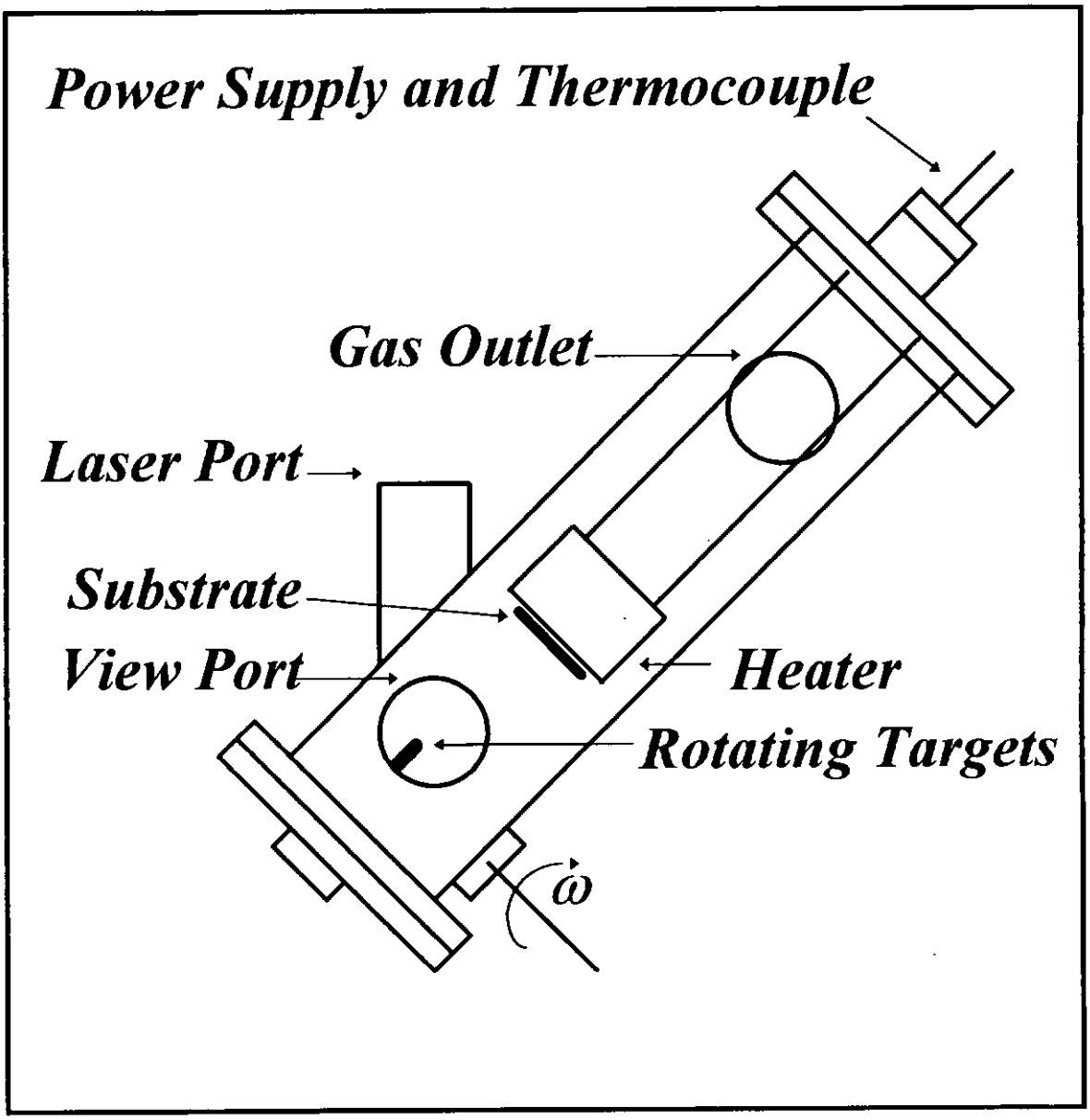

Figure 4.1 The schematic diagram of the 5 litres vacuum chamber.

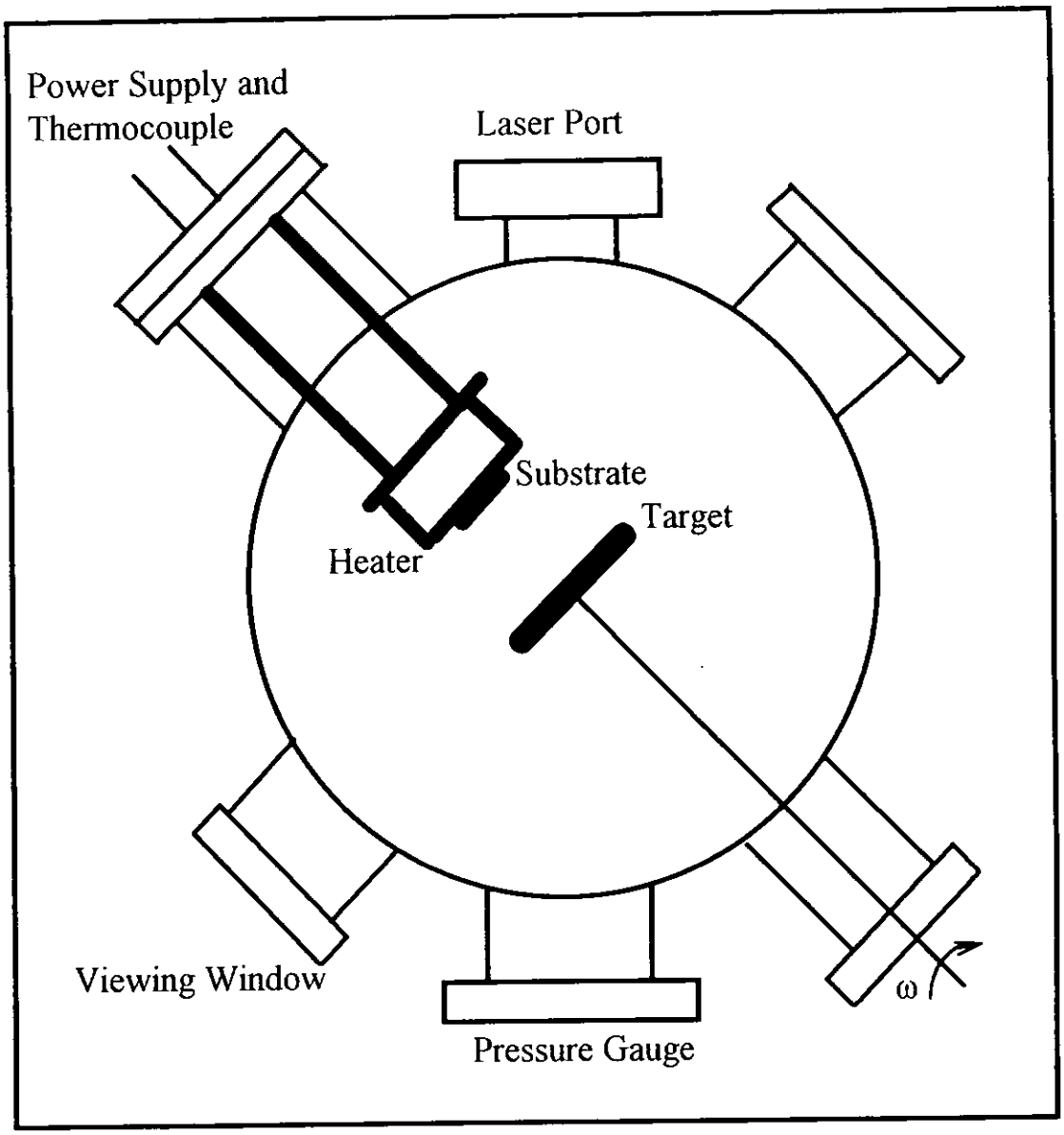

Figure 4.2 The schematic diagram of the 10 litres vacuum chamber.

4.1.1.3 Target Holders

Two target holders and target arrangements were used. They are depicted in Figures 4.3 and 4.4. The rotating multiple target holder configuration has been developed by us for in situ deposition of multilayer thin films of different materials. Laser is directed through the chamber window to irradiate on the rim of the rotating

target at 45° to rotating axis. The film thickness is controlled by the number of laser shot used. After the deposition of one layer the shraft is shifted to a pre-defined position such that the laser ablates a different target. In this manner we can deposit layers of many different materials in succession without breaking the vacuum.

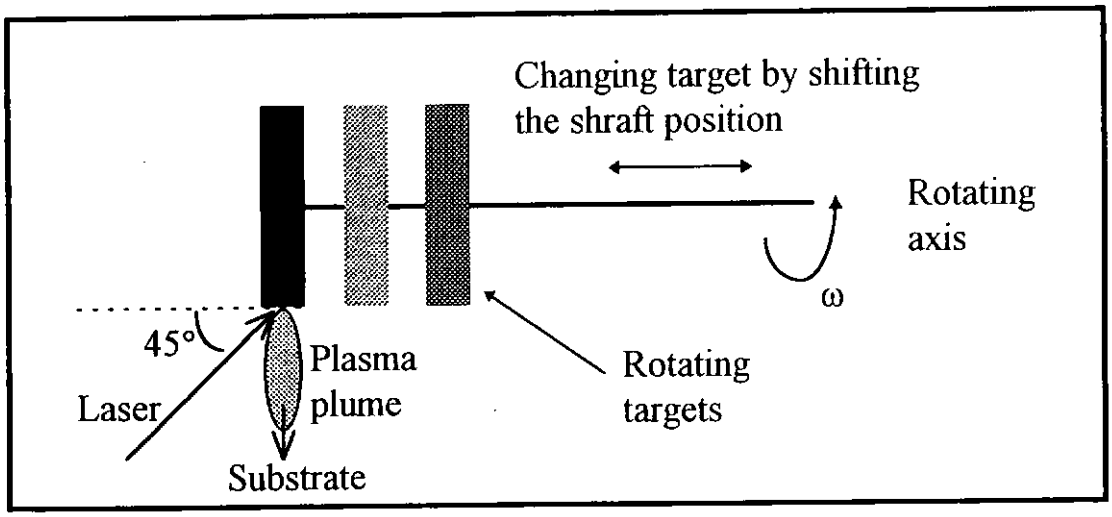

Figure 4.3 The schematic diagram of rotating multiple targets holder.

The split target arrangement has also been developed by us. It allows us to fabricate multilayer and granular thin film of various composition ratio very easily. Two half-circle of different material targets are put together to form a single split target. Thickness and composition of the deposited films can be conveniently varied at will by changing the relative laser ablated track lengths on the split targets. This in turns can be achieved by making use of the off centre rotation illustrated in Figure 4.4.

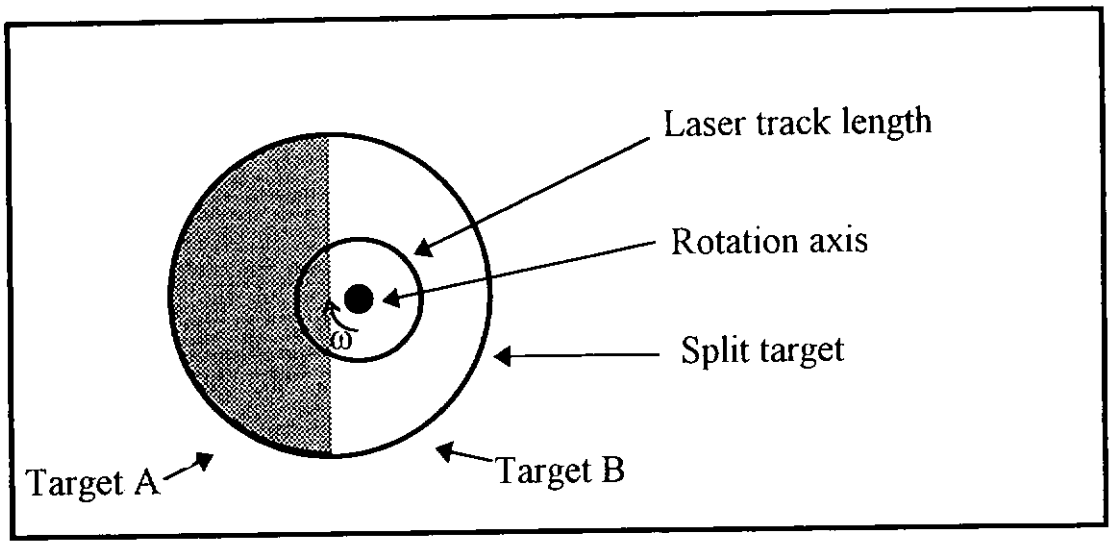

Figure 4.4 The schematic diagram of split target.

During the deposition, the target was rotated by a d.c. magnet motor (RS part no.: 2511G-244). The targets were kept rotating in order to avoid pitting on the target surface. A more detailed description on the working principle of split targets and results will be presented in Chapter 5.

4.1.2 X-ray Diffractometer (XRD)

The crystalline structures of the thin films were characterized by using an X-ray diffractometer (Philip mode X'pert system) operated in four-circle mode. The CuK_α radiation of $\lambda = 0.154$ nm was used. The K_β line was filtered off by a Ni filter. Figure 4.5 shows the schematic diagram of Bragg diffraction of a crystal. When X-rays fall on atoms in the crystal lattice, each atom scatters a small fraction of the incident beam. Thus, the reflected beams from all atoms in the crystal planes

involved may interfere and the resultant reflected beam is only strong if the path difference from successive planes is a whole number of wavelength of the incident X-ray radiation. Thus, reinforcement only occurs for planes p and q when AB + BC = $n\lambda$ where n is an integer and λ is the wavelength of the X-rays. If d is the distance between planes of the atoms and θ is the angle between the X-rays beam and the crystal plane, then AB + BC = 2d sinθ and the reflect beam has maximum intensity when

$$2d\sin\theta = n\lambda \text{ (Bragg's Law)} \tag{4.1}$$

and the d value was calculated as:

$$d = \frac{a}{\sqrt{(h^2 + k^2 + l^2)}} \tag{4.2}$$

where a is the lattice constant of the crystal structure and h, k and l are the reciprocal lattice indices for a-axis, b-axis and c-axis respectively.

For example, to calculate the 2θ angle of Si(400):

a = 0.543 nm for Si(100),

λ = 0.154 nm for K_α radiation of Cu in X-ray,

then $d = \frac{0.543}{\sqrt{4^2 + 0 + 0}}\ nm = 0.13575\ nm$

hence, 2θ = 69.11°

We have used only one X-ray scanning mode, namely the θ-2θ for the characterization of the crystal structure of the thin film. Figure 4.6 shows the simple working diagram of the θ-2θ X-rays scan. For a fixed X-rays emitter, when the sample rotates θ degree, the receiver will also rotates twice as much simultaneously. For this scanning mode, it is commonly used to determine the crystal phase formation with the orientation normal to the substrate surface. We used this technique to study the phase aggregate of the thin films.

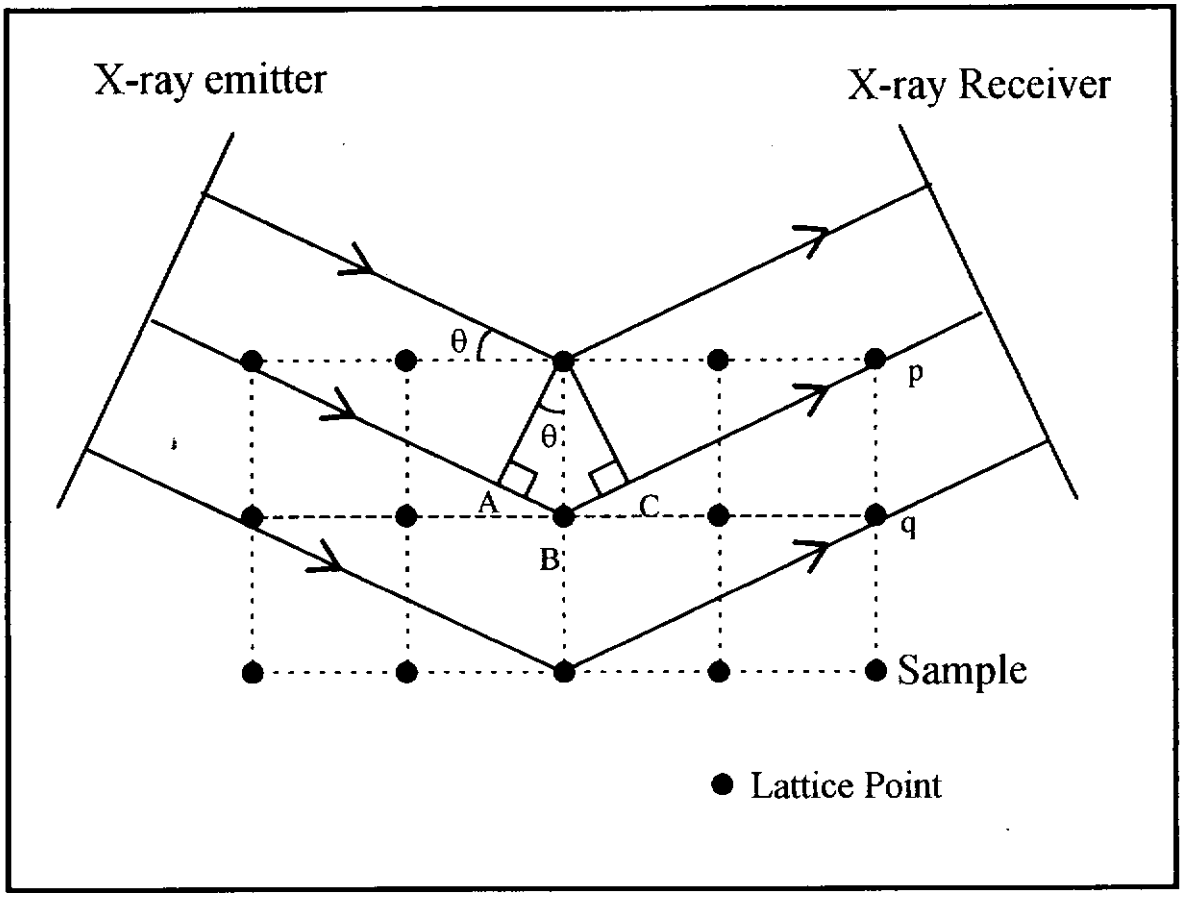

Figure 4.5 The schematic diagram of X-ray diffraction of a crystal.

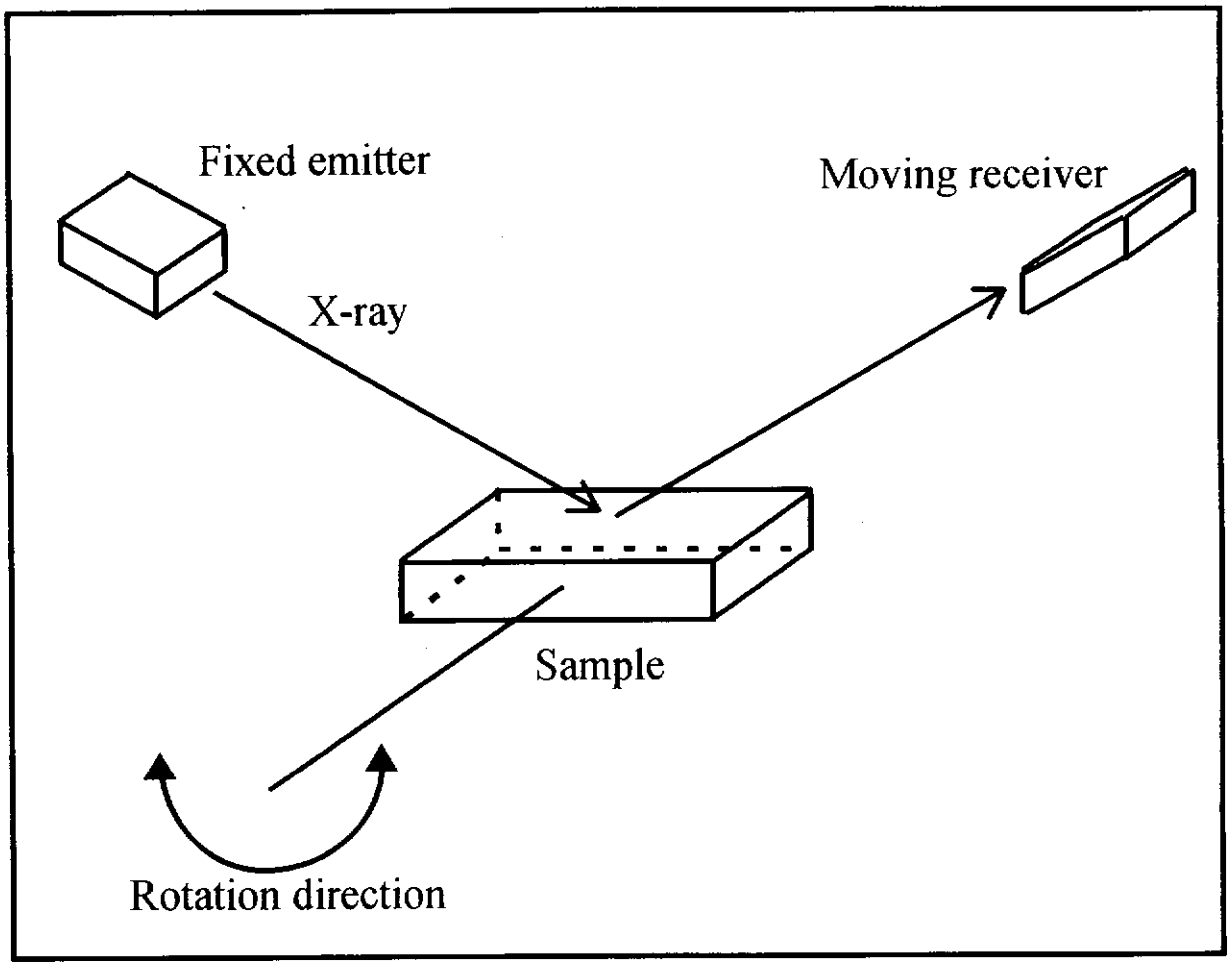

Figure 4.6 The rotation axis of the sample relative to the X-ray emitter and receiver.

The crystal size of the film can also determinate by the XRD. As the principle of XRD is the path different between two adjacent atomic planes, a strong signal can only be obtained at Bragg's angle. With other incident angle , other plane of the crystallites were involved. The reflective beam of X-rays of these planes cancel each other . However, as the particle size decreases, the number of atomic plane decreases, then not all the reflected rays are canceled. Therefore, peak broaden can occur. This is called the particle size effect of peak broadening. The crystallite size broadening (β_τ) of a peak can be written in terms of the mean crystallite dimension (τ) using the Scherrer equation [Jenkins, Ron and Snyder, Robert L., 1996]

$$\tau = \frac{K\lambda}{\beta_\tau \cos\theta} \qquad (4.3)$$

where β_τ is the line broadening due to the effect of small crystallites. β_τ is given by (B-b), where B is the breadth of the observed diffraction line at full width half maximum (FWHM), and b is the instrumental broadening or breadth of a peak from a specimen that exhibits no broadening beyond inherent instrumental peak width. Note that β_τ must be given in radians; K is the shape factor, which usually takes a value of about 0.9. Then equation (4.3) becomes

$$\tau = \frac{0.89\lambda}{(B-b)\cos\theta} \qquad (4.4)$$

If the equipment setting is suitable, crystallite sizes as small as 1 nm can be measured.

4.1.3 Alpha-step

Alpha-step surface profiler (Tencor Instruments, mode 1500) was used to determine the thickness of the thin film. The resolution of this instrument is 1 nm. For these measurement, a sharp edge in the film is needed. Therefore, during deposition of the film, a small piece of silicon wafer acting as a mark was placed on substrate to produce a sharp film edge. When the alpha-step needle moves on the surface of the film and meet the sharp edge, it will suddenly step down and the thickness of the film can be determined. A schematic drawing of the operation of the Alpha-step profile is shown in Figure 4.7.

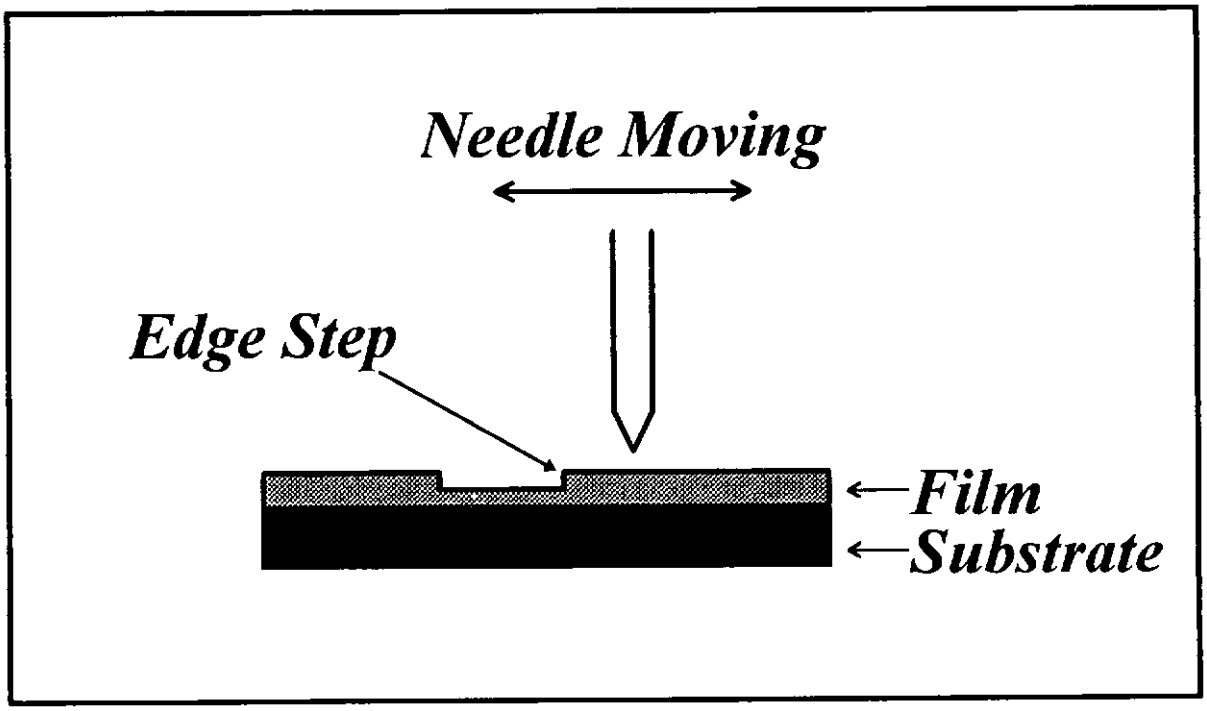

Figure 4.7 Film thickness measurement by α-step

4.1.4 Four-terminal Probe

The sample resistivity (ρ) is defined as $\rho = RA/l$ where R, A and l correspond to resistance , cross section area and length of a current path in the sample respectively. Figure 4.8 shows the schematic diagram for the resistivity measurement. There are four electrodes for current flow and for tapping the voltage drop while a constant current I of about 1 mA is sent passing through the sample between the pair of outer electrodes, the potential different between the two inner electrodes is measured. Due to the geometry of the measurement setup, the above equation need to be corrected by a factor to eliminate the geometry effect [Uhlir, A., 1995]. The equation for the four point probe becomes

$$\rho = \frac{\Delta V \pi t}{I \ln 2} \qquad (4.5)$$

where ΔV, t and I are the potential different between inner electrodes of the sample, thickness of the sample and constant input current respectively.

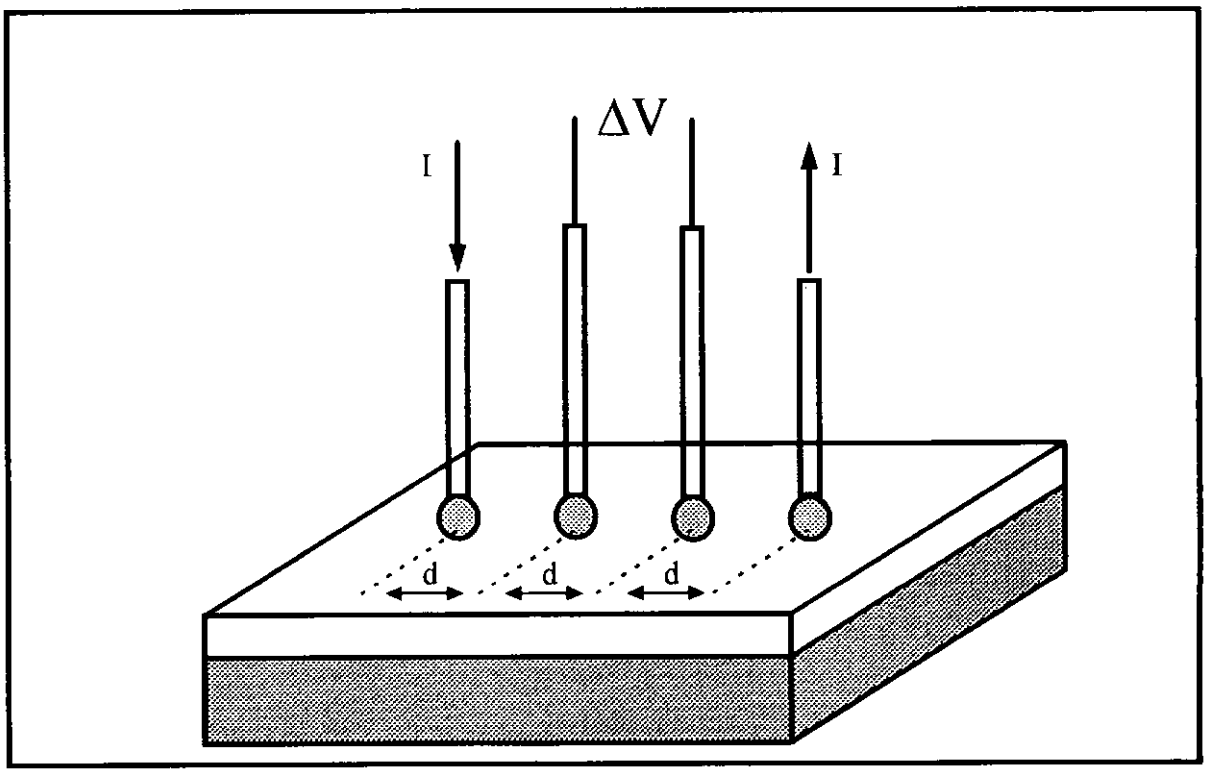

Figure 4.8 The schematic diagram of resistivity measurement.

The constant current source for the four point probe measurement was generated by a negative feedback circuit shown in Figure 4.9. The circuit is composed of a standard 741 Operational Amplifier, two resistors and the measuring sample. The current can be maintained constant in flowing through the feedback loop even if the resistance of the sample changed widely. The value of the voltage supply and the resistance of the resistors were selected in order that the circuit can produce a constant current of 1 mA. For samples having too large or too small resistance, different values of constant current need to be used to get measurable signals or to avoid saturation of the output of the Operational Amplifier, which is limited to about 14 V. Similarly, Figure 4.10 shows the constant current circuit for

the Pt thermometer which was used as a temperature sensor for range from room temperature to 77 K.

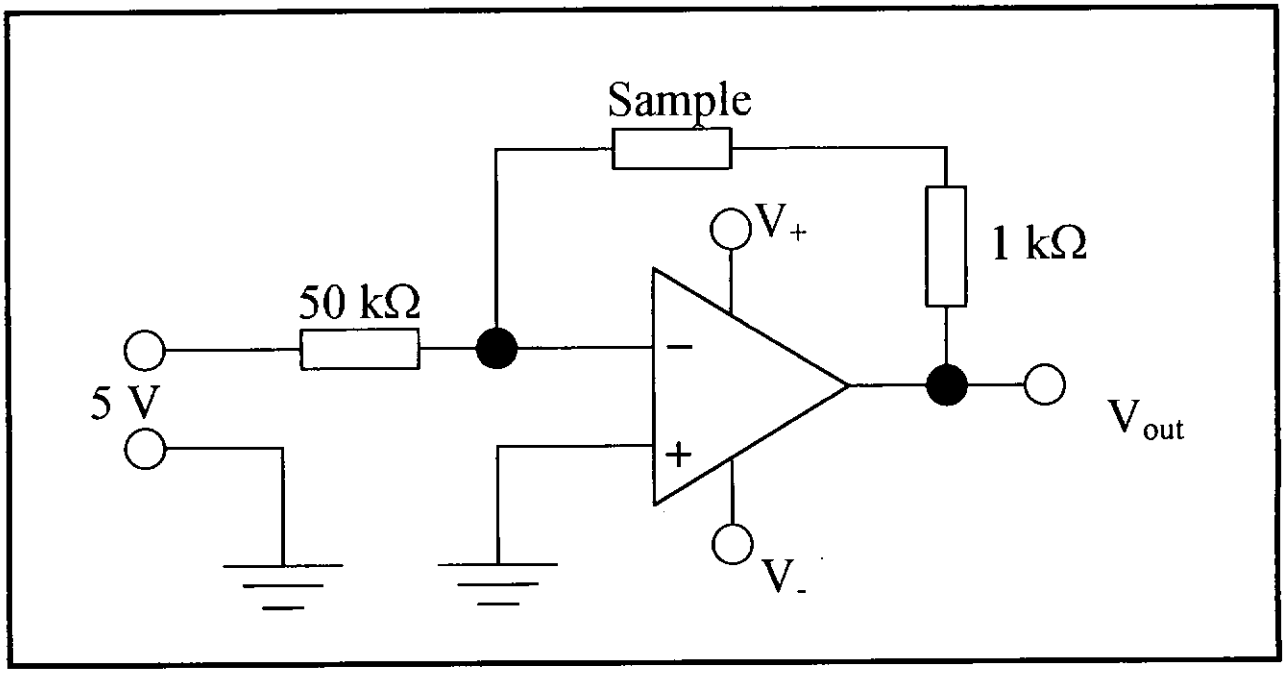

Figure 4.9 The constant current circuit of the sample.

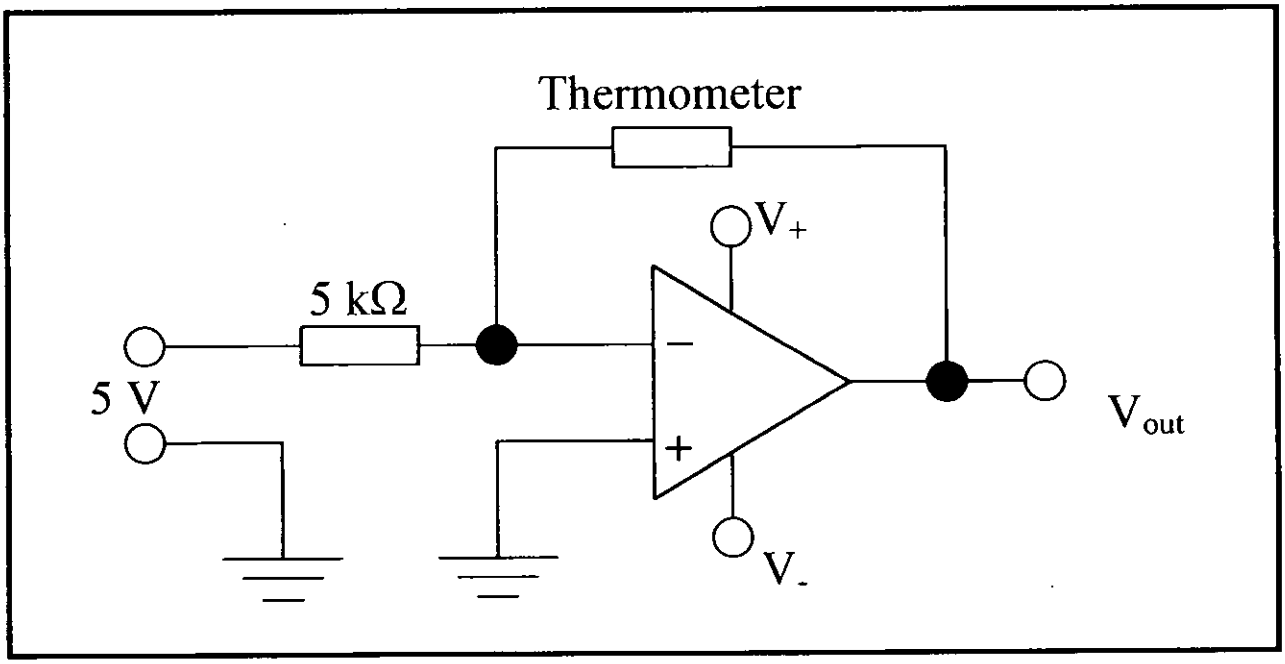

Figure 4.10 The constant circuit of the thermometer.

4.1.5 Electromagnet

For the magnetoresistance ratio (MR) measurement of the samples, a constant dc magnetic field was applied perpendicular to the current flow and either perpendicular or parallel to the plane of the samples. For our study, the maximum magnetic field used was 1 Tesla. It was generated by an electromagnet of a LDJ Model 9500 Vibrating Sample Magnetometer (VSM). The magnetic field strength was computer controlled and it can vary from 0 to ± 1 Tesla.

4.1.6 Atomic Force Microscope (AFM)

The AFM, a very recent invention [Binning et al, 1986a], produces images that are much closer to simple topology and can image nonconducting surfaces [Binning et al, 1983, 1986a and 1986b; Feenstra, R.; 1988; Martin, Y, 1988]. The AFM records interatomic forces between the apex of a tip and atoms in a sample as the tip is scanned over the surface of the sample. When the AFM is operated in a mode that senses the repulsive forces between tip and sample, the tip actually touches the sample. In the AFM machine, however, the probe tip is so sharp and the tracking force is so small that the tip can trace over individual atoms without damaging the surface of the sample. The AFM can also be operated in other mode that senses the attractive force between the tip and the sample. The feedback system then prevents the tip from touching and damaging the sample. But in this mode of operation it generally results a decreased lateral resolution. So far, most images obtained in this way are of micrometer-scale objects.

The probe tip can be made of a small fractured diamond fragment attached to a spring in the form of a cantilever. The small repulsive tracking force between the tip and the sample, usually in the range of 10^{-6} to 10^{-9} N, is recorded by measuring minute deflections of the cantilever. The typical spring constant for a cantilever would be about 1 N/m. If the microcantilever is made of silicon oxide with silicon etching technology [Albrecht et al, 1988] it can be even lighter and has a higher resonant frequency, less sensitivity to vibrations and more stable for atomic force microscope. Thus, a cantilever with a vibration frequency of 10 kHz would have a vibration amplitude less than 0.01 nm and would be suitable for atomic resolution imaging with minimal vibration isolation.

The essential parts of an AFM are shown in Figure 4.11. All AFMs use the principle of negative feedback to control the tip-sample separation. The atomic forces between sample and tip are measured using a laser and detector to measure the cantilever motion. The measured force is compared to a user selectable reference force to determine the error. The negative feedback loop moves the sample as needed to eliminate the measured error and maintain the desired interaction force. The sample is moved vertically (Z direction) using a piezoelectric (PZT) scanning tube position actuator. The PZT scanning tube also moves the sample in the X and Y direction for the raster scan. The sample is raster scanned under the tip while the feedback adjusts the sample position for a constant force. The sample's position in the Z-axis direction, commanded by the feedback, corresponds to the topography of the surface. To construct a 3 dimensional image of the surface, the computer records these Z-axis movements as a function of the sample's X and Y direction.

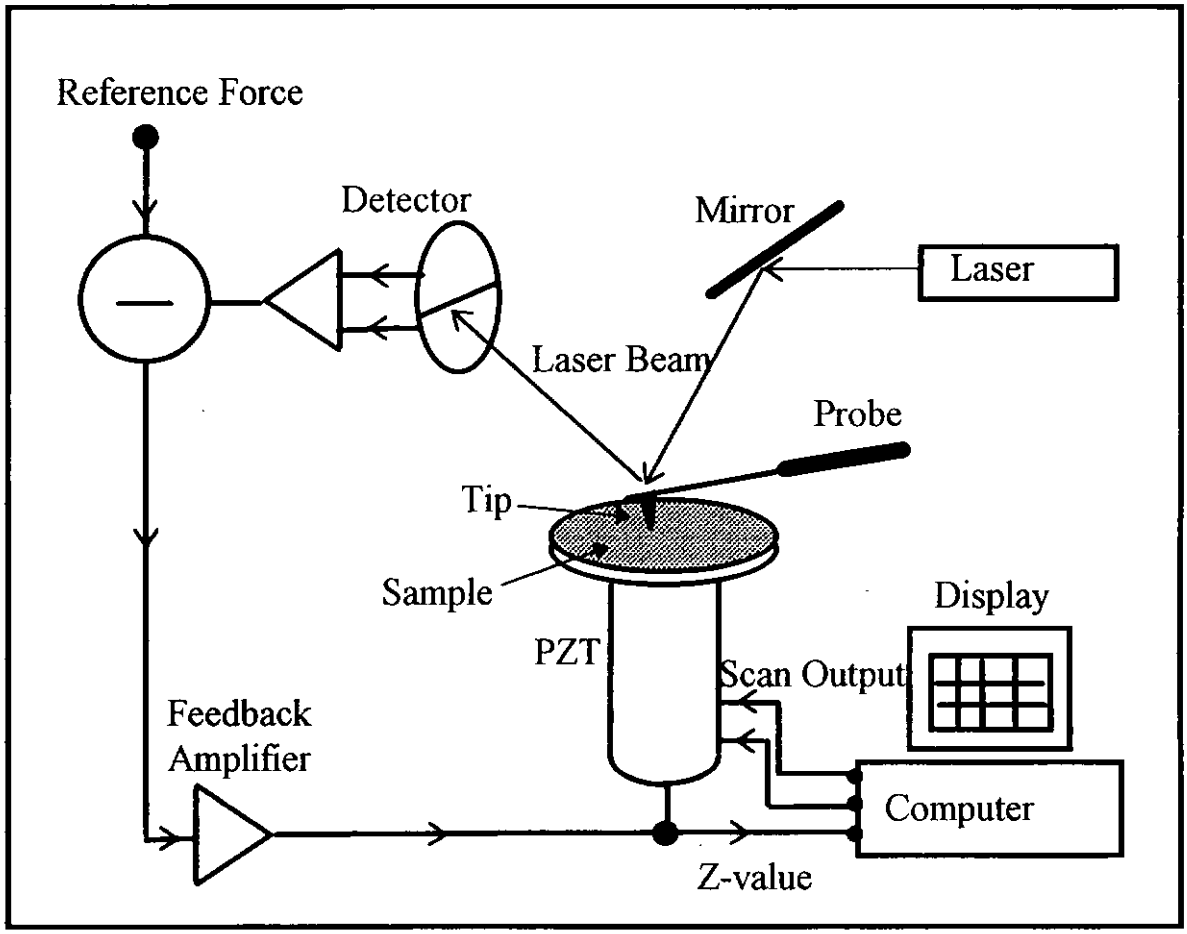

Figure 4.11 Schematic diagram of the atomic force microscope.

We used these recent techniques of AFM (Burleigh; Metris-2000) to characterize the topology of the samples. We have also attempted to determine the size of crystallites and to distinguish the grains of the two immiscible materials.

4.2 Experimental Procedures

4.2.1 Films Fabrication

The CoAg granular and multilayer thin films were fabricated by the PLD method. The CoAg was chosen as the material system in our investigation. The reason behind is that the CoAg system is known to have the largest GMR effect. It has been studied by many groups using sputtering method to prepare the samples. However, only two research groups have use PLD to process this material system and the MR ratio reported is not large. It is therefore worthy to fabricate the CoAg granular and multilayer thin film by PLD and to investigate the physics involved.

In depositing CoAg granular and multilayer thin films, a CoAg split target was mounted on a rotating target holder. The experimental setup is shown in Figure 4.12. By carefully control of the target rotation speed, laser repetition rate and the ablation track ratio, we can conveniently vary the film thickness in multilayer system and the composition ratio in granular films. The results of our studies will be presented and discussed in the Chapter 5 and Chapter 6.

In addition to the CoAg system, we have also investigated the Ti/Si system. Before studying the multilayer and granular films, we have prepared some single metallic thin film deposited on Si(100). However, we found an anomalous R-T profile for Ti thin film deposited on Si (100) substrate. Moreover, the Ti on Si shows an unexpected large positive magnetoresistance effect. The findings of this investigation will be reported in details in Chapter 7.

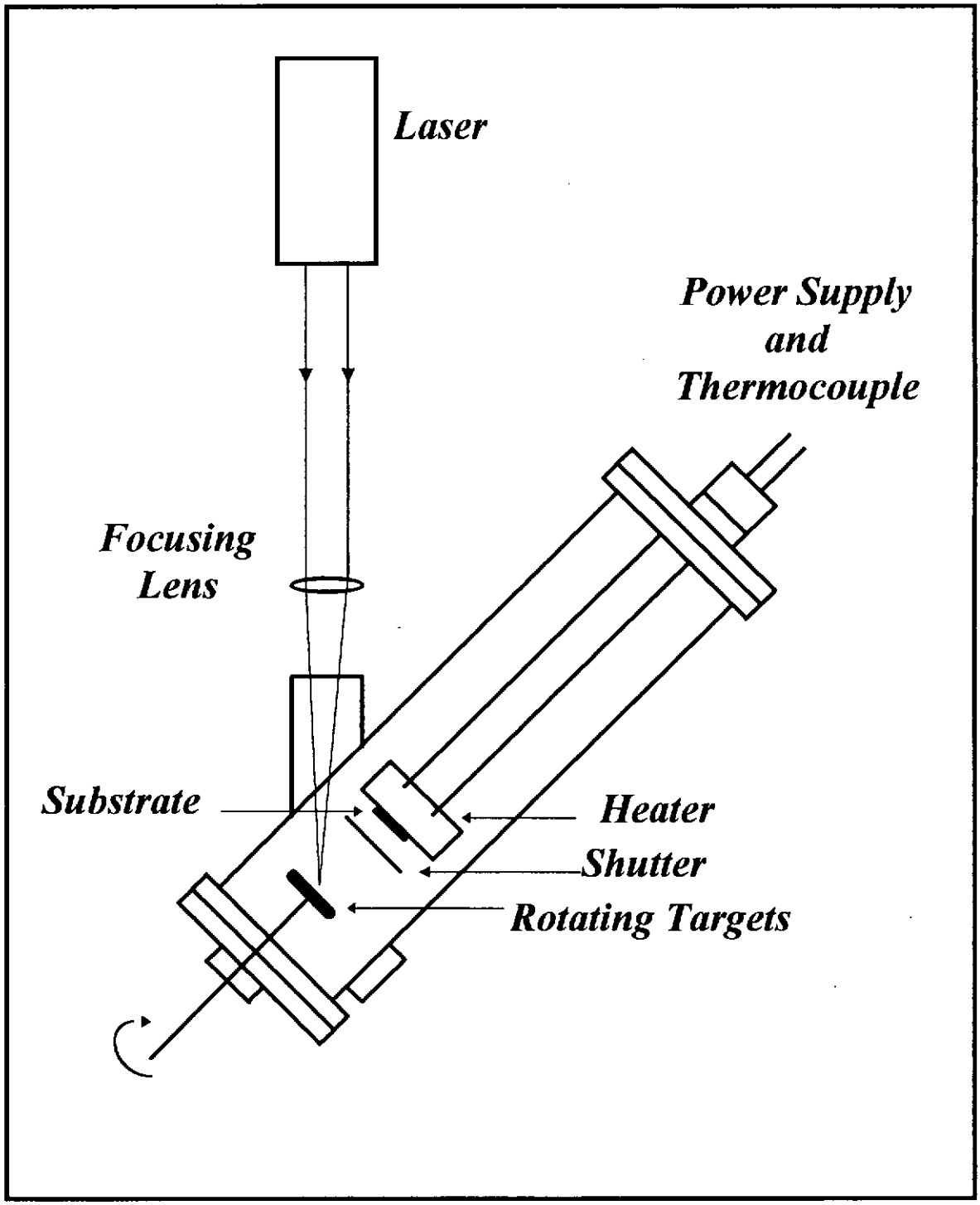

Figure 4.12 The schematic diagram of pulsed laser deposition system using split target for fabrication of multilayer and granular films.

All our films were grown on Si(100) substrates and the Si wafers were processed by a standard cleaning and etching treatments. i.e. degreased by alcohol in

ultrasonic for 5 mins and etched by 10% HF for 3 mins and rinsed by acetone and distillate water. The processed Si wafer was pasted on the top of the heater which was placed parallel with the targets. The CoAg films were fabricated by KrF pulsed laser in the small chamber which was evacuate ~ 4×10^{-6} Torr. The targets to substrate distance was about 3.5 cm. The Ti/Si films, however, were fabricated by the XeCl pulsed laser in the large chamber. The target to substrate distance was about 4 cm and the chamber was kept at < 10^{-5} Torr. The substrate temperature was set in a range from room temperature to 750 °C. After the vacuum and substrate temperature had reached the desired values and became stable, the laser was switched on. In most cases, both lasers were operated at a repetition rate of 10 Hz and the beams were focused onto the targets by a converging lens of f = 30 cm. The targets were conditioned for ~ 300 laser pulses for every film deposition process. The rotating target materials were ablated in vacuum and deposited on the heated substrates. Assuming a constant deposition rate, the deposition time can be conveniently converted to the film thickness. Two kinds of films, namely as-deposited films and post-annealed films, were fabricated. The as-deposited films, were obtained by cooling sample to room temperature immediately after the deposition. Unlike processing of ceramic films, no special cooling temporal pattern was attempted as we deem it unnecessary. For the post-annealed ones, the thin films were kept at a certain temperature, which was equal or greater than the deposition temperature, for a prolonged period of 0.5 to 60 mins in situ. The post-annealing process was mainly used to improve the crystallinity of the films.

4.2.2 Electrical Properties Measurement of The Thin Films

The electrical properties of both the CoAg and Ti films on Si were studied. The measuring method was a standard dc four-terminal probe mentioned in 4.1.4. After the films were made, four conducting wires were adhered on the film surface by silver paste. A constant Current was allowed to flow in the sample through the two outer electrodes. The voltage drop between the two inner electrodes was recorded as the a y-axis input signal of a chart plotter. The voltage output of the platinum thermometer, which has been calibrated for temperature in Kelvin was fed to the x-axis of the plotter. The resistivity of the samples was calculated according to the equation of $\rho = \frac{\Delta V \pi t}{I \ln 2}$, where ΔV is the potential different between the inner electrodes, t is the thickness of the film and I is the constant current passing through the sample. Therefore the resistivity of the samples from room temperature (300K) to liquid nitrogen temperature (77K) can be obtained and the R-T profile of the films were plotted. The recorded R-T profiles were then digitized to ASCII data format for further processing by computers.

4.2.3 Magnetic Properties Measurement of The Thin Films

The magnetic property measurement of the CoAg and Ti films were confined to the magnetoresistance MR ratio dependence as functions of temperature and field. In our measurements, we have used a magnetic field set up in the gap between the two electromagnet poles of a VSM. Indeed, the measurement of magnetoresistance profiles were similar to the measurement of the field-free R-T profiles as mentioned above. The film was installed on a sample holder, which consisted of a Pt-wire thermometer and o-ring seal for a quasi-thermal insulation from the outside. The sample was cooled down to 77 K by immersing the sample holder in liquid nitrogen. It was then put into the constant magnetic field region. As the sample temperature gradually rose to room temperature, the R-T profile of the sample under the influence of the magnetic field can be obtained. This is to be compared with the field-free R-T profile and the MR can be deduced according to equation 2.1.

For some Ti/Si based films we have used the magnetic measurement set-up offered in the HKUST. In this set-up sample temperature of 4 K to 300 K and magnetic fields up to ± 50 kOe are available.

Chapter 5

Split Target

5.1 Introduction

A so called "split target" technique has been developed in our laboratory in 1993 for the purpose of studying the differential resputtering of the materials from the PLD films [Hau et al, 1995; Hau, 1995]. We have, in the present work, adopted this technique to fabricate multilayer films with different layer thickness and granular film with varied composition. Figure 5.1 shows the schematic diagram of the split target arrangement, in which two half circle sector targets are put together. The split target is kept rotating in order to avoid localized erosion by laser ablation. Using this setup both the multilayer and granular thin films can be easily fabricated by the PLD method. In preparing the CoAg multilayer and granular films, we therefore use two half circle sector targets of pure Ag and Co. They were put together, forming a circular split target of 1" diameter.

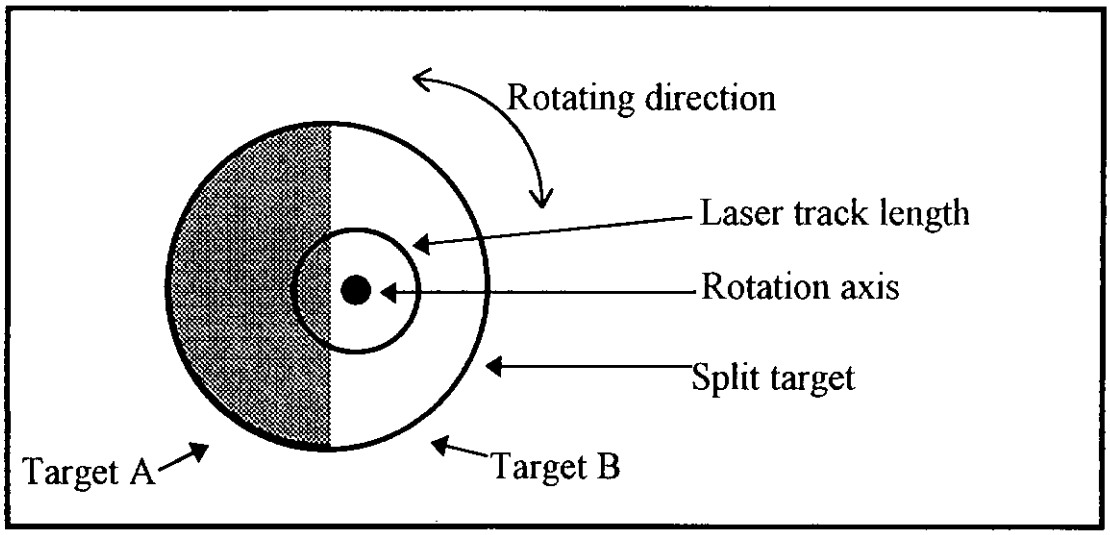

Figure 5.1 The schematic diagram of split target.

5.2 Fabrication of Multilayer and Granular Films

If the pointing direction of the laser is fixed and the beam is directed to irradiate the flat surface of the split target while the target is rotating, one would ablate the target materials A and B in alternate fashion and produce a circular erosion track on the target surface. If the target rotation speed is kept low and the laser repetition rate high, then, during one rotation cycle, the amount of materials from A and from B will be large enough to form layers. Films of many tens of layers can be easily produced in this manner. The film thickness can be simply controlled by altering the rotational speed and/or the laser repetition rate . On the other hand, if the rotational speed is fast and the laser repetition rate is low, i.e. ablation of A or B is not more than a few times by the laser within one rotation cycle, no layers will be formed. Granular structured films consisting A and B materials will be developed instead. Furthermore, by making the rotation center different from the geometric

centre of the split target, one can change the composition ratio of A to B in the granular films. The changes can be simply deduced from the ablation track length ratio on A and B. This is illustrated schematically in Figure 5.2.

In metallic GMR multilayer and granular films the control of the layer thickness and the composition ratio are of paramount importance. Thus, our split target PLD technique is a simple and convenient way to fabricate and to study the behavior metallic of GMR films as well as to explore new GMR materials systems.

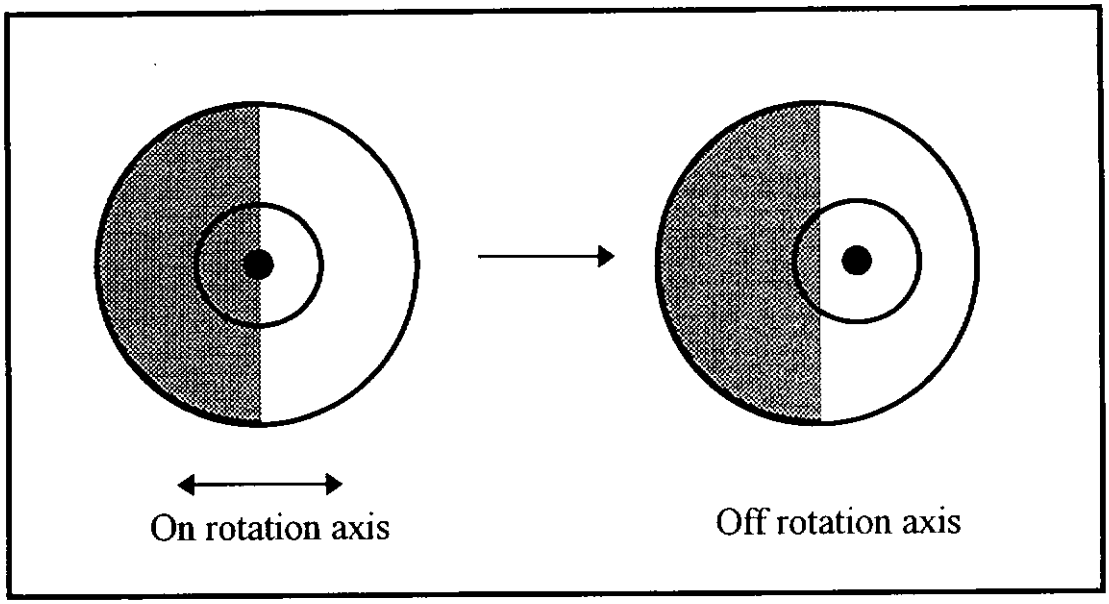

Figure 5.2 The schematic diagram of the split target off rotation axis.

5.3 Laser Track Length Ratio against Atomic Percentage of Co in CoAg

We have fabricated a series of granular CoAg thin films in order to study the relationship between the track length ratio and the atomic percentage of Co. The targets Co and Ag were bought from Electronic Space Products International and Noble Metal Research Center, China respectively. They were circular discs of 1 inch in diameter and 0.25 inch in thickness. The target Co, Ag and the atomic composition of the CoAg granular films were measured by the Energy Disperse X-ray (EDX) spectroscopy. The purity of Co and Ag targets are 99.9% and 99.99% respectively. For the granular films, we have selected three different spots for measuring the composition of the thin films. The selected spots are 150×130 μm^2, which is much greater than the granular size so that it is large enough for accurate reflection of the average composition of the films. The track length ratios of Co to Ag were directly measured from the laser ablation track marks on the spilt target surface.

Figure 5.3 shows the atomic percentage of Co against the track length percentage of Co. Figure 5.4 shows the atomic percentage of Ag against the track length percentage of Ag. Solid lines representing a linear relationship between atomic percentage and track length ratio are added in both figures for reference purpose. It can be seen that the Co atomic % is upshifted from the reference line whereas the Ag atomic % is downshifted. Thus it suggests that for the same number of laser shots the deposition yield is higher for Co and lower for Ag.

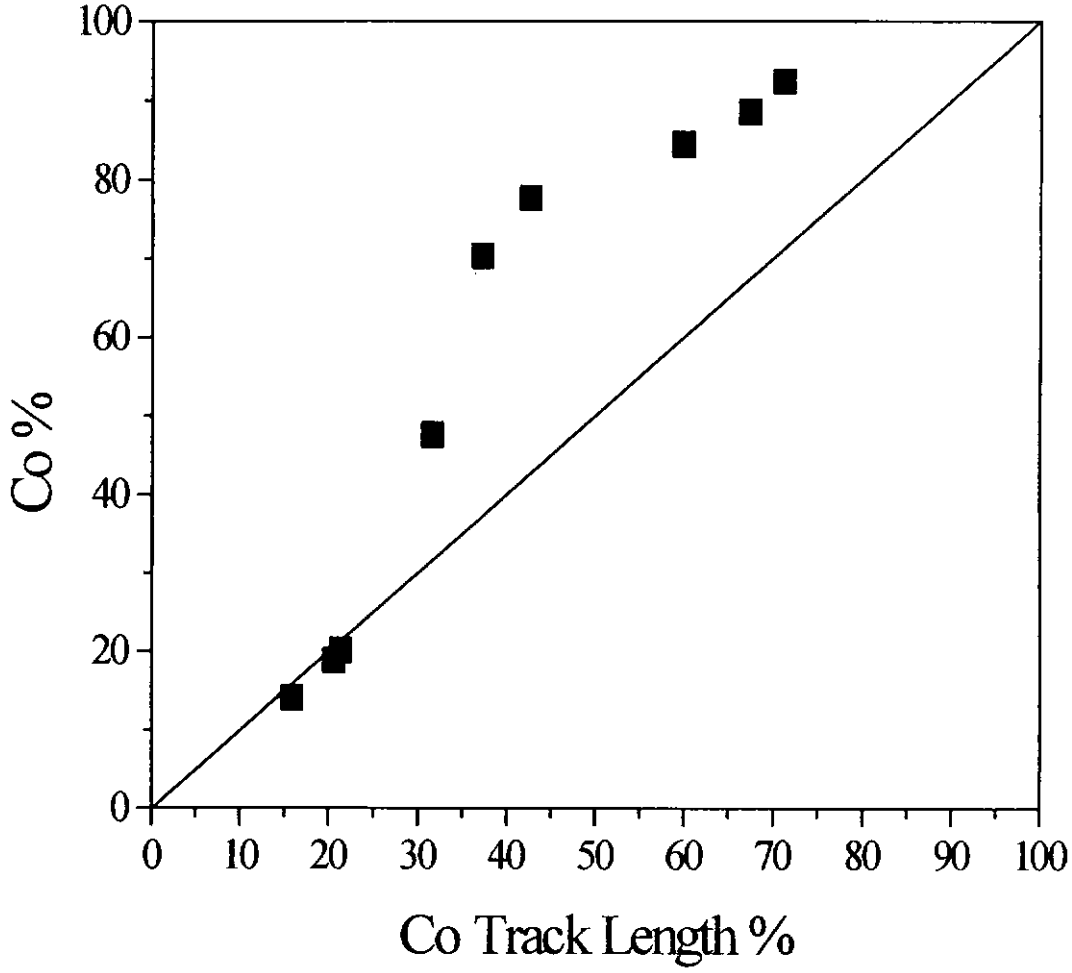

Figure 5.3 The Co atomic % against Co track length ratio. The ■ are data points and the solid line represent a linear relation. Ablation fluence of 2 Jcm^{-2}.

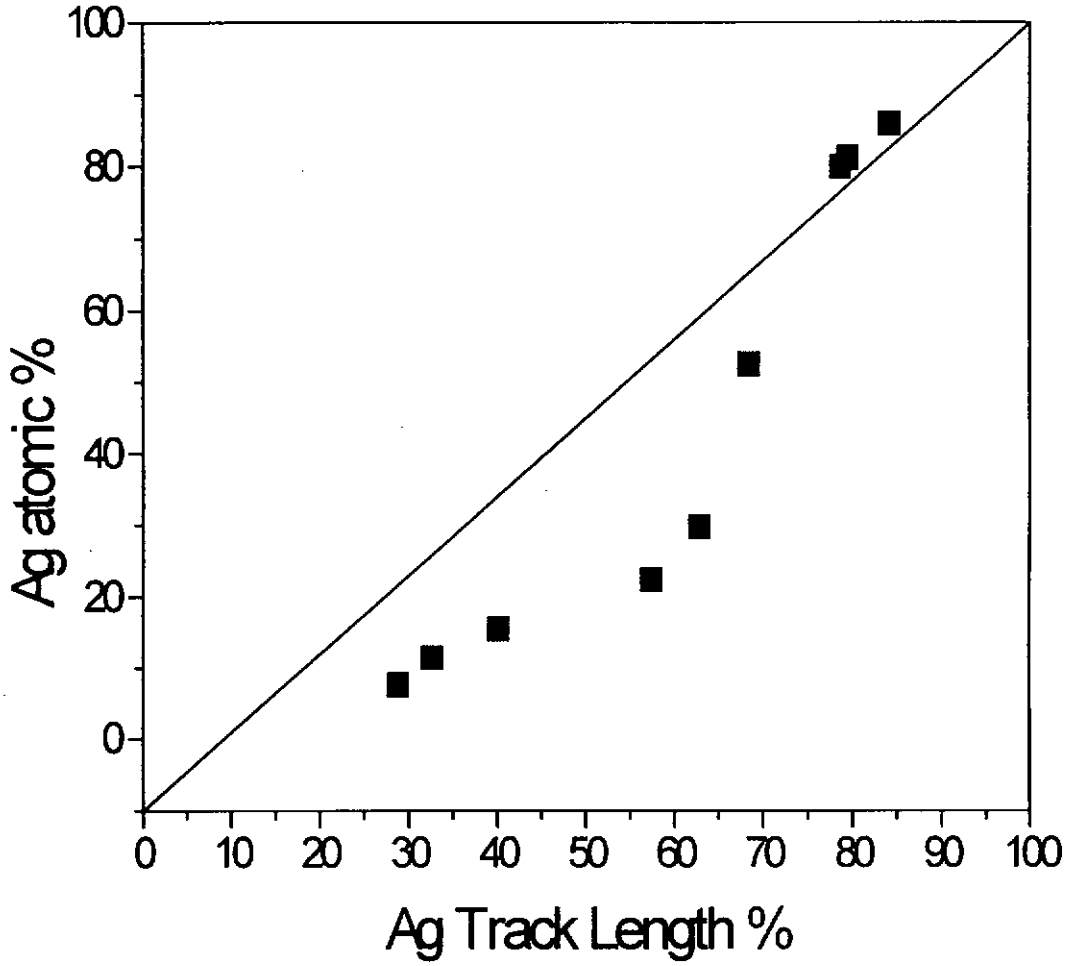

Figure 5.4 The Ag atomic % against Ag track length ratio. Ablation fluence of 2 Jcm^{-2}.

Using these two figures as the calibration data, we can estimate the atomic compositions of the two materials in the films by looking at the track length ratio. In practice, we can position the target to obtain the desired track ratio prior to the actual film grow process. In this way, we can vary and optimize the composition of the film easily.

Chapter 6

Cobalt Silver Multilayer and Granular Films on Silicon(100)

6.1 Introduction

There are many ferromagnetic metal-noble metal systems that exhibit GMR effect. The CoAg system, however, is attractive for GMR effect studies and potential application for several reasons [Parker, M. R., 1994]. Firstly, the highest GMR values reported for any granular thin films have been achieved in CoAg mixtures [Wang et al, 1994]. Secondly, Co and Ag can segregate essentially completely under the proper fabrication conditions. The segregation occurs because the surface free energy [Mezey et al, 1982] of Co (2.71 J/m^2) is more than twice that of Ag (1.30 J/m^2) causing the Co to cluster. In addition, there is a very poor lattice match since fcc Ag has a lattice parameter that is 15% larger than that of fcc Co. Furthermore, the heat of formation between Co and Ag is positive (+26 kJ/g atom) so that there is no tendency for formation of the compound CoAg or for alloying [Miedema, M. B., 1976]. Other materials system such as the CoCu system is less favorable for complete segregation since the last three effects are smaller; the surface free energy of Cu (1.93 J/m^2) is closer to that of Co, the lattice mismatch is only 2%, and the heat of formation CoCu is +13 kJ/g atom.

In the present studies we have concentrated our effort in fabrication and characterization of CoAg multilayer and granular films using the split target PLD method. Nevertheless, the same technique is expected to apply in processing other ferromagnetic metal-noble metal systems.

6.2 Magnetoresistance of CoAg Granular Films

Figure 6.1 shows the typical resistance and MR% against temperature profiles of our CoAg granular thin films. The solid line represent the resistance of the film without the external magnetic field. It is a fairly normal metallic film R-T profile. The resistivity decreases almost monotonously from room temperature to about 77 K. The discontinues line, on the other hand, represents the resistance of the film at 1 Tesla magnetic field. This line shows similar temperature dependence as the field-free resistance profile. The absolute resistance value, however, is lower.

The square dots presents the deduced MR% of the CoAg film. Although the field induced change of resistance remains more and less the same, larger MR% is obtained at the lower temperature. By definition, the MR% is the change of resistance divided by the absolute resistance of the film. When the absolute resistance decreases, the MR% will increase. Under 1 Tesla magnetic field, MR ratios of 9% at about 77 K and 5.5% at room temperature are observed. These values are comparable to those reported by other groups [Dupuis et al, 1996; Zhang et al, 1997]. Direct comparison is not possible due to the fact that our measurements are limited to a maximum field of 1 Tesla and a minimum temperature of 77 K. (cf.

with 5 Tesla and 4 K for others). However, by extrapolation, we have in fact obtained granular films of similar MR%.

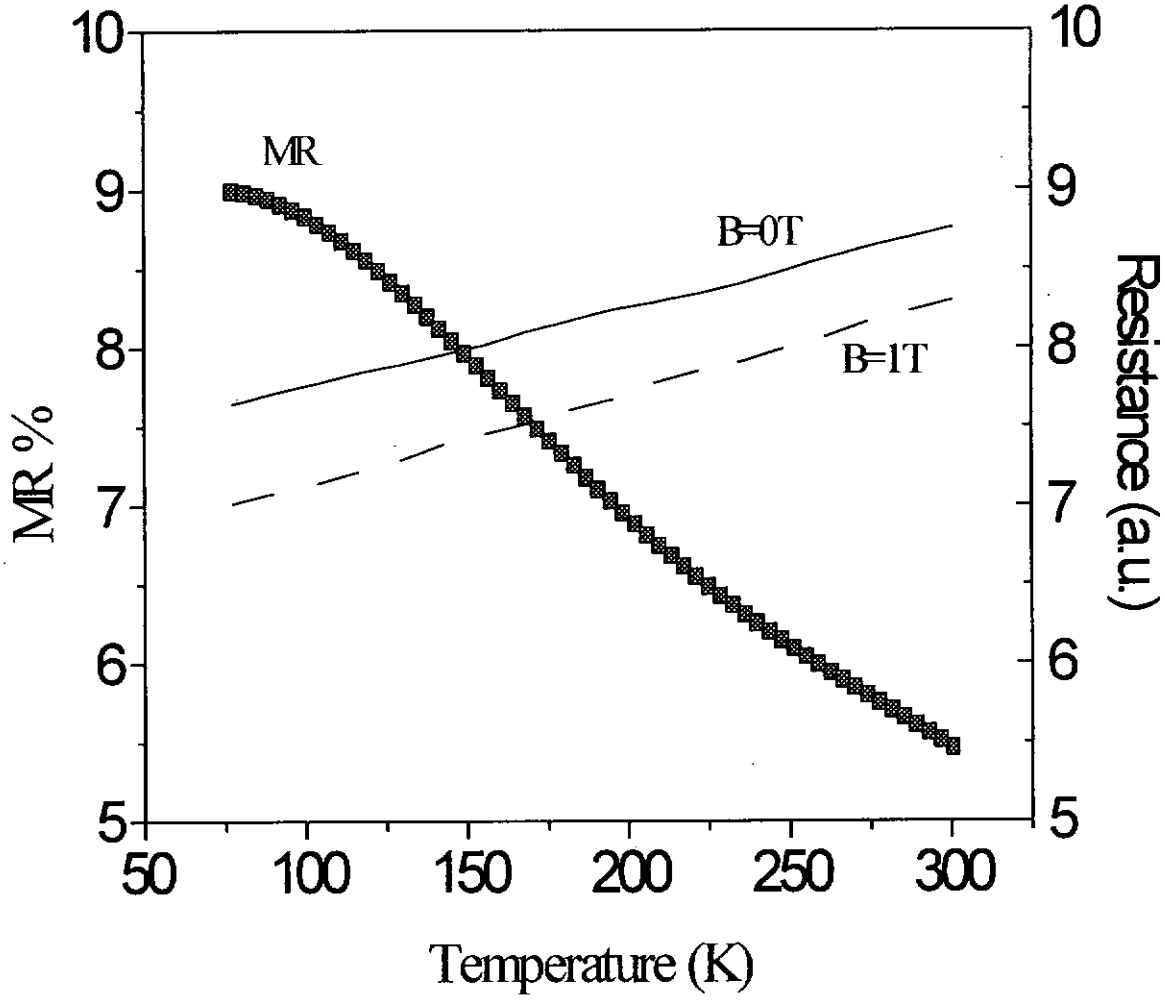

Figure 6.1 Resistance against temperature and MR% against temperature of typical CoAg profiles.

6.3 Atomic Percentage of Co Dependence on MR%

In magnetic granular thin film the largest GMR has been reported in CoAg system. The Co concentration in granular film will directly affected the magnetoresistance ratio for the films prepared by MBE [Azizi et al, 1995] and sputtering [Conde et al, 1994]. The greatest GMR in CoAg granular film, fabricated by sputtering, with the atomic percentage of the Co is around 20% [Berkowitz et al, 1992; Xiao et al 1992; Parkin, 1993]. In our study of CoAg granular films prepared by PLD method the MR% dependence on the Co concentration were examined. Films with Co atomic fraction from 15 to 65% were fabricated. The results are shown in Figure 6.2. At the range of 15 to around 20% atomic fraction of Co, the MR% increases with Co. As the concentration of Co inside the Ag matrix increases and the scattering centers or scattering surface increases so that the MR effect improves. Besides, the magnetic granular-granular inter distance will decrease as the concentration of the Co increases. The MR% has a maximum at around 20% of Co and thereafter the MR% decreases as the atomic Co% increases. The magnetic granular-granular inter distance in this range gets longer than the electron mean free path and it is likely that the coupling between the magnetic regions diminishes and the MR effect becomes less prominent. As the concentration of Co increases, Co granules tend to agglomerate to large clusters. When the cluster size is greater than the electron mean free path, the MR effect will also decrease.

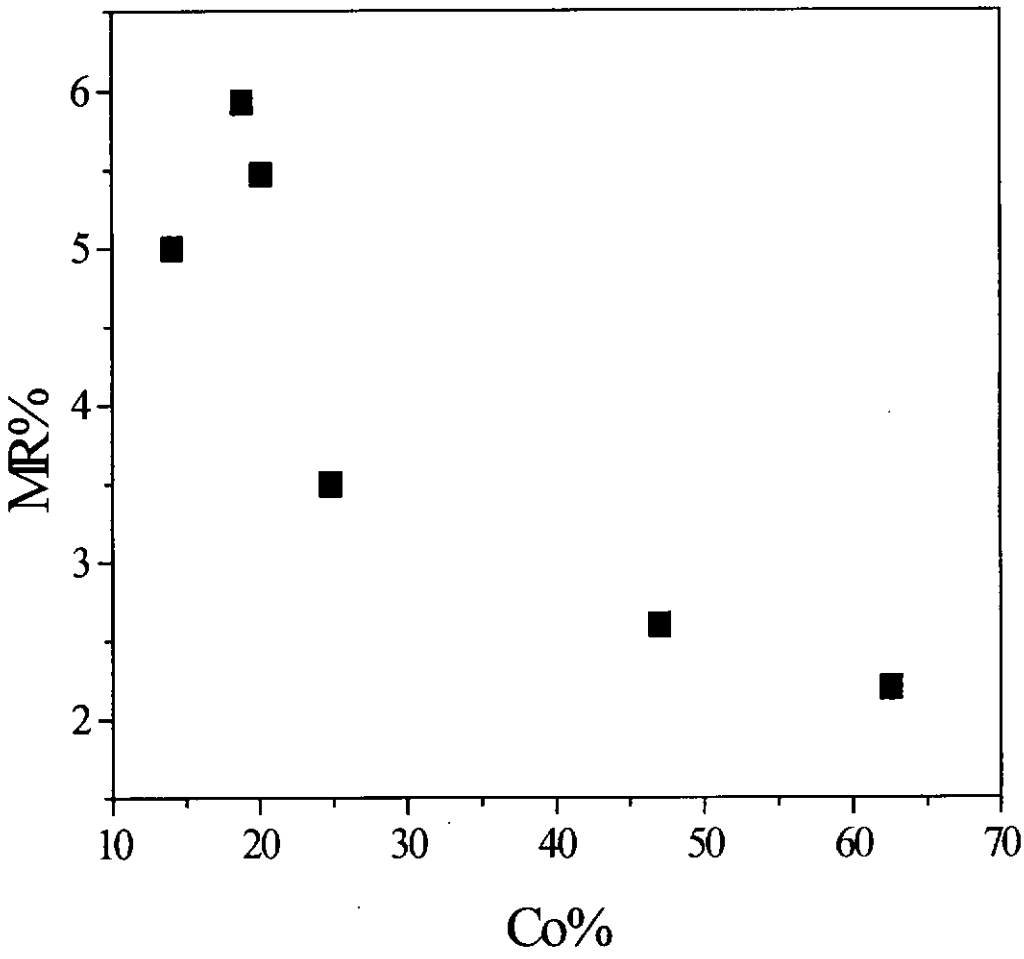

Figure 6.2 The MR% against atomic Co% of CoAg thin film profile measured at 77 K.

6.4 Post-annealing and Crystallinity of CoAg Granular Films

It has been reported that in CoAg granular films prepared by sputtering method, the post-annealing has significant effect on the MR%. This is due to the fact that post-annealing can greatly promote segregation and improve the film crystallinity and hence the grain sizes. As the magnetic coupling is very sensitive to the separation of the magnetic entities and the interfacial areas, complete Co-Ag segregation is therefore desired. However, enlarged grain size will increase the separation and reduce the interfacial area, and will inevitably degraded the MR effect. In fact some researchers have deliberately prepared the granular films at below room temperature and then post-anneal them at slightly higher temperatures in attempts to reduce the grain size. We have studied the crystallite size as a function of post annealing temperature. X-ray diffraction patterns of the post-annealed samples are depicted in Figure 6.3. All Co peaks overlap with those of Ag and their FWHM can not be evaluated easily. Ag on the other hand, has strong and isolated peaks. Crystallite sizes of Ag were deduced from the FWHM of the diffraction peaks by the equation 4.4 and are tabulated in Table 6.1. They are also displayed graphically in Figure 6.4. As expected, the cystallinity improves as annealing temperature. A rather sharp change appears at 300-400 °C. It is believed that at this temperature range, complete Co-Ag segregation occurs and both the Co and Ag tend to form larger crystallites. Optimal MR% is therefore likely to occur at temperatures just below ~300 °C. This is in agreement with most other reports on granular CoAg films. However, the measured MR% of all our samples shows similar values. Post-annealing temperatures appear to

have no observable effect on the MR%. Indeed, if we compare the MR of PLD CoAg granular films with those obtained by sputtering, the later generally produce a much bigger MR%. In order to unravel this discrepancy, we have used AFM to examine the topography of the PLD produced Co, Ag and CoAg granular films.

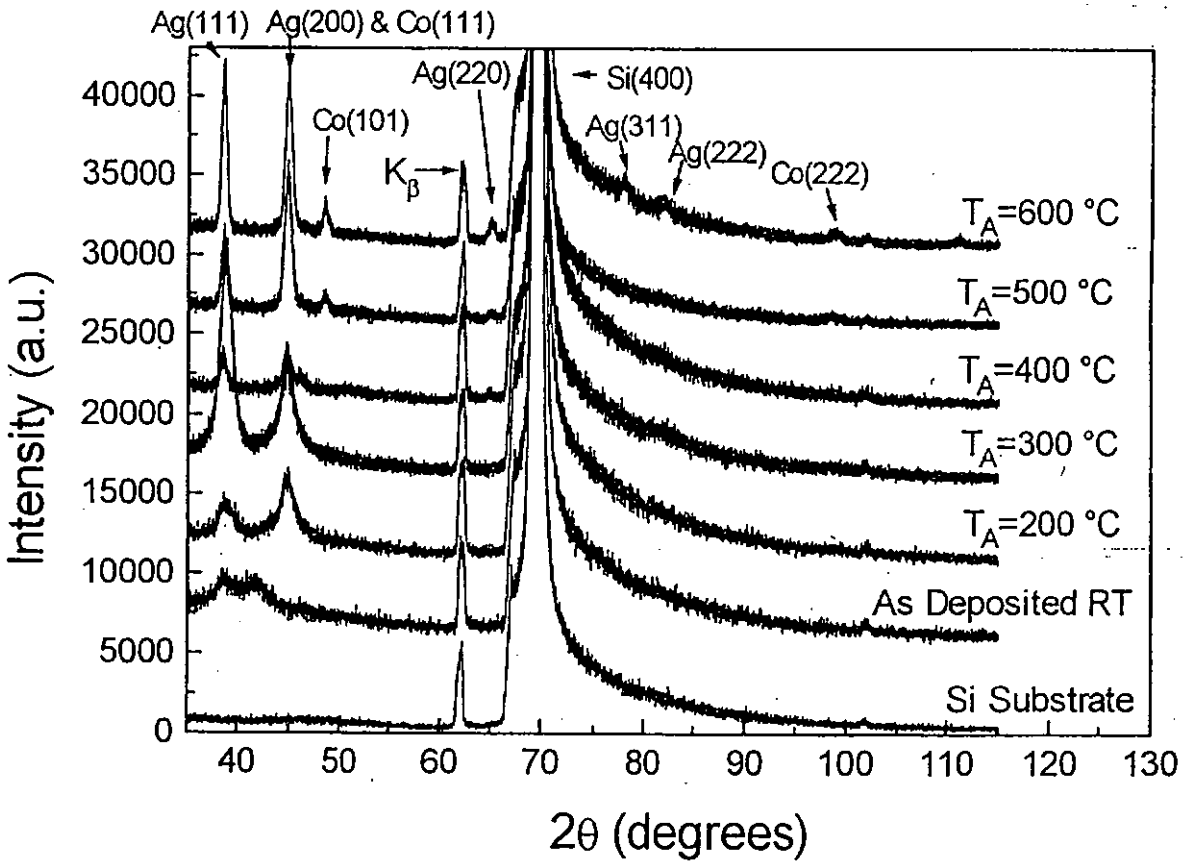

Figure 6.3 X-ray diffraction patterns of Si(100) substrate, $Co_{60}Ag_{40}$ sample deposited at room temperature (fcc alloy) and granular fcc Co in fcc Ag after annealing at 200 °C, 300 °C, 400 °C, 500 °C, 600 °C for 30 mins. The diffraction patterns have been shifted vertically.

T_a (°C)	FWHM (°)	Crystallites Size ε (nm)
600	0.612	74.2
500	0.613	73.6
400	0.622	68.2
300	1.360	9.7
200	1.629	7.4
As deposited	1.907	5.9

Table 6.1 FWHM of the diffraction peaks and crystallite sizes of Ag of different post-annealing temperatures.

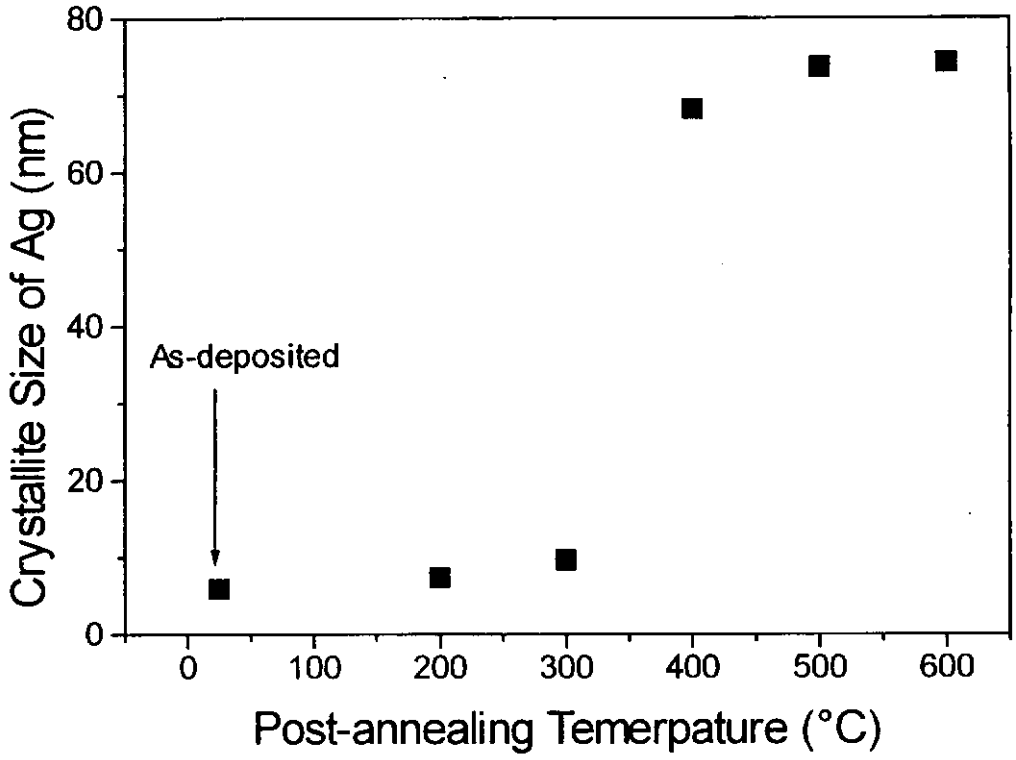

Figure 6.4 The crystallite size of Ag against the post-annealing temperature.

6.5 AFM Studies of Co, Ag and CoAg Granular Films

We have prepared pure Co and Ag single layer films as well as the CoAg granular films. From some of our AFM studies, it is concluded that under our ablation laser fluence of ~2 J/cm^2 less than 100 shots of laser ablation on target is enough to deposit a complete layer on the substrate. Figure 6.5 shows the Ag/Si film was produced by 1,000 laser shots of similar laser fluence. Here the Ag appears in large grains (>10 nm). It has been shown that by post-annealing the films at 200 °C the grains become larger and smooth. Figure 6.6 shows the AFM picture of Co/Si film produced by irradiating 1,000 laser shots on the pure Co target at room temperature. No apparent grains of Co were observed. The surface was littered with densely populated voids. The AFM data of CoAg granular film are shown in Figure 6.7. The film was prepared by alternately ablating the Co and Ag targets for 8 and 32 shots, respectively for 30 mins. The film was then annealed at 200 °C for 1/2 h. From the data it is apparent that the granular film consists of large grains same as those of pure Ag films. We believed that these CoAg granular films are composed of grains of Ag with the Co filling the grain boundary. This structure is therefore different from the ideal GMR CoAg granular films, in which the Co granules are embedded in a semi-continuous Ag matrix. This observation can thus explain the reduced MR% in the PLD prepared CoAg granular films. From this point of view, the post-annealing temperature only have minimal effect on the MR%.

The ablated species by PLD process are known to have high kinetic energy. This energy can, in principle, dissipated onto the film surface during deposition. As a consequence the film surface temperature can be raised to high values and film crystallization at room temperature is possible. The details of the dynamics of the Co and Ag grain growth are not known. A thorough investigation of the grain growth processes by PLD is therefore needed and can form topics for future studies.

6.6 CoAg Multilayer Films

Based on the idea of GMR multilayer films described in Chapter 2 and the scheme of PLD of split target set out in Section 5.2, we have attempted to grow CoAg multilayer films up to 30 layers thick. The spacer layer (Ag) thickness of a few angstroms to tens of angstroms have been tried. However, all our CoAg multilayer films show a relative small MR of ~1% irrespective of the spacer thickness. From the AFM pictures of Figures 6.5, 6.6, it is seen that the PLD films tend to have a rather large outgrowth and grain size even at room temperature deposition. It is further suggested that the fine control of layer thickness down to angstroms level in this CoAg system by PLD be in vain. All our CoAg "multilayer films" are in fact not true multilayers. Consequently the films have much smaller MR% and in general show no apparent dependence on the spacer thickness.

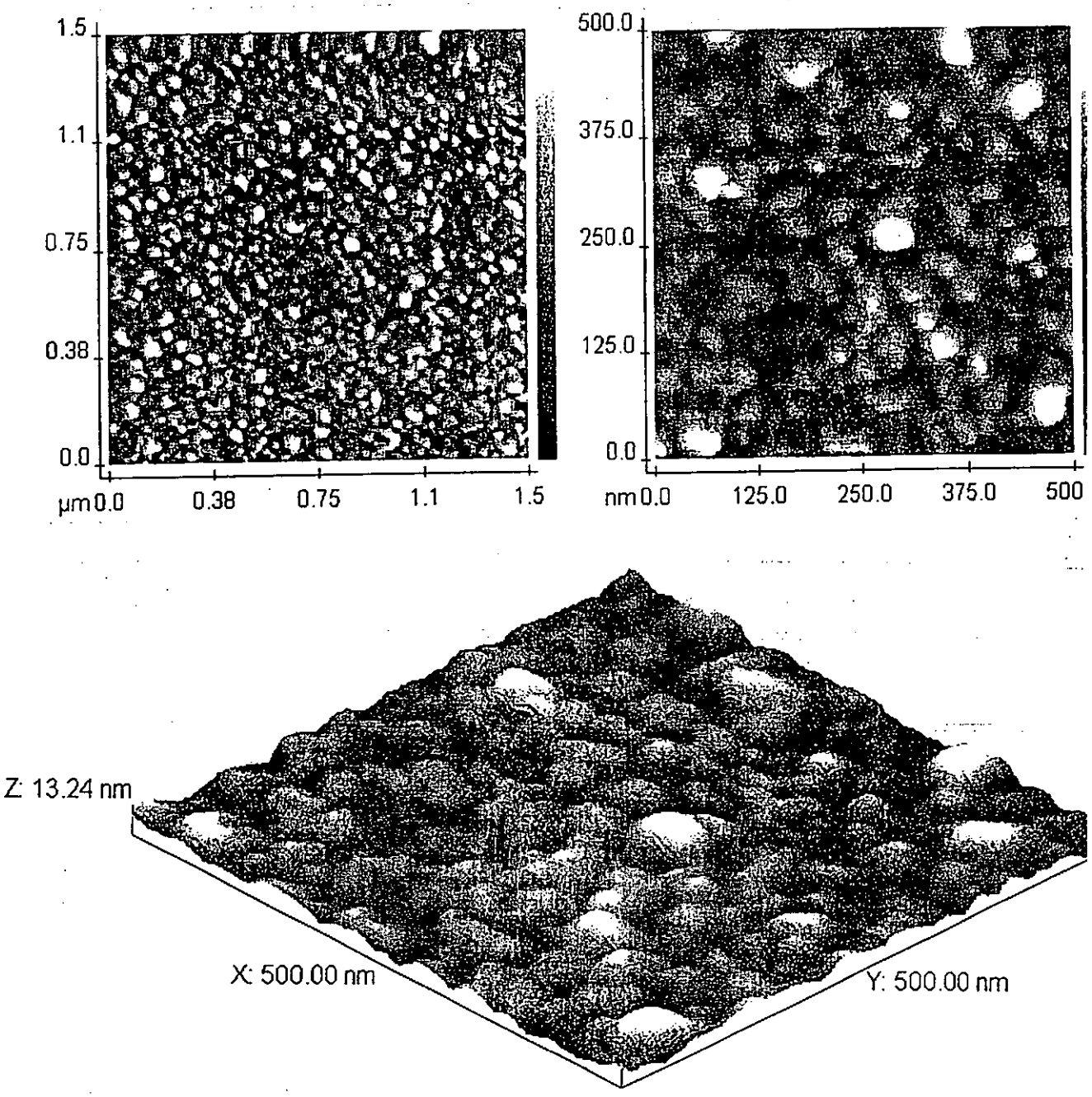

Figure 6.5 The AFM data of 1000 shots of Ag on Si substrate with different scale.

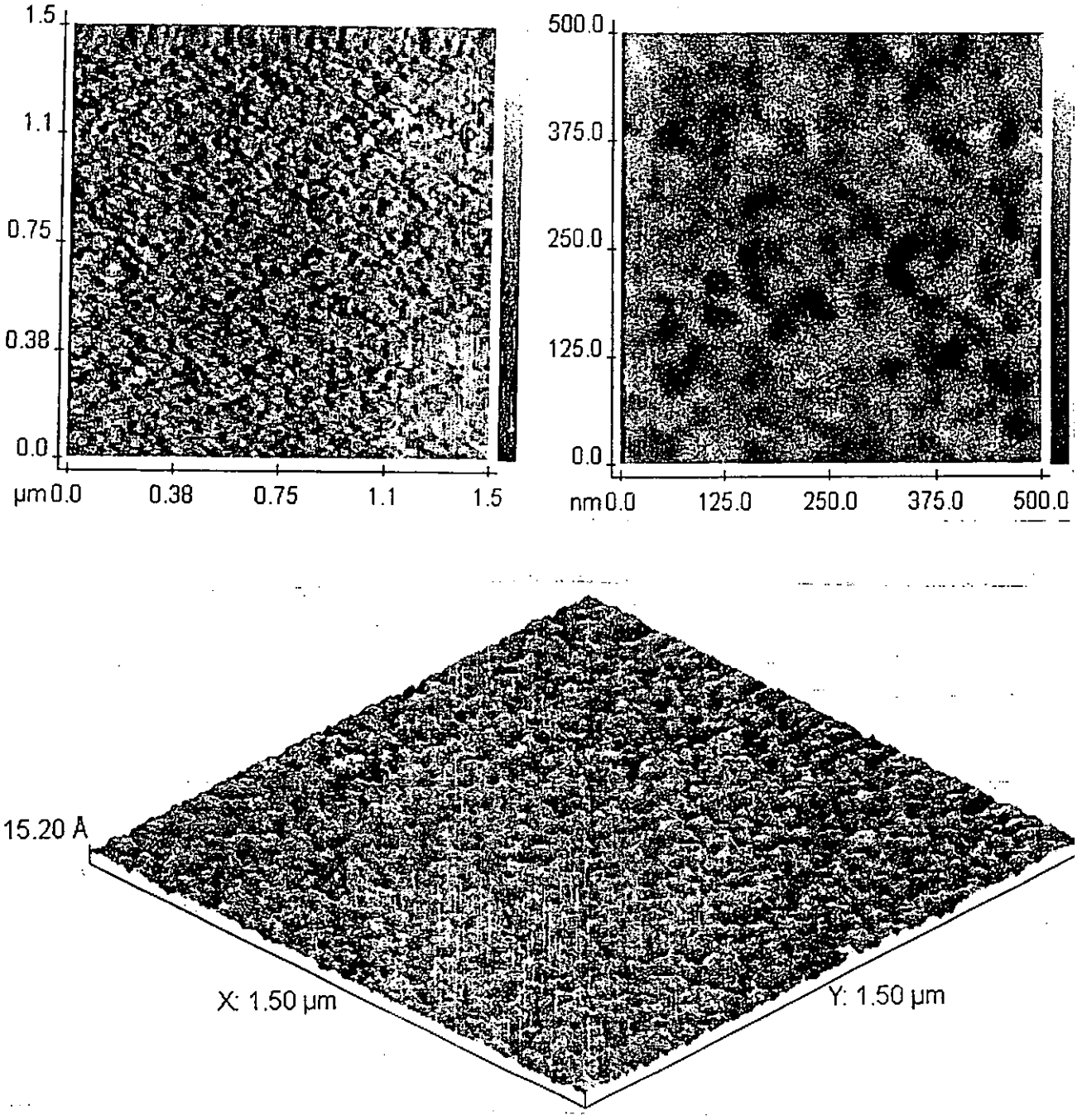

Figure 6.6 The AFM data of 1000 shots of Co on Si substrate with different scale.

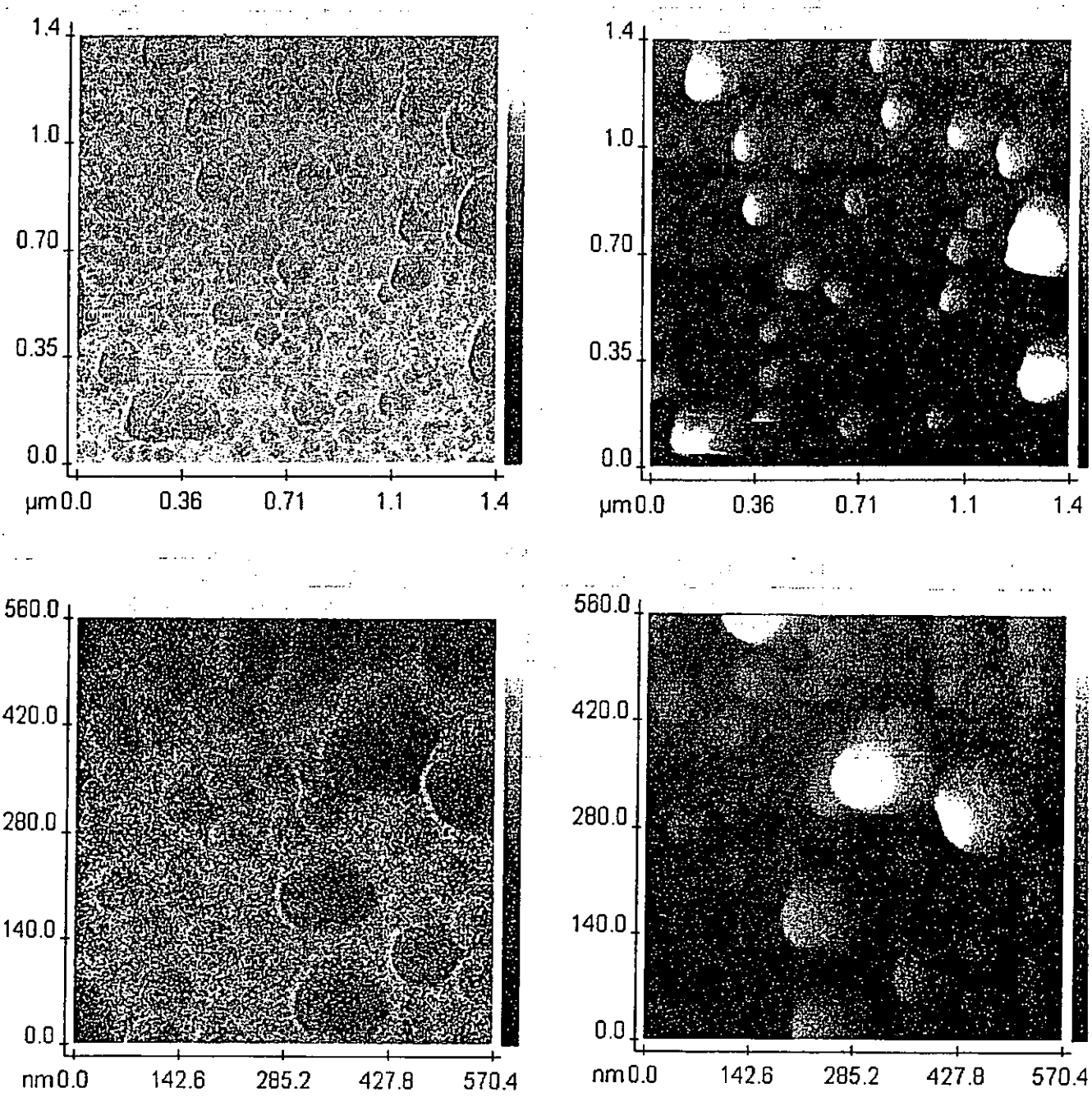

Figure 6.7 The AFM data of $Co_{20}Ag_{80}$ granular film on Si substrate with different scale. (On the left hand side is lateral force data and on the right hand side is topology data.)

Chapter 7

Fabrication and Characterization of Ti Thin Film on Si Substrate

7.1 Introduction

We have studied the metallic granular and multilayer systems. The giant magnetoresistance of all these systems is always negative. However, we have also examined systems of metal films deposited on Si. In these investigations we have observed of an exceptionally large positive magnetoresistance and an anomalous R-T profile in Ti films deposited on Si by PLD method. The studies of the effect of film thickness, substrate temperature and post-annealing effect on the positive magnetoresistance and the R-T profiles are reported in the following section.

7.2 R-T Profile and Positive Magnetoresistance of Ti Film on Si Substrate

Figure 7.1 shows the R-T profiles of the Ti film deposited on Si. We have used the XeCl pulsed UV excimer laser with λ = 308 nm to deposit Ti film on silicon(100) substrate. The laser fluence was about 2 J/cm^2 with a laser repetition rate of 10 Hz. The target was a Ti metal with high purity. The deposition was carried out in an ambient gas pressure of 1×10^{-5} torr in the 10 litres vacuum chamber. The substrate temperature was held at 600 °C during deposition. The rotating

multiple targets holder illustrated in Figure 4.3 was used. The ablation lasted for about 3 mins and produced a film of about 10 nm thick. It is seen from the figure that the R-T profiles display a metallic-like behavior at temperatures above 170 K. From 170 K to 160 K, however, the R-T curves show an anomalous transition and the resistance of the film increases rapidly by more than an order of magnitude. As the temperature decreases further, the R-T curves show a semiconductor-like feature. It is possible that the Ti/Si form an amorphous alloy layer at the interface. The transition is probably due to a temperature induced semiconductor-to-metal transition. When a magnetic field is applied perpendicular to the plane of the film, the resistance of the film increases noticeably in the metallic-like region giving a large PMR. A maximum MR of +37% is obtained at temperature near the transition. The MR gradually decreases to about +10% at room temperature.

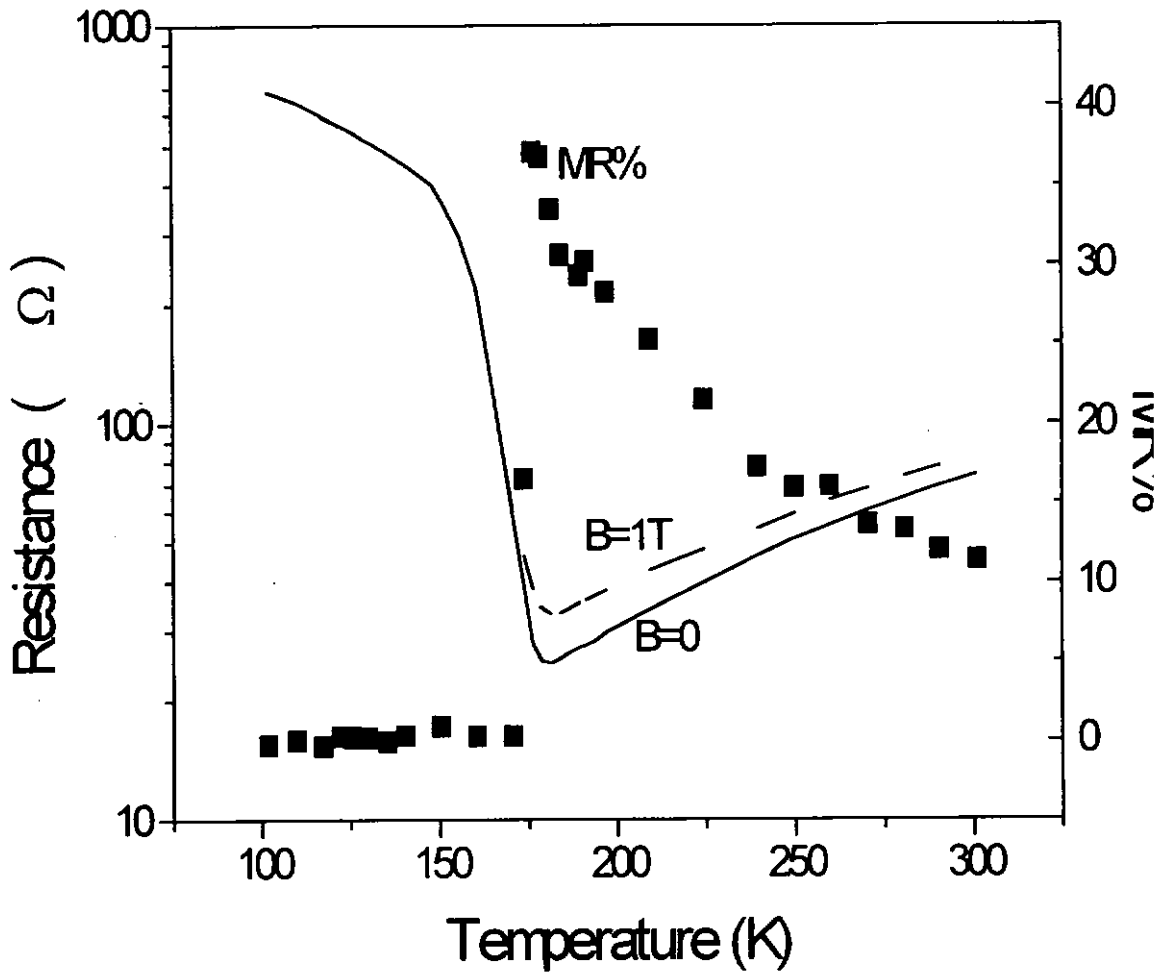

Figure 7.1 Typical Ti/Si based thin film resistance against temperature and MR against temperature profiles deposited for 3 mins and 600 °C.

7.3 Thickness (Deposition Time) Dependence

Initially we were not certain whether the semiconductor-to-metal transition and the PMR were originated in the interfacial layer. We therefore have examined the effects of Ti film thickness. In these thickness studies, apart from varying the laser ablation duration, all other deposition conditions remained unchanged. Ti was

deposited on silicon substrate for different deposition time while the substrate temperature was kept at 200 °C for all samples. The thicknesses of Ti films were deduced from a sample of 192 nm thick Ti film produced by a 60 mins laser ablation. Assuming the deposition yield per laser shot is constant, the film thickness is roughly proportional to the deposition time (number of laser shots). The results are tabulated in Table 7.1. Generally, shorter deposition time produces thinner films. It has been shown in Figure 7.2 that thinner films produce a conspicuously larger PMR. For example, the 64 nm thick film shows a maximum MR of +11% whereas the 3 nm film gives a value of +23%. This suggests that the MR effect is primarily produced by the interfacial layer. Due to the technical difficulties, we did not attempt to fabricate thinner films in the present work.

Sample	$t_{deposition}$ min	Thickness nm	MR%
STi3	0.5	1.6	20
STi1	1	3.2	23
STi2	3	9.6	12.5
STi4	5	16	10
STi6	10	32	8
STi7	20	64	11
STi26	30	96	7.1
STi27	40	128	6.4
STi5	60	192	8

Table 7.1 Results of Ti/Si film thickness studies. The substrate temperature was kept at 200°C.

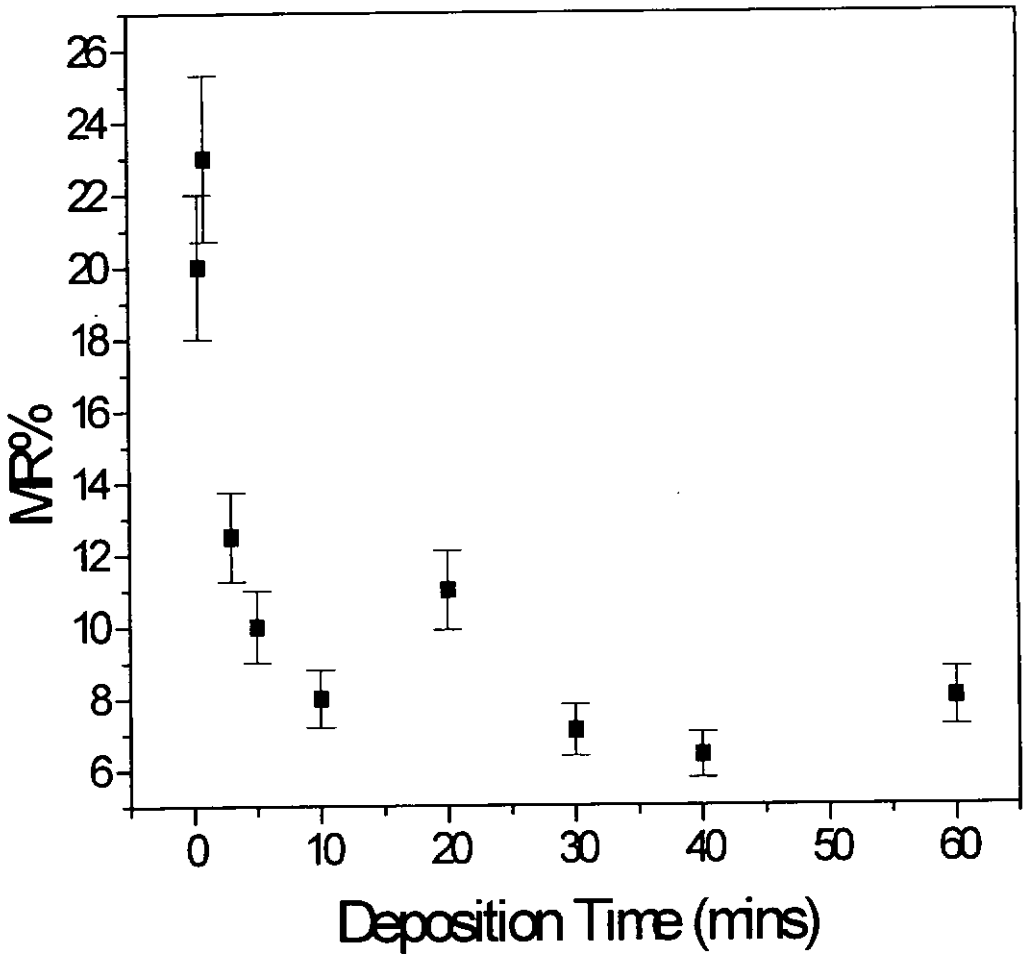

Figure 7.2 The MR against deposition time profile of Ti/Si based films deposited at substrate temperature 200 °C.

7.4 Substrate Temperature Dependence

Table 7.2 shows the results of a series of substrate temperature dependence studies. Figure 7.3 depicts the MR% as a function of substrate temperature. It is seen that the MR% increases with the substrate temperature up to 600 °C, the maximum value in this study. Apparently a much larger MR% can be obtained at even higher temperatures. It is believed that at high substrate temperatures the interfacial Ti/Si alloying becomes more prominent and leads to an enhanced MR effect. Optimization of the MR% values at temperatures higher than 600 °C have not been investigated in the present studies.

Sample	$T_{substrate}$ K	MR%
STi22	50	11.6
STi10	100	12.5
STi12	200	16.7
STi14	300	14.3
STi16	400	16.1
STi18	500	20.4
STi20	600	37.0

Table 7.2 Positive MR% as a function of substrate temperature.

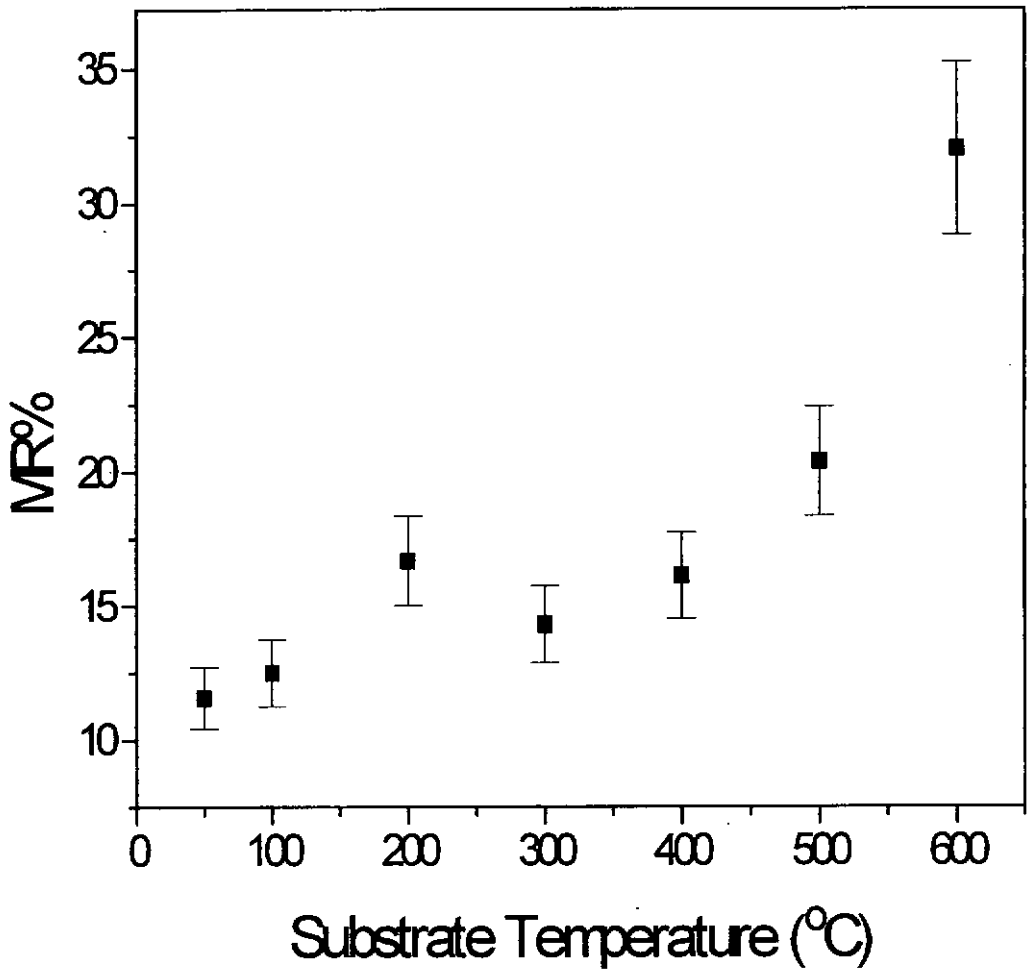

Figure 7.3 The positive MR% against substrate temperature profile of Ti/Si based films deposited for 3 mins.

7.5 Annealing Temperature Dependence

Table 7.3 shows the results of MR dependence on the annealing temperatures Figure 7.4 shows profile of the MR% against the post-annealing temperature. All these samples were deposited at 200 °C to ~ 10 nm thick. They were then post-annealed for an hour in temperatures ranging from 200 °C to 600 °C. The MR % is shown to decrease rapidly from 200 °C to 300 °C. Further increase of the post-annealing temperature, however, have minor effect on the MR% (apart from a small increase in MR% with temperature). The quickly deteriorated MR at 200 °C - 300 °C post-annealing temperature is thought to be the result of excessive oxidation of Ti. Our experimental chamber was kept at vacuum of about 1×10^{-5} torr. The corresponding monolayer formation time is about tens of seconds. It is likely that a prolonged annealing at temperature above 200 °C - 300 °C causes a substantial amount of Ti being oxidized, and hence increases the resistance of the film and produces a much reduced MR. At higher post-annealed temperatures similar effect occurs with perhaps a slight improvement in the Ti/Si alloying.

Sample	$T_{annealing}$ °C	MR%
ST28	200	20.0
ST36	300	10.7
ST30	400	10.6
ST34	500	10.8
ST32	600	13.0

Table 7.3 1 hour annealing temperature series with 3 mins deposition time and 200 °C substrate temperature.

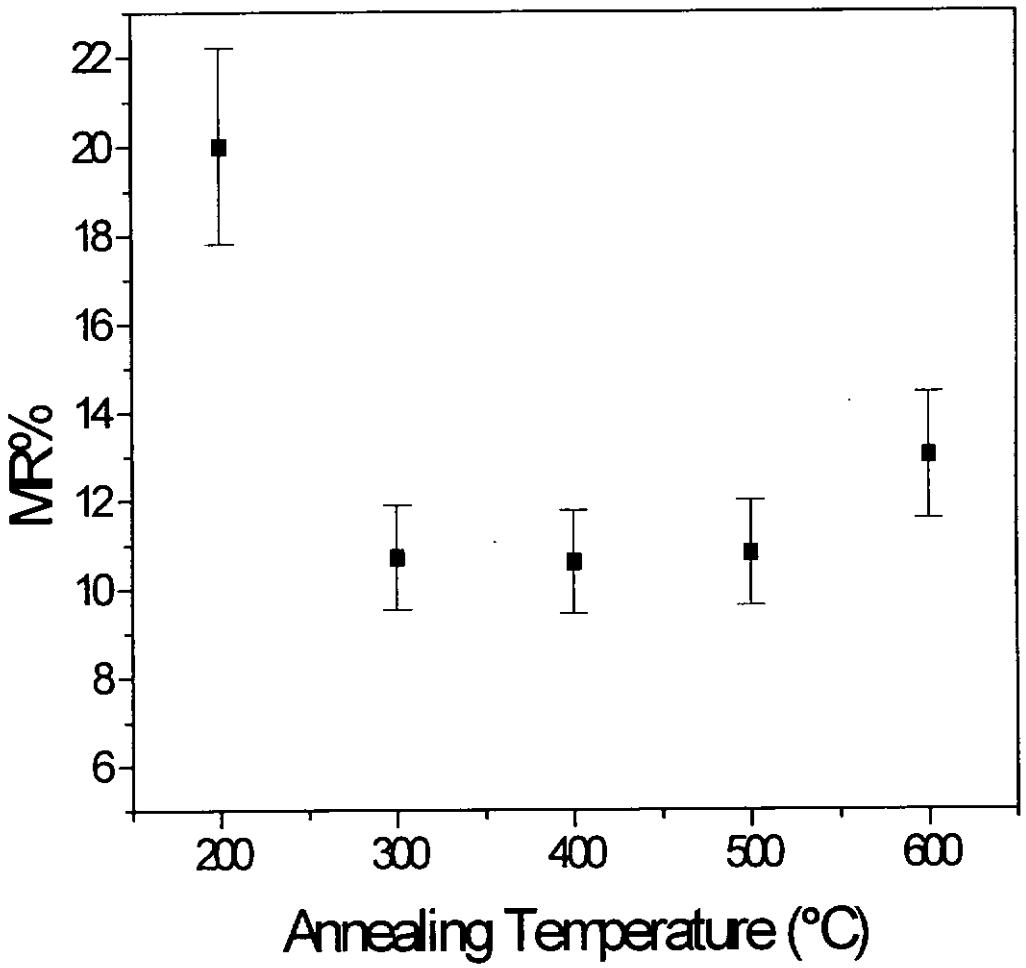

Figure 7.4 The MR against annealing temperature profile of Ti/Si based films deposited for 3 mins at 200 °C.

7.6 Scanning Field Profile

For this particular measurement, we have use the scanning field set-up in the Hong Kong University of Science and Technology (HKUST) which can provide a scanning field of 0 – ± 50 kOe (0 – ± 5 Tesla) and sample cooling down to 4 K. Figure 7.5 shows the resistance of our Ti/Si based film under the influence of the scanning magnetic field at temperature near the semiconductor-to-metal transition. It is a symmetric profile with the resistance lying between 121 Ω and 166 Ω, At the low magnetic field region from -15 kOe to 15 kOe, the resistance responded quadratically with increasing applied magnetic field. At higher magnetic field region, the resistance increased linearly with the field. No sign of saturation is observed even at the maximum field of ± 50 kOe used.

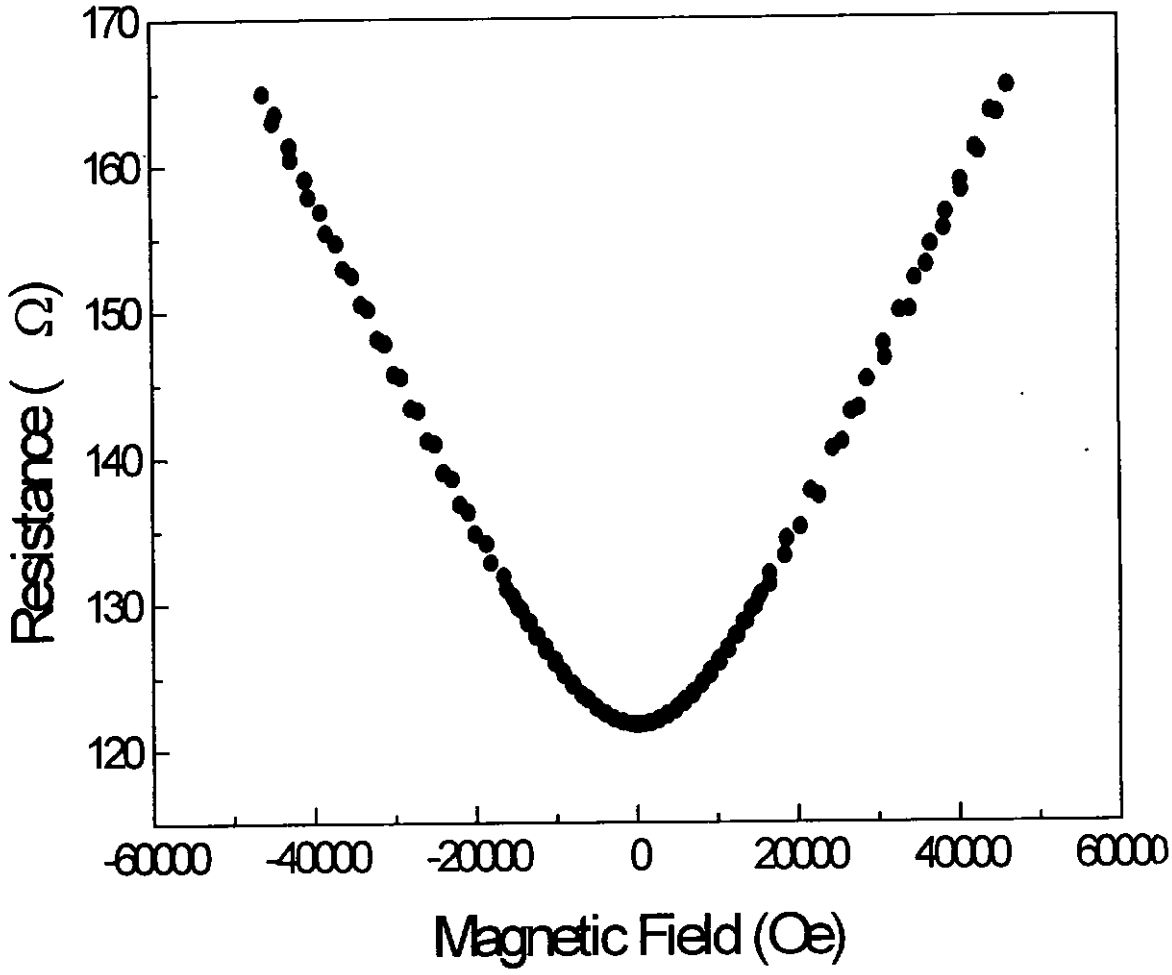

Figure 7.5 The resistance against magnetic field profile of Ti/Si based film.

The profile in Figure 7.5 is converted to a field dependent MR% profile shown in Figure 7.6 according to the definition of MR stated in equation 2.1. The maximum MR% thus obtained is 37% at 50 kOe and -50 kOe.

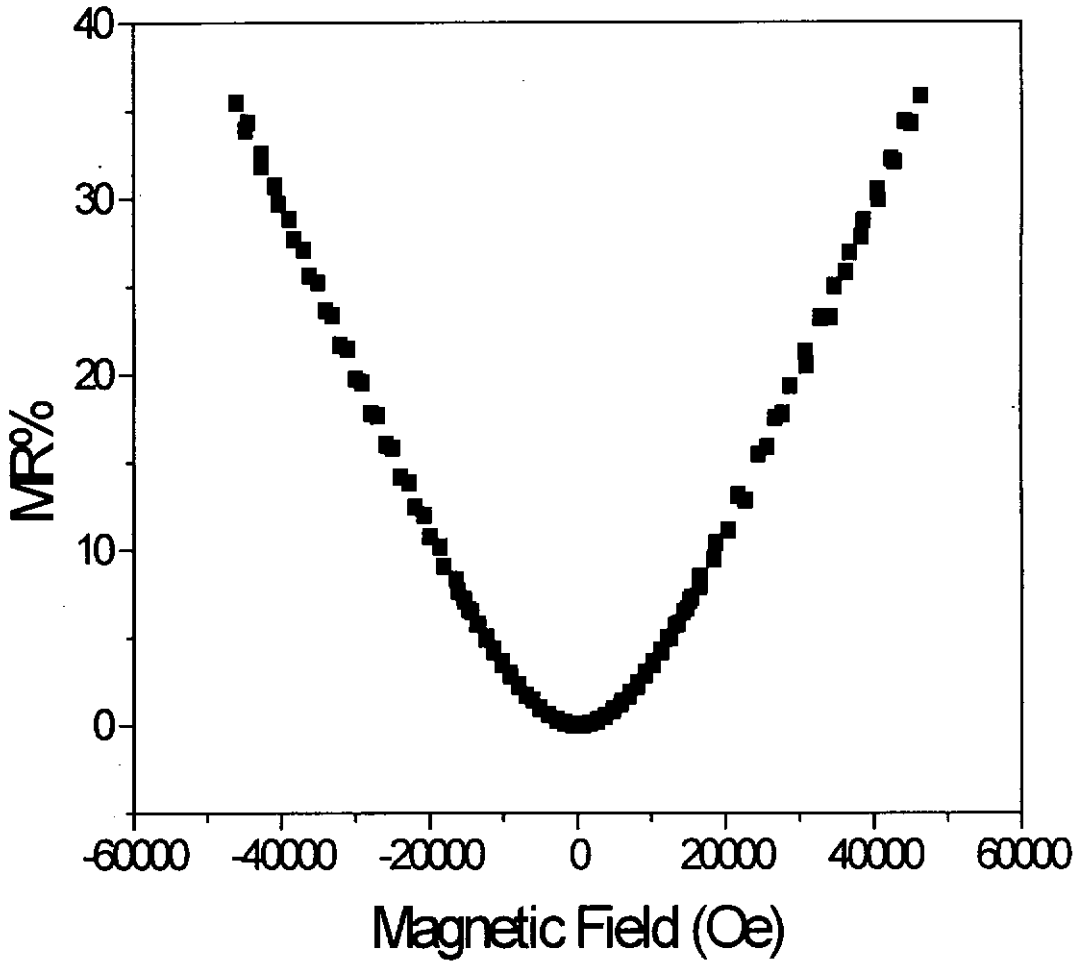

Figure 7.6 MR% against magnetic field profile of Ti/Si based film.

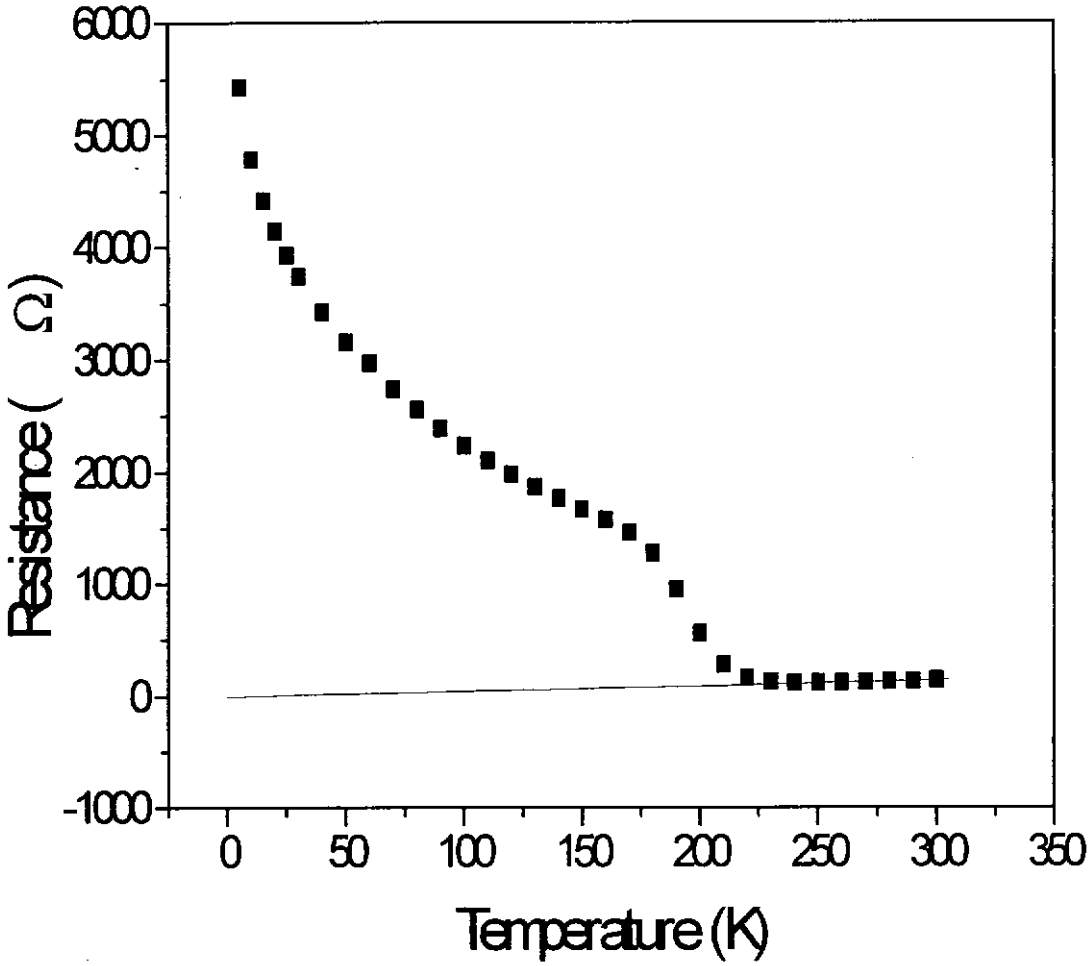

Figure 7.7 R-T profile of the Ti/Si based film. The solid line is a best fit for the data above 220 K.

7.7 R-T Profile of the Ti/Si Based Film

Figure 7.7 shows the R-T profile of one of the Ti/Si based films. It is seen that at temperatures above 220 K the film is metallic-like with the resistance extrapolated to zero at 0 K. A rather sharp transition occurs at about 200 K. At that point the resistance suddenly increases by more than an order of magnitude. Thereafter the R-T of the film behaves like semiconductor. As we have mentioned earlier, the large PMR only occurs in the metallic-like regime. No observable MR is seen in the semiconductor-like region at low temperature.

7.8 Discussion and Conclusion

The observation of a large PMR in the Ti/Si based films is somewhat unexpected. The temperature induced semiconductor-to-metal transition is also unexpected. The conductivity σ of the Ti/Si based film as a function of 1/T plotted in Figure 7.8 illustrates the transition clearly. Work reported by Raaijmakers et al has shown that Ti film deposited on crystallized Si forms a prominent interfacial layer of $TiSi_x$ [Raaijmakers et al, 1990]. This is displayed on their high resolution TEM pictures (reproduced in Figure 7.9 here). A schematic drawing is shown in Figure 7.10 for clarity.

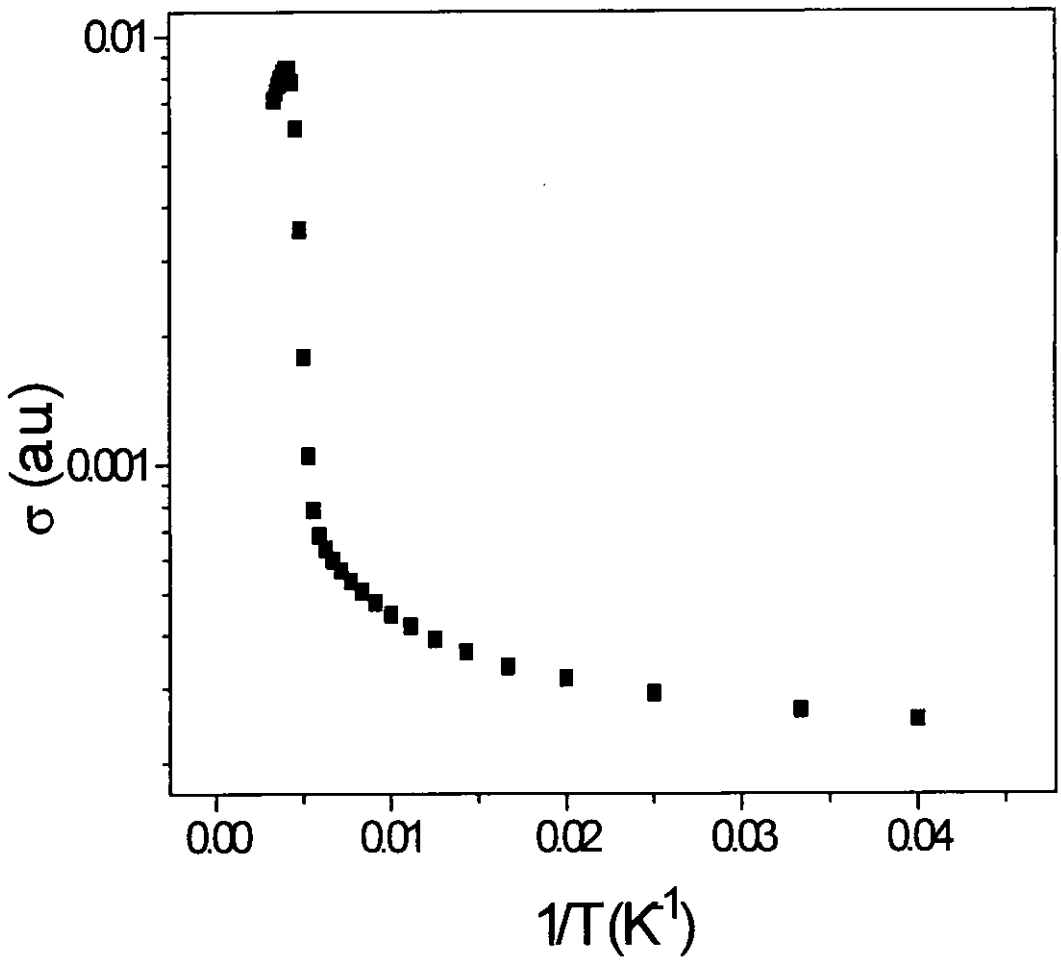

Figure 7.8 The conductivity of a Ti/Si based film as a function of 1/T, showing the metal-semiconductor transition.

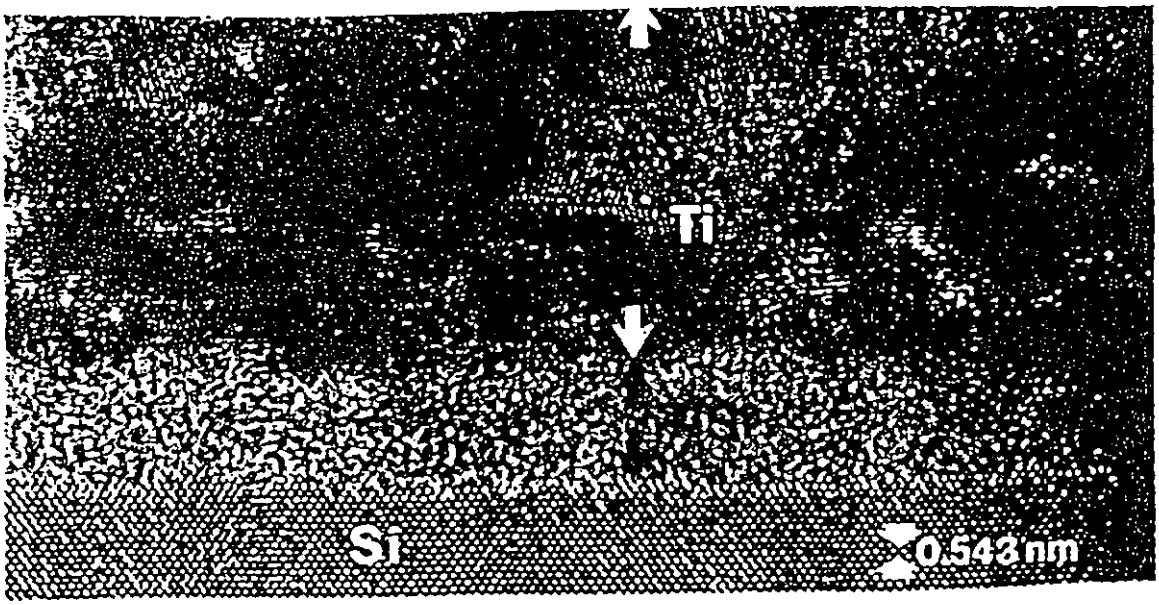

Figure 7.9 High-resolution bright-field electron micrographs of a Ti/TiSix/Si sample (reproduced from [Raaijmakers et al, 1990]).

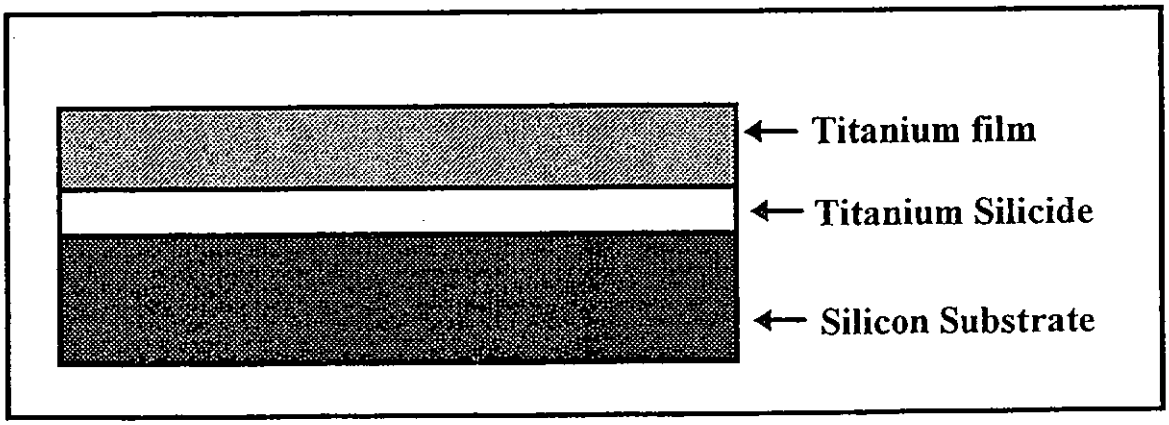

Figure 7.10 A schematic drawing of Ti/$TiSi_x$/Si trylayer.

This interfacial layer can be considered as a region of heavily doped Si. The Ti ion is a localized impurity which causes the temperature induced semiconductor-to-metal transition [Mott, N. F., 1990].

The application of a magnetic field can reduce the conduction bandwidth of the impurity band in the metallic regime leading to a metal-to-semiconductor transition, hence PMR. Details of the originating mechanism for the observed anomalous R-T profile and the PMR of Ti/Si have yet to be determined. More systematic experimental and theoretical investigation are needed for better understanding of these very interesting and potentially useful materials system.

Conclusion and Suggestions for Future Work

In the present experimental investigation we have used a split target arrangement to fabricated CoAg multilayer and granular thin films with different layer thickness and varied composition respectively on Si(100) substrate by the conventional PLD technique. The relationship of laser track length percentage and the atomic percentage of Co and Ag are non-linear and different for these two materials. For the same number of laser shots the deposition yield is higher for Co than for Ag. Using the calibration data of deposition yield for different materials, we can fabricate films of desired composition easily by arranging appropriate track length ratio on the split target. The studies of atomic percentage of Co dependence on MR ratio suggests that the optimum MR% is obtained with the atomic fraction of Co at around 20%. AFM characterization results indicate that the granular films are composed of grain of large Ag with the Co filling the grain boundary. This structural configuration produces a much smaller MR effect. The outgrowth and large grain size of Ag film produced by PLD prohibit the fine control of the film thickness and leads to poor quality CoAg multilayers.

Apart from the CoAg multilayer and granular films, we have also studied the Ti/Si based films. This is essentially a trilayer system consisting of $Ti/TiSi_x/Si$ layered structure. Clear and sharp temperature induced semiconductor-to-metal transition was observed. A change of resistance by over an order of magnitude occurs at the

transition temperature. In addition, large PMR is observed in the metallic regime of the Ti/Si films. A maximum MR of +37% and +10% are obtained at the temperature near the transition and at room temperature respectively under 1 Tesla of magnetic field applied perpendicular to the plane of the sample. No sign of field saturation is observed even at the maximum field of ± 50 kOe used.

The observation of large PMR in this rather simple structured material system is unexpected. In fact some of our other preliminary investigations show that the Cu/Si based films also has prominent PMR. The semiconductor-to-metal transition, however, occurs at about room temperature. The change of resistance at the transition can be greater than two orders of magnitude. In this report we have only concerned with the Ti/Si system. We expect, however, that there might be other metals, apart from Ti and Cu, deposited on Si will show similar PMR and semiconductor-to-metal transitions. In view of the large PMR and sharp temperature induced resistance change, potential applications in magnetic and temperature sensor are envisaged. The present studied material system is particular interesting in that, apart from being simple, the Ti film is actual deposited on Si substrate at low temperature. Thus it is compatible to Si processing technology and is eminently suitable for integrated microelecrtonic device.

However, before any practical devices fabrication can be carried out, more detailed and systematic studies, both in the experimental and theoretical aspects, are needed.

From the present studies, some further work of interest are summarized as follows:

For multilayer and granular films

1. To study the large MR effect of other material systems (e.g. Co/Cu, NiFe/Ag).
2. To investigate new material systems (e.g. $Fe_{16}N_2$, FeMn/Co/CuCo and NiFe/Cu/Co/Cu/NiFe (spin valves)).

For Ti/Si films

1. To further investigate the origin of the positive magnetoresistance and the anomalous R-T profiles of the Ti/Si films.
2. To explore other materials such as Cu, apart from the Ti, deposited on Si that exhibit the large positive GMR effect and sharp semiconductor-to-metal transition.
3. To study the temperature dependence of the semiconductor-metal transition by doping with different materials.

Reference

Al'tshuler, B. L. and Aronov, A. G.
Electronic-Electronic Interactions in Disordered systems, ed. by Efros, A. L. and Pollak (North-Holland, Amsterdam, 1984)

Albrecht, T. R. and Quate, C. F.
J. VA. Sci. Technol., Vol. A6, p.271 (1998)

Askar'yan G. A., Pokhorov, A. M., Chantutiya, G. F. and Shipulo, G. P.
Sov. Phys. JETP, Vol. 17, p.6 (1963)

Azizi, A., Thompson, S. M., Ounadjela, K. Gregg, J., Vennegues, P., Dinia, A., Arabski, J. and Fermon, C.
"Correlation between the structure and transport properties of granular CoAg system prepared by MBE"
J. M. M. M., Vol. 148, p.314 (1995)

Baibich, M. N., Broto, M. J., Fert, A., Nguyen Van Dau, F., Petroff, F., Etienne, P., Creuzet, G., Friederich, A. and Chazelas, J.
Phys. Rev. Lett., Vol. 61, p.2472 (1988)

Bennett, L. H. and Watson, R. E.
Magnetic Multilayers, p.2 (1994)

Berkowitz, A. E., Mittchell, J. R., Carey, M. J., Young, A. P., Zhang, S., Spada, F. E., Parker, A., Hutten, A. and Thomas, G.
Phys. Rev. Lett. Vol. 68, p.3745 (1992)

Binash, G., Grunberg, P., Saurenbach, F. and Zinn, W.
Phys. Rev. B, Vol. 39, p.4828 (1989)

Binning, G., Rohrer, H., Gerber, Ch. and Weibel, E.
"The first atomic-resolution STM image"
Phys. Rev. Lett., Vol. 50, p.120 (1983)

Binning, G., Quate, C. F. and Gerber, C.
Phys. Rev. Lett., Vol. 56, p.930 (1986a)

Binning, G. et al
"The first atomic resolution AFM image"
Euro. phys. Lett., Vol. 1, p.31 (1986b)

Bunshah, R. F.
Deposition Technologies for Films and Coating (Noyes Pub. Ridge, Park, N. J.) (1982)

Bykovskii, Yu. A., et al.
Sov. Phys. Tech. Phys., Vol. 23(5) , pp.578-581 (1978)

Cali, C., Daneu A.,.Orioli A. and Riva-Sanseverino, S.
Appl. Opt., Vol. 15(5), pp.1327-1330 (1976)

Chaiken, A., Lubitz, P., Krebs, J. J., Prinz, G. A. and Harford, M. Z.
Appl. Phys., Vol. 70, p.5864 (1991)

Chang, L. D.,.Tseng, M. Z., Hu, E. L. and Fork, D. K.
Appl. Phys. Lett., Vol. 60(14), pp.1753-1755 (1992)

Cheung, J. T., Gergis I. M., James, J. and DeWames, R. E.
Appl. Phys. Lett., Vol. 60(25), pp.3180-3182 (1992)

Conde, F., Gomez-Polo, C. and Hernando, A.
"Superparamagnetic behavior and giant magnetoresistance in as-obtained Co-Ag metastable alloys"
J. M. M. M., Vol. 138, p.129 (1994)

Coqblin, B.
"The Electronic Structure of the Rare-Earth Metals and Alloys"
The Magnetic Heavy Rare-Earths (1977)

Curl, R. F. and Smalley, R. E.
Sci. Am. October, pp.54-63 (1991)

Daughton, J. M
Ferroelectrics, Vol. 116, p.175 (1991)

Daughton, J. M.
Thin Solid Films, Vol. 216, p.162 (1992)

Dieny, B., Humnert, P., Speriosu, V. S., Metin, S., Gurney, B. A., Baumgart, P. and Lefakis, H.
Phys. Rev. B., Vol. 45, p.806 (1992)

Dijkkamp, D., et al.
Appl. Phys. Lett., Vol. 51, pp.619-621 (1987)

Doll, G. L., Sell, J. A., Taylor. C. A., II and Clarke, R
Phys. Rev., Vol. B43, pp.6816-6819 (1991)

Edwards, D. M.
"MAGNETIC COUPLING IN MULTILAYERED MAGNETIC FILMS"
ASPECTS OF MODERN MAGNETISM, p.105 (1996)

Enrech, M. R., Skomski, Coey, J. M. D. and Lunney, J. G.
"Characterization, transport, and magnetic properties of Co/Pd Multilayers produced by pulsed laser deposition"
Appl. Phys., Vol. 73 (10), p.6421 (1993)

Falicov, L. M., Meija-Lira, F. and Moran-Lopez, J. L.
Magnetic Properties of Low-Dimensional Systems II (Springer, Berlin, Heidelberg, 1990a)

Falicov, L. M., Pierce, D. T., Bader, S. D., Gronsky, R., Hathaway, K. B., Hopster, H. J., Lambeth, D. N., Parkin, S. S. P., Prinz, G., Salamon, M., Schuller, I. K. and Victoria, R. H.
Mat. Res., Vol. 5, p.1299 (1990b)

Fert, A. and Campbell, I. A.
J. Phys., Vol. F6, p.849, (1976)
Fert, A.
Materials Science Forum, Vol. 59&60, p.439 (1990)

Fork, D. K., Fenner, D. B., Connell, G. A. N., Phillips, J. M. and Geballe, T. H.
Appl. Phys. Lett., Vol. 57, pp.1137-1139 (1990)

Fork, D. K., Nashmoto, K. and Geballe, T. H.
Appl. Phys. Lett., Vol. 60(13), pp.1621-1623 (1992)

Freeman, A. J.
An excellent reference book on the magnetism of the RE metal in Magnetic Properties of Rare Earth Metals, p.245 (1972)

Fritsch, G., Schulte, A. and Luscher, E.
Amorphous and Liquid Materials, NATO ASI Series E, No. 118, ed. by Luscher, E., Fritsch, G. and Jacussi, G. (Nijhoff, Dordrecht, 1987)

Fullertton, E. E, Conover, M. J., Mattson, J. E., Sowers, C. H., and Bader, S. D.
Appl. Phys. Lett., Vol. 63, p.1435 (1993)

Greer, J. A. and Van Hook, H. J.
Mater. Res. Soc. Symp. Proc., Vol. 191, pp.171-176 (1990)

Hamelin, B.
Nucl. Inst. Methods, Vol. 135, p.299 (1976)

Hass, G. and Ramsey, J. B.
Appl. Opt., Vol. 8 (6), pp.1115-1118 (1969)

Hathaway, K. B.
"Simple Model of the Magnetoresistance in Multilayer"
Ultrathin Magnetic Structure II, p.100 (1994)

Hau, S. K.
"Split Target"
Deposition of ceramic films using pulsed excimer laser, PhD. Thesis, p.67 (1995)

Hau, S. K., Wong, K. H., Chan, P. W. and Choy, C. L.
"Intrinsic resputtering in pulsed-laser deposition of lead-zirconate-titanate thin film"
Appl. Phys. Lett., Vol. 66, p.245 (1995)

Horwitz, J. S., Grabowaki, K. S., Chrisey, D. B. and Leuchtner, R. E.
Appl. Phys. Lett., Vol. 59(13), pp.1565-1567, (1991)

Howson, M. A., Paja, A., Morgan, G. J. and Walker, M. J.
Z. Phys. Chem. Vol. 157, p.693 (1985)

Huang, J. C. A., Yao, Y. D., Liou, Y., Lee, S. F., Yang, W. T., Cahng, C. P., Liao, S. Y. and Lee, C. H.
"Novel epitaxial growth and magnetotransport characterization of single crystal Co(1120)/Cr(100) superlattices on Mo Buffer layers"
Appl. Surf. Sci., Vol. 92, pp.480-483 (1996)

Humphreys, R. G., Satchell, J. S., Chew, N. G., Edwards, J. A., Cullis, A. G. and Dosser, O. D.
Less-Common Metals, Vol. 151, p.271 (1989)

Iwabuchi, M., Kinoshita, K., Ishibashi, H. and Kobayashi, T.
"Reduction of pinhole leakage current of $SrTiO_3$ films by ArF excimer laser deposition with shadow mask ("Eclipse method")'
Jpn. J. Appl. Phys., Vol. 33, p.L610 (1994)

Jenkins, Ron and Snyder, Robert L.
Introduction to X-rays powder diffractometry, p.1-4, p.47-82 (1996)

Kasuya, T., Prog. Theoret.
Phys. Vol. 16, p.45 (1956)

Lee, P. A. and Ramakrishnam, T. V.
Rev. Mod. Phys., Vol. 57, p.287 (1985)

Lee, W. Y., Salem, J., Lee, V., Huang, T., Savoy, R., Deline, V. and Duran, J.
Appl. Phys. Lett., Vol. 52, p.2263 (1988)

Leung, Y. S.
"STO/TiN/Si"
Fabrication and Characterization of Pulsed Laser Deposition of $La_{1-x}Ca_xMnO_3$ Based Heterostructures, p.93 (1998)

Levry, Peter M.
"Giant Magnetoresistance in Magnetic Layered and Granular Materials"
Solid State Physics, Vol. 47, p367 (1994)

Lindqvist, P. and Fritsch, G.
"Magnetoresistance of Amorphous Cu-Ti alloys: The spin-orbit scattering time within weak localization"
Phys. Rev. B, Vol. 40, p.5792 (1989)

Lynn, J. W. and Kjems, J. K. et al
J. Appl. Crystallography, Vol. 9, p.454 (1976)

Maiman, T. H.
Nature, Vol. 187, p.493 (1960)

Majkrzak, C. F.
Applied Optics, Vol. 23, p.3524 (1984)

Majkrzak, C. F. and Shirane, G.
J. Phys. Paris, Vol. C7, p.215 (1982)

Martin, T., Williams, C. C. and Wickramasinghe, H. K.
"A recent review"
Scanning Microscopy, Vol. 2, p.3 (1988)

Meyerand, R. G. and Haughty, A. F.
Phys. Rev. Lett., Vol. 9, p.403 (1963)

Mezei, F.
Commun. Phys., Vol. 1, p.81 (1981)

Mezey, L. Z. and Giber, J.
Jpn. J. Appl. Phys., Vol. 21, p.1569 (1982)

Miedema, A. R.
Philips Tech. Rev., Vol. 36, p.217 (1976)

Moon, R. M., Riste, T. and Koehler, W. C.
Phys. Rev., Vol. 181, p.920, (1969)

Mott, N. F.
"Chapter 5, Interacting Electrons in Non-crystalline Systems. Impurity Bands and Metal-Insulation Transitions in Doped Semiconductors"
Metal-Insulator Transition, pp.145-169 (1990)

Narayan, J., et al.
Appl. Phys. Lett., Vol. 61(11), pp.1290-1292 (1992)

Norton, G. M., Kotula, P. G. and Carter, C. B.
Appl. Phys., Vol. 70(5), pp.2871-2873 (1991)

Olivier, M., Strom-Olsen, J. O., Altounian, Z. Cochrane, R. W. and Trudeau, M.
Phys. Ren. B. Vol. 33, p.2799 (1986)

Ousset, C., Rakoto, H., Broto, J. M., Dupuis, V., Askenazy, S., Durand, J. and Marchal, G.
Phys. Rev. B, 36, 5432 (1987)

Pardavi-Horvath, Martha
""Classical" magnetoresistance Galvanomagnetic effect"
Magnetic Multilayers, pp.356-359 (1994a)

Pardavi-Horvath, Martha
"GMR in magnetic multilayers"
Magnetic Multilayers, p.360 (1994b)

Parker, E. H. C.,ed.
The Technology and Physics of Molecular Beam Epitaxy, Plenum, New York (1986)

Parker, M. H.
"Giant Magnetoresistance in Granular Materials"
J. Appl. Phys., Vol. 75 (10), p.6894 (1994)

Parkin, S. S. P., More, N. and Roche, K. P
Phys. Rev. Lett., Vol. 64, p.2304 (1990)

Parkin, S. S. P., Bhadra, R. and Roche, K. P.
Phys. Rev. Lett., Vol. 66, p.2152 (1991a)

Parkin, S. S. P. and Mauri, D.
Phys. Rev. B. Rapid Comm., Vol. 44, p.7131 (1991b)

Parkin, S. S. P.
Phys. Rev. Lett., Vol. 67, p.3598 (1991c)

Parkin, S. S. P.
"Giant Magnetoresistance and Oscillatory Interlayer Coupling in Polycrystalline Transition Metal Multilayers"
Ultrathin Magnetic Structures II, p.148 (1994)

Parkin, S. S. P., Farrow, R. F. C., Rabedeau, T. A., Marks, R. F., Harp, G. P., Lam, Q., Chappert, C., Toney, M. F., Savoy, R. and Geiss, R.
Euro. Phys. Lett., Vol. 22, p.455 (1993)

Prusseit, W., et al.
Appl. Phys. Lett., Vol. 61(11), pp.1841-1844 (1992)

Raaijmakers, Ivo J. M. M. and Kim, Ki-Bum
" A comparison of the reaction of titanium with amorphous and moncrystalline silicon"
J. Appl. Phys., Vol. 67, p.6256 (1990)

Ramesh, R., et al.
Appl. Phys. Lett., Vol. 57(15), pp.1505-1507 (1990)

Ready, J. F.
Appl. Phys. Lett., Vol. 3(1), pp.11-13 (1963)

Rengan, A., and Narayan, J.
Laser Ablation of electronic materials (Foragassy, E. and Lazare, S.,eds. Elsevier, North Holland, The Netherlands, pp.363-376 (1992)

Rubinstein, M., Das, B. N., Koon, N. C., Chrisey, D. B., and Horwitz, J.
"Granular giant magnetoresistance materials and their resonances"
Appl. Phys., Vol. 76 (10), p.6823 (1994)

Ruderman, M. A. and Kittel, C.
Phys. Rev., Vol. 96, p.99 (1954)

Sato, H., Schroeder, P. A., Slaughter, J. M., Pratt, Jr. and Abdul-Razzaq, W.
"Supperlattices Microstruct.", Vol. 4, p.45 (1997)

Saxena, A. M. and Majkrzak, C. F.
AIP Conf. Proc., Vol. 89, p.193 (1981)

Schad, R., Potter, C. D., Belien P., Verbanck G., Moshchalkov V.V., and Bruynseraedd Y.
Appl. Phys. Lett., Vol. 64, p.3500 (1994)

Schoenborn, B. P., Caspar, D. L. D. and Kammerer, O. F.
J. Appl. Crystallography, Vol. 7, p.508 (1974)

Schuller, I. K.
"The Physics of Metallic Supperlattices: An Experimental Point of View"
Physics, Fabrication, and Applications of Multilayered Structures, ed. by Dhez, P. and Weisbuch, C., p.139 (Plenum, New York, 1998)

Schwartz, H. and Tourtellotte, H. A.
Vac. Sci. Technol., Vol. 6(3), pp.887-891 (1969)

Shinjo, T. and Takada, T.
"Metallic Supperlattices"
Ferromagnetic Materials, Vol. 3, ed. by E. P. Wohlfarth (Elsevier, Amsterdam, 1987)

Smith, H. M. and Turner, A. F.
Appl. Opt., Vol. 4, pp.147-148 (1965)

Tsui, F., Uher, C. and Flynn, C. P.
"Positive Giant Magnetoresistance in Dy/Sc Superlattices"
Phys. Rev. Lett., Vol. 72, p.3084 (1994)

Turchin, V. F.
At. Energy, Vol. 22 (1967)
Velu, E., Dupas, C., Renard, D., Renard, J. P. and Seiden, J.
Phys. Res. B, Vol. 37, p.668 (1998)

Uhir, A.
Bell System Tech. J., p.105 (1995)

Venkatesan, T., Wu, X. D., Inam, A. and Wachhtman, J. B.
"Observation of two distinct components during pulsed laser deposition of high T_c superconducting films"
Appl. Phys. Lett., Vol. 52, p.1193 (1988)

Wang, Jian-Ding and Xiao, Gang
Phys. Rev. Lett., Vol. 49, p.3982 (1994)

White, R. L.
IEEE Trans. Mag., Vol. 28, p.2482 (1992)

White, R. M.
Appl. Phys., Vol. 34, p.3559 (1963)

White, R. M.
"Quantum Theory of Magnetism"
Springer, Berlin, Heidelberg, (1983)

Wu, Wenbin, Wong, K. H., Chan, P. W. and Cheung, Jeffrey T.
"Particular-free a-$YBa_2Cu_3O_{7-x}$/$La_{0.5}Sr_{0.5}CoO_3$/a-$YBa_2Cu_3O_{7-x}$ sandwiched thin film on (100)$SrTiO_3$ fabricated by pulsed laser deposition with shadow mask"
Materials Letters, Vol. 33, pp.225-230 (1997)

Xiao, J. Q., Jiang, J. S. and Chein, C. L.
Phy. Rev. Lett., Vol. 68 , p.3749 (1992)

Yosida, K.
Phys. Rev., Vol. 106, p.893 (1957)

Zeitsev-Zatov, S. V., Martynyuk, R. A. and Prostasov, E. A.
Sov. Phys. Solid State, Vol. 25, pp.100-103 (1983)

Zhang, Wei, Boyd, Ian W., Cohen, Neil S., Bui, Quang T., Pankhurst, Quentin A., Elliott, Martin, Herrenden-Harkerand, William.
"Phase segregation and giant magnetoresistance behavior in as-deposited Co-Ag film frown by pulsed laser deposition."
Appl. Phys., Vol. 81 (8), p.5211 (1997)

Zhang, Wei, Boyd, Ian W., Elliott, Martin. Herrenden-Harkerand, Willian
"Growth of giant magnetoresistance metallic granular CoAg films by pulsed laser deposition"
Magn. Magn. Matter, Vol. 165, p.330 (1997)

ZHANG, Ling-yun, YANG, Guo-lin, Li, Bo-zang, PU, Fu-ke (PU, Fu-cho)
Temperature Effect on Giant Magnetoresistance in Magnetic Multilayers, Vol. 13, No.1 (1996)